# SYNTHESIS AND CHARACTERIZATION OF PRISTINE AND LANTHANUM MODIFIED $WO_3$ NANOPARTICLES FOR THE PHOTOCATALYTIC DEGRADATION OF ORGANIC DYES

---


**by**

**Nthabeleng Sylvia Lehutso**

**(201602371)**


**Dissertation in fulfilment of the requirement for the degree**

**MASTER OF TECHNOLOGY**

**in**

**CHEMISTRY**

**in the**

**FACULTY OF SCIENCE**

**of the**

**UNIVERSITY OF JOHANNESBURG**


**Supervisor : Dr. L.N. Dlamini**

**Co-supervisor : Prof. J.C. Ngila**

# DECLARATION

I hereby declare that this dissertation, which I herewith submit for the research qualification

**MASTER OF TECHNOLOGY DEGREE IN CHEMISTRY**

to the University of Johannesburg, Department of Applied Chemistry, is, apart from the recognised assistance of my supervisors, my own work and has not previously been submitted by me to another institution to obtain a research diploma or degree.

_____ on this 04 day of September 2019

*(Candidate)*

_____ on this 04 day of September 2019

*(Supervisor)*

_____ on this 04 day of September 2019

*(Co-supervisor)*

# DEDICATION

I dedicate this work to God the all mighty for blessing me with this milestone and getting me through it. My loving husband Ephraim Motekedi Lehutso, the man who has been a pillar of strength, and our sweet daughter Tshegofatso Lehutso for the love and support they showed me through the sleepless nights and missed weekend outings. My grandmother Mamane Moitheri Tseisi who always believed in me and encouraged me my whole life. My mother Malerato Mookho Lucia Tseisi who is full of love, she has always been there and made sure I got hold of education. To my entire family for their love and support. My pastors, Pastor Goodwill Mkhavhela and wife Pastor Thandi Mkhavhela, who have been a guide and an inspiration that it is never too late to get education. I love you all.

# ACKNOWLEDGEMENTS

This project has been a good journey with many high and low points. However, with every journey comes interaction with extraordinary friends. I am honoured and humbled to recognize the input, commitment, support, sacrifice and dedication of the following people and institutions:

- My Heavenly father, who has never left me not forsaken me throughout this journey.
- My supervisors: Dr. L.N. Dlamini, and Prof. J.C. Ngila for your unconditional assistance in this journey.
- Dr. L.N. Dlamini, I am grateful to for your endeavours in guaranteeing a solid research and learning conditions. Always available, never held back constructive criticism, clear and goal orientated. Your input is very much appreciated. May God bless you and expand your legacy.
- Financial support from the National Research Foundation (NRF), Water Research Commission (WRC), ESKOM and the University of Johannesburg, Department of Applied Chemistry.
- Dr. S.P. Malinga, I am grateful for sacrificing your time, to provide inputs and moral support during our research group presentations.
- Mr. L.C. Mahlalela, Mr. M.M. Thwala, and Mr. S. Simelane, I truly appreciate you for your great assistance throughout the project. Your ideas and inputs helped me to get through and complete the project. May God richly bless you.
- Mr. E. Ngigi for your assistance in the characterization of my samples whenever I needed help. For that, I am truly thankful.
- To the rest of my research group members, Mr. D. Vlotman, Mr. S. Dube, Mr. Q. Zwane, Mr. C. Kgoetlana, Ms. D. Majotena, Ms. R. Bhembe, and Mr. P. Nhlophe and Ms. M. Kamogelo, thank you for your input and support. May God bless you.
- Members of the Department of Applied Chemistry in the Faculty of Science at the University of Johannesburg, I express my gratitude for your friendship and unconditional support during my studies

# PRESENTATIONS

The work outlined in this dissertation has been presented at conferences as shown below:

1. N.S. Lehutso, J. C. Ngila, and L. N. Dlamini, Synthesis and characterization of pristine and modified tungsten oxide nanoparticles for the degradation of organic dyes, Annual UJ-ESKOM workshop programme. University of Johannesburg, Doornfontein campus, Johannesburg, South Africa, 25th November 2016.

2. N.S. Lehutso, J. C. Ngila, and L. N. Dlamini, Synthesis and characterization of pristine and modified tungsten trioxide nanoparticles, Department of Applied Chemistry: Postgraduate research day. University of Johannesburg, Doornfontein campus, Johannesburg, South Africa, 13th -14th July 2017.

3. N.S. Lehutso, J. C. Ngila, and L. N. Dlamini. Synthesis and characterization of pristine and modified tungsten trioxide nanoparticles, Annual UJ-ESKOM workshop programme, Annual UJ-ESKOM workshop programme. University of Johannesburg, Doornfontein campus, Johannesburg, South Africa, 8th November 2017.

4. N.S. Lehutso, J. C. Ngila, and L. N. Dlamini, Synthesis and characterization of pristine and lanthanum modified tungsten trioxide nanoparticles for the photodegradation of organic dyes, Annual Postgraduate Research Conference (APRC), University of Johannesburg, Bunting Road Campus, Johannesburg, South Africa, 19th October 2018.

# ABSTRACT

South Africa is rich in naturally occurring resources including water, coal, oil, land. Individuals and industries use these resources as raw material inputs on a daily basis. However, they create significant amounts of pollution such as persistent organic pollutants (POPs). Such pollutants can be classified as inorganic, microbial and organic. Organic pollutants such as organic dyes are found in textile effluents that escape to the environment. They are designed to have a high degree of stability to fading upon sunlight exposures, chemicals and microbial attack leading to the ineffectiveness of current conventional wastewater treatment methods.

Conventional wastewater treatment methods have been reported to be ineffective in the degradation of textile dyes because of their chemical stability. These methods have low effectiveness, with limited flexibility, they require specialized equipment and further handling of the generated waste. These methods are reported to have the ability to effectively remove colour, but for but lack the ability to completely degrade the dye molecules. Developed methods such as advanced oxidation processes (AOPs) use of photocatalytic semiconductors. These semiconductors have been researched and reported to have the characteristics to effectively treat wastewater by completely degrading a diversity of organic pollutants.

A widely used semiconductor is monoclinic tungsten trioxide ($WO_3$). It is viewed as an ideal candidate for photocatalytic applications. It is a photocatalyst that is responsive in the visible region, it absorbs light in the region up to 480 nm. $WO_3$ has small band-gap energy which has been reported to range from 2.4−2.8 eV and high oxidation power of valence band (VB) holes and thus displays enhanced photoabsorption in visible-light irradiation. This gives $WO_3$ the advantage to be used as an indoor pollutant treatment as well as outdoor applications. Hence, this project aims to utilize lanthanum-doped $WO_3$ for the photodegradation of refractory

organic dyes. Lanthanides as dopants are reported to improve the photocatalytic activity of the catalyst by increasing the adsorption capacity for pollutants, as well as, reducing the electron-hole recombination rates.

In this study, pristine tungsten trioxide ($WO_3$) nanoparticles were synthesized using the impregnation method with tungstic acid ($H_2WO_4$) and nitric acid as precursors, Lanthanum nitrate hydrate was used as a source of lanthanum (La) dopant. The as-synthesized nanoparticles were annealed at 450ºC for 3 hrs. The nanoparticles were characterized using X-ray diffraction spectroscopy (XRD), transmission electron microscopy (TEM), coupled with energy dispersive X-ray (EDX), scanning electron microscopy (SEM), Fourier transform infrared spectroscopy (FTIR), Raman spectroscopy, zeta potential, UV-visible spectroscopy (UV-vis), X-Ray photoelectron spectroscopy (XPS) and Ion chromatography (IC).

Spectroscopic instruments such as XRD, Raman and FTIR confirmed the nanoparticles were composed of monoclinic polymorphs. The spherical morphology was confirmed by TEM and SEM, with EDX confirming the presence of tungsten, oxygen and lanthanum in the samples. The band gap energy obtained from the DRS measurements were found to be 2.45, 2.42 and 2.57 eV for *m*-$WO_3$, 1-La-$WO_3$, and 5-La-$WO_3$ nanoparticles respectively. XPS was used to determine the valence band maximum (VBM) which was used to calculate the conduction band and estimate the band edge position. XPS band edge positions were in agreement with the UV-vis band edge positions. Zeta potential confirmed the point of zero charge for the nanoparticles to be at pH 3.8. Ion chromatography confirmed the evolution of the chlorides and sulphate ions from the degradation of Methylene blue and Congo red respectively.

# TABLE OF CONTENTS

# LIST OF FIGURES

# LIST OF TABLES

# LIST OF ABBREVIATIONS

| | |
|---|---|
| AOPs | Advanced oxidation processes |
| AMD | Acid mine drainage |
| ATR | Attenuated total reflection |
| BE | Binding energy |
| CB | Conduction band |
| COD | Chemical oxygen demand |
| CR | Congo Red |
| CSO | Combined sewage overflow |
| DI | Deionised water |
| DRS | Diffuse reflectance mode |
| EDX | Energy dispersive x-ray spectroscopy |
| $E_g$ | Band gap energy |
| eV | Electron volt |
| FTIR | Fourier transform infrared spectroscopy |
| IC | Ion chromatography |
| KE | kinetic energy |
| LO | liquid oxidation |
| MB | Methylene Blue |
| MO | Methylene orange |
| NHE | Natural hydrogen electrode |
| NPs | Nanoparticles |
| PEC | Photoelectrochemical |
| PCP | Pentachlorophenol |
| POPs | Persistent Organic Pollutants |

| | |
|---|---|
| pzc | Point-of-zero-charge |
| RhB | Rhodamine blue |
| SA | South Africa |
| SAED | Selected area electron diffraction |
| SC | Semiconductor |
| SEM | Scanning electron microscopy |
| SEs | Secondary electrons |
| SPR | Surface plasmon resonance |
| TEM | Transmission electron microscopy |
| UV | Ultraviolet |
| VBM | Valence band maximum |
| VB | Valence band |
| VOC | Volatile organic compound |
| WO | Wet oxidation |
| WWTPs | Wastewater treatment plants |
| XC | Exchange correlation |
| XRD | X-ray diffraction spectroscopy |
| XPS | X-ray photoelectron spectroscopy |

# CHAPTER 1
# INTRODUCTION

## 1.1 Problem statement

South African National Water Act (Act number 36 of 1998) stated that it recognises the necessity to guard the quality of water resources in order to ensure that the nation's water resources are sustainable in the interest of all water users.[1] However, due to agricultural, industrial, and domestic activities, water is polluted by a variety of pollutants such as suspended solids, metals, organic and inorganic substances. This water pollution has become a worldwide problem as the quality of water continues to deteriorate and thus leading to water-related diseases.[1–3] The availability of clean water for human needs has become a challenge and the scarcity of satisfactory sanitation prior to discharge of wastewater requires concepts for monitoring and implementation plans.[4]

Wastewater from textile industries has been classified as the most contaminating because of the large volumes they generate and the toxic components of the effluent.[5] During the dyeing process, a portion of the dye does not bind to the fabrics and is washed out. The released unfixed dyes contain high concentrations of toxic compounds, which are released into waste wastewater treatment plants (WWTP) or unlawfully released to surface waters. However, most WWTP in South Africa (SA) are not equipped to effectively treat the pollutants.[6,7] Removal of organic dyes using nanomaterials in conjunction with conventional treatment plants is thus of interest. As nanomaterials exhibit unique properties that will enable the removal of toxic pollutants even at low concentration, at which the current conventional processes fail.

This project aims to utilize doped $WO_3$ for the photodegradation of refractory organic dyes. This will be achieved by synthesizing and characterizing pristine and modified tungsten trioxide nanoparticles, which will then be applied for the photodegradation of organic dyes such as Congo red and Methylene blue.

## 1.2 Justification

Water pollution is a distinct facet of the overall water crisis and access to safe drinking water is basic human rights. South Africa is a water-stressed country and though it has built many dams, water resources within these dams are still susceptible to the presence of polluted effluent.[8] It is reported that the greater concern to the environment is pollution that is due to the textile effluent that has increased in recent years.[9]

Different types of dye are used in many industries such as textile, paint, ink, plastic and cosmetics. Synthetic dyes used in textile industries in the dyeing and printing processes, generate large quantities of toxic chemical compounds which remain in the wastewater from numerous stages of textile processing.[10] A significant amount of these dyes may collect in the soil, particularly in the areas near the textile processing industries. It is reported that when ingested, these organic dyes split into aromatic amines which cause cancer, and when released into the aquatic environment they disturb the natural growth of aquatic life by decreasing the dissolved oxygen capacity and by blocking sunlight.[11–13] Methylene blue (MB) and Congo red (CR) are some of the widely used dyes in textile industries. They have been reported as hazardous due to their recalcitrant nature under conventional wastewater treatment methods.[4] Wang et al.[14] reported that inhalation and ingestion of MB result in adverse effects including breathing difficulties, nausea, vomiting, profuse sweating, and mental confusion. Ventura-camargo & Marin-morales [15] reported CR to be a known human carcinogen.

The release of these organic dyes into water stream poses a serious concern to the environment, human and animal health and should be adequately treated before being discharged. The use of photocatalytic semiconductors for water decontamination has been widely reported as being effective for the degradation of a variety of organic pollutants. In this study, the focus is on fabricating modified nanostructured tungsten trioxide, which is known for its photocatalytic properties.

The outcome of this study will provide photocatalytic mechanisms that will degrade the organic dye components to non-toxic compounds.

## 1.3 Aim and objectives

The aim of the study was:

To synthesise and characterize the pristine and lanthanum modified tungsten trioxide ($WO_3$) nanoparticles for the photodegradation of organic dyes.

The objectives of the study were:

i. To synthesize pristine and lanthanum doped tungsten trioxide nanoparticles.
ii. To characterize pristine and lanthanum doped tungsten trioxide nanoparticles using XRD, Raman spectroscopy, SEM, TEM, BET, DRS and XPS.
iii. To monitor and measure the photodegradation efficiency of the synthesized tungsten trioxide nanoparticles on organic dyes using UV-vis spectroscopy and IC



## 1.4 Dissertation outlines

From this chapter the dissertation continues as outlined below:

**Chapter 2** outlines the literature review on water pollution, different types of pollution found in water. The study chapter further elaborates on dye pollution, classification of dye pollutants, and treatment of water pollution, advanced oxidation processes as well as heterocatalysis overview.

**Chapter 3** details the synthetic route, characterization techniques as well as the photodegradation activity of the prepared nanoparticles.

**Chapter 4** reports the results and discussions of the findings in **Chapter 3**.

**Chapter 5** summarises the key findings of the research work and further provides recommendations on addressing gaps this study could not cover.

**References** are listed at the end of each chapter.

## 1.5 References


1. Mahlambi, M. M., Ngila, C. J. & Mamba, B. B. Recent Developments in Environmental Photocatalytic Degradation of Organic Pollutants: The Case of Titanium Dioxide Nanoparticles - A Review. *J. Nanomater.* **2015,** 1-30 (2015).
2. Omole, D. O. & Ndambuki, J. M. Sustainable Living in Africa: Case of Water, Sanitation, Air Pollution and Energy. *Sustainability* **6,** 5187-5202 (2014).
3. Ebrahiem, E. E., Al-Maghrabi, M. N. & Mobarki, A. R. Removal of organic pollutants from industrial wastewater by applying photo-Fenton oxidation technology. *Arab. J. Chem.* **10,** S1674-S1679 (2017).
4. Lahkimi, A., Oturan, M. A., Oturan, N. & Chaouch, M. Removal of textile dyes from water by the electro-Fenton process. *Env. Chem Lett* **5,** 35-39 (2007).
5. Hettige, A. I. & Lanka, S. Reduction of Colour in Treated Wastewater from Textile Industry Using Sawdusts as Bio-sorbents. *Trop. Agric. Res.* **26,** 666-676 (2015).
6. Ghaly, A. E., Ananthashankar, R., Alhattab, M. & Ramakrishnan, V. V. Production, Characterization and Treatment of Textile Effluents: A Critical Review. *J Chem Eng Process Technol* **5,** 1-19 (2014).
7. Ogugbue, C. J. & Sawidis, T. Bioremediation and Detoxification of Synthetic Wastewater Containing Triarylmethane Dyes by Aeromonas hydrophila Isolated from Industrial Effluent. *Biotechnol. Res. Int.* **2011,** 1-11 (2011).
8. Sershen, Rodda, N., Stenstrom, T., Schmidt, S., Dent, M., Bux, F., Hanke, N., Buckley, C. & Fennemore, C. Water security in South Africa: perceptions on public expectations and municipal obligations, governance and water re-use. *Water SA* **42,** 456-465 (2016).
9. Carmen, Z. & Daniela, S. Textile Organic Dyes - Characteristics, Polluting Effects and Separation/Elimination Procedures from Industrial Effluents - A Critical Overview. *InTech* **2741,** 55-80 (2016).
10. Kehinde, F. & Aziz, H. A. Textile Waste Water and the advanced Oxidative Treatment Process, an Overview. *Int. J. Innov. Res. Sci. Eng. Technol.* **3,** 10-12 (2014).

11. Amini, M., Pourbadiei, B., Ruberu, T. P. A. & Woo, L. K. Catalytic activity of MnOx/$WO_3$ nanoparticles: Synthesis, structure characterization and oxidative degradation of methylene blue. *New J. Chem.* **38,** 1250-1255 (2014).
12. Senan, R. C. & Abraham, T. E. Bioremediation of Textile Azo Dyes by Aerobic Bacterial Consortium Aerobic Degradation of Selected Azo Dyes by Bacterial Consortium. *Biodegradation* **15,** 275-280 (2004).
13. Imran, M., Shaharoona, B., Crowley, D. E., Khalid, A., Hussain, S., & Arshad, M. The stability of textile azo dyes in soil and their impact on microbial phospholipid fatty acid profiles. *Ecotoxicol. Environ. Saf.* **120,** 163-168 (2015).
14. Wang, L., Zhang, J. & Wang, A. Fast removal of methylene blue from aqueous solution by adsorption onto chitosan-g-poly (acrylic acid)/attapulgite composite. *Desalination* **266,** 33-39 (2011).
15. Ventura-camargo, B. D. C. & Marin-morales, M. A. Azo Dyes: Characterization and Toxicity - A Review. *Text. Light Ind. Sci. Technol.* **2,** 85-103 (2013).

# CHAPTER 2
# LITERATURE REVIEW

## 2.1 Introduction

Underground waters in developed areas is normally inclined to severe contamination by various pollutants in the form of water pollution, air pollution and soil pollution.[1,2] Though it is reported that South Africa has ratified the Stockholm Convention, the production, import and use of POPs are banned. However, there are potential sources that are still present.[3] Persistent Organic Pollutants (POP's) comprise a variety of organic pollutants characterized by high toxicity, bioaccumulation, and ability to persist through long-range transport. It is reported that POPs produced and used in industrial centres, urban centres and agricultural areas are the primary source of environmental pollution.[4]

Over the past few decades, air pollution has been identified as a major problem globally as it has been recognized that this fine particulate matter has contributions to diseases such as cardiovascular and respiratory symptoms.[5] On the other hand, the soil has been reported as an important reservoir for POPs even after their phase-out for many years. POPs residues in soil have been associated with the contamination of food, groundwater which poses a serious threat to human health and the environment.[4] Textile dyeing processes and agricultural activities use water excessively and discharge the contaminated water. The dyes are able to resist light, biological wastewater treatments, and other degradative environmental conditions because of the complexity of their aromatic structures.[6,7] Since these POPs resist degradation and bioaccumulate, they migrate through the atmosphere and waterways for thousands of kilometres from their source, accumulating in terrestrials and aquatic ecosystems.[4]

Traditional methods that have been employed for the removal of organic dyes include coagulation, membranes and adsorption.[8] However, these existing technologies were

reported to be unable to eliminate harmful materials without generating potentially dangerous by-products.[9] For this reason, advanced oxidation methods have been applied in the removal of organic pollutants, these methods employed the combination of powerful oxidizing agents with UV or near-UV light.[10]

## 2.2 Water pollution

Drinking water can be provided by different water sources such as oceans, wells, rainwater, lakes and rivers. The challenges arise due to the diversity of the concentration of the common inorganic and organic pollutants, and trace amounts of disinfectant by-products.[11] Water Pollution as described in National Water Act is the direct or indirect modification of the physical, biological and, chemical properties of a water resource making it undesirable for any beneficial use, harmful to human beings and aquatic organisms, and affecting other legitimate uses of water.[12]

Water sustains life and hence the need to preserve and protect it from pollution. Wastewater contaminants may include organic, inorganic, and diverse trace contaminants from pesticides, pharmaceuticals and personal care products. In addition, industrial wastewater may encompass organic compounds and heavy metals.[13] The consistent effects of disposal of human waste, water quality, health status, and transmission of disease via the faecal-oral route have been reported.[14]

Water wastage resulting from industries is a worldwide problem. It is common knowledge that resources of freshwater are scarce, hence the need to govern them. The accessibility of freshwater for different human requirements for the years to come appears to turn into a challenge.[7] The weakening of water quality is a genuine concern and prompts an expansion in treatment costs. Another outcome of water contamination is its inevitable effect on wellbeing. Many diseases affecting humans such as diarrhoea, cholera and other bacterial diseases are triggered and kept up by terrible water quality. Contaminated water may likewise affect food quality through the growth of microorganisms in harvests. The build-up of metals and substances that disturb the

endocrine systems present in the water could adjust the organic qualities of crops, making them increasingly hard to be well-maintained and compromising their capacity to adjust to fluctuating climatic conditions.[15]

Increasing industrialization and urbanization has been related to environmental pollution. Various industries discharge toxic effluents, which influence water assets, soil affinity, aquatic life forms and the integrity of the ecosystem. Flooded agribusiness is caught in this discussion, among different reasons, as a result of its contribution to contamination of groundwater over the leakages that result in the pollution of surface water through their runoff.[16] Nowadays, the synthetic dye industries have achieved a critical spot in the improvement of the general public because it supplies its produces to a great diversity of industries.[17] Industries including printing, textile, cosmetics and leather are accounted for to utilize dyes to tint their final product. They also consume significant amounts of water and thus produce a substantial amount of colour-tinted wastewater. Dye contaminated water is extremely hard to treat because the dyes are recalcitrant organic molecules, are stable to light and resist aerobic digestion.[18]



### 2.2.1 Inorganic pollutants

Water polluted by heavy metals adds to the economic concerns due to their intense toxicity to human wellbeing and biological frameworks. In general, heavy metals are reported to be foundational poisons that affect the kidneys, destruct the nerve tissue, and disturb physiological development. Inorganic contaminants are found in water, wastewaters, and industrial effluents including mining, tanning etc. and may include Cadmium (Cd), Nickel (Ni), Copper (Cu), Chromium (Cr), Zinc (Zn), and Lead (Pb).[19,20] South African mines contribute to the economy. However, mining effluents have been reported to detriment the quality of land-dwelling and aquatic ecosystems due to the generation of acid mine drainage (AMD). It is reported that Johannesburg generates 360 mL/d from gold mines, which is discharged onto the nearby aquatic ecosystem and

fast-tracking the degradation of waterbodies downstream. This acid advances weathering and leaching of toxic elements.[21]

Tanning Industry is considered one of the main sources of pollution. Its waste in the aquatic system is characteristic of a complex mixture including inorganic pollutants such as hexavalent chromium. Hexavalent Chromium is reported to be one of the inorganic pollutants from the tannery waste, its use in leather production is to bind with the insoluble fibrous protein to convert to leather, a process that forms a crucial step of intervention in pollution control.[22] Hexavalent Chromium in this form has proven to be of the greatest occupational and environmental health concern. It does not form insoluble precipitates in aqueous solutions, making through an immediate precipitation technique not practical. It has been reported that it can enter the body through food, drinking water and inhaled air. Infection is evidenced by a runny nose, sneezing, nosebleeds, and ulcers. Ingestion can cause kidney and liver damage, nausea, and death.[22,23]

### 2.2.2 Microbial pollutants

Microbial pollution originates from agricultural activities in our country such as plants (fields, runoff water from fields, fertilisation), animal production, faecal nature related to humans (sewage treatment systems), agrarian wastewater and wastewater from the processing industry runoff into streams or lakes. Some microbial populations can increase in drinking water distribution systems.[24,25] In fertilization, pollution is reported to be related to agricultural nitrogen enrichment which is important for growth and yields. However, the excess of nitrogen can lead to increased pollution of rivers and ground waters.[26]

Microbial pollution resulting from animal production (pasture, farms), contaminate ground and surface water resources with microorganisms such as viruses, bacteria, and parasites. Whereas pollution from faecal nature related to humans results from releases

of water treatment plants, disinfecting stations, medical clinics, and wastewater from the processing industry runoff into streams or lakes. The current disinfection practices and rules as far as chlorine residuals have been accounted for to be incapable for the eradication of faecal pollution indicators and pathogens since large amounts of these organisms could, in any case, be identified in the final effluent, bringing about the deterioration of the quality of receiving water bodies. Microbial pollution is in this manner a source of impairment of the compliance of supply for small scale to private water supplies.[25,27]

### 2.2.3 Organic pollutants

Organic pollution starts from different industries including the industrialization, agricultural activities, municipal wastewater, other ecological and worldwide changes. These pollutants are unsafe and harmful to the environment.[28] There are different types of organic pollutants which have been found in various water bodies. They include fertilizers, hydrocarbons, oils, pesticides, plasticizers, biphenyls, pharmaceuticals. These compounds mostly encompass a large number of organic materials that are challenging to degrade.[29]



Organic pollutants that have been found to taint water assets have been connected to different symptoms and embryotoxicity, mutagenicity, teratogenicity, and cancer-causing nature just as wellbeing issue to individuals.[28–30] Organic dyes are intended to have a more prominent liking for the substrate than the medium from which it is applied and also a high level of stability to washing off when exposed to sunlight, microbial attack and when washed with chemicals. Subsequently, the current conventional wastewater treatment methods including adsorption, flocculation, and biological degradation are typically ineffective.[31,32]

## 2.3 Dye pollution

The use of synthetic chemical dyes has expanded impressively in the course of the most recent couple of years in different industrial processes such as paper and pulp manufacturing, colouring of material, leather treatment, plastics.[33] The textile industry is critical in light of the fact that its materials are utilized in varying ways including clothes for wearing. Dyes and colours are known to have a long history. It is accounted for that natural plants as well as insect sources were at first utilized by the dye industry and thereafter turned to synthetic dyes. Synthetic dyes normally consist of aromatic rings, methoxy, methyl, nitro or sulfo group. Their use and manufacture of synthetic dyes have continued due to their ease and simplicity of synthesis.[6,34]

However, textile industries use substantial amounts of chemicals and water during their textiles wet processing stage. These chemicals, running from inorganic to polymers and organic products are utilized for scouring, desiring, dyeing, bleaching and printing.[33] The textile industry devours a significant quantity of water in its manufacturing processes, largely in the dyeing and finishing stages. Amid the colouration stage, a large percentage of the synthetic dye that does not bind to the material is lost to the wastewater stream. In cotton textiles production, cotton fibres separated from the cottonseeds and then spun into cotton yarns. Thereafter the yarns are meshed effectively into fabrics which then undergo numerous wet processing stages including dyeing. The final step in manufacturing is the finishing, this step uses chemicals to treat the cloths for obtaining a better quality.[30]

The wastewater released from textile plants is delegated the most polluting when compared to other industrial divisions, mainly due to the volume produced together with the composition of the effluent. It is reported that 10,000 diverse textile dyes with yearly generation of 7.105 metric tons are available commercially around the world. More than 1000 tons of about 30% of the dyes are utilized on a yearly basis. Furthermore, only

about 100 tons or less of the 90% of the textile products are utilized every year.[35] Most of these dyes can by-pass the conventional methods of wastewater treatment and proceed in the environment because they are stable towards the light, water, temperature, chemicals and soap. Moreover, an increase in colour fastness and the resistance of dyes to degradation have made them increasingly obstinate to biodegradation.[32]

## 2.4 Classification of Dyes

There are three main categories used to classify textile industries namely: cellulose, synthetic and protein fibres. The sort of dyes and chemicals used in this industry are found to contrast depending on the textures fabricated. These dyes display structural diversity and depending on the surface charge, they can be grouped into anionic dyes such as direct dyes, reactive dyes and acid dyes, the cationic dyes such as basic dyes and the non-ionic disperse dyes.[6,30] Examples of anionic dyes are depicted in **Figure 2.1**.



Naphthol dyes, direct dyes, reactive dyes and indigo dyes are a portion of the anionic dyes used to colour cellulose fibres which are sourced from plants such as linen, lyocell, cotton, ramie, rayon, and hemp.[30] Basic and reactive dyes are widely utilized in textile industries on account of their bright colour which is their favourable characteristics. Furthermore, they are e are effectively water-soluble, less expensive to create, and simpler to apply to fabric.[36] Reactive dyes show a wide scope of diverse chemical structures comprising functional groups like azo, phthalocyanine, anthraquinone, formazin, and oxazine as a chromophore. Wastewater treatment has for the most part centred on the use of reactive dyes in dyeing cotton fibres. This makes up about a portion of the world's fibre intake. A large segment of the applied reactive dyes is reported to be released into wastewater because of the process of hydrolysis in an alkaline dye bath that passes through. Traditional wastewater treatment plants have

limited removal efficiency towards these reactive and anionic dyes, and this has led to colour-tinted waterways.[36]

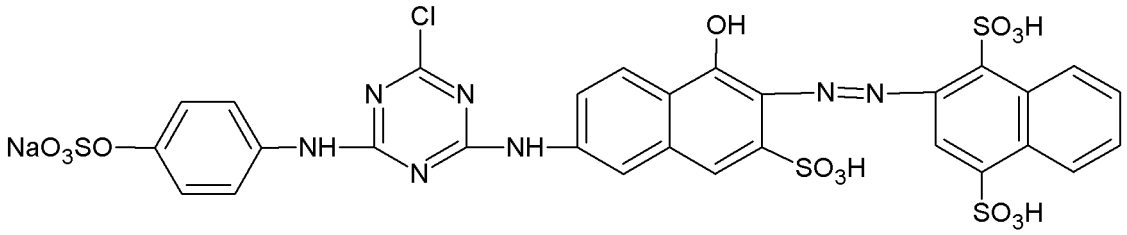


C. I. Reactive Orange 122, RO122.[37]

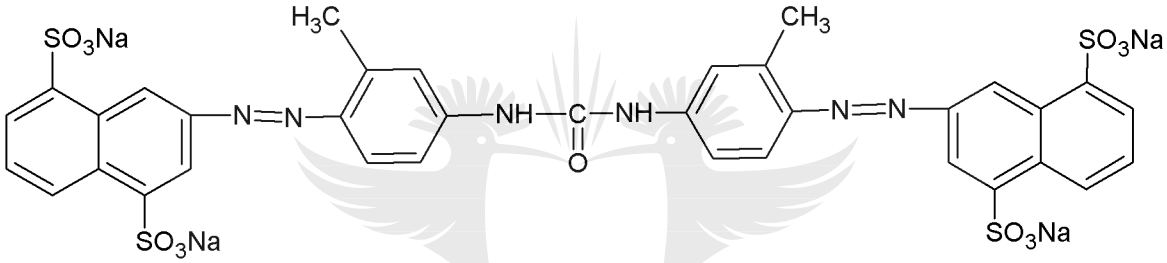


C.I. Direct Yellow 50 (DY).[38]

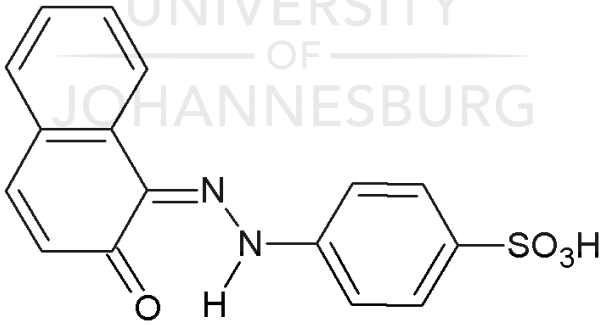


C.I. Acid orange 7.[39]

**Figure 2. 1:** Examples of anionic dyes

Direct dyes are quite large molecules with high attraction specifically for fibre. They are used in dyeing cotton, rayon, linen, ramie, hemp and lyocell. They do not form strong

with the fibre molecules from which they are applied. These weak bonds result in them having a poor quick drying property after their application on fabrics and thus require elevated temperatures of 79.4-93.3 °C for the application. Congo red is one of the direct diazo dye frequently utilized in the paper industry. It is a refractory and a notable carcinogen owing to the aromatic amine group in the structure. Acid dyes and Lanaset dyes are utilized in dyeing protein fibres sourced from animals such as wool, mohair, angora, and silk.[6,30] Anionic dyes have been reported to cause severe organic and colour pollution in the water. They display a variety of chemical structures containing azo anthraquinone, phthalocyanine, and showcase toxic effects and can thus be mutagenic and carcinogenic to both human beings and aquatic life.[28,30]

Other different dyes, such as basic dyes, and dispersed dyes are used in dying synthetic fibres like nylon, polyester, acetate, spandex, acrylic and polypropylene.[6,28,30] Cationic basic dyes are soluble in water, their chemical backbone comprises of azo, anthraquinone, methane, thiazine, and triarylmethane, with applications in modified nylon, acrylic, papers, and polyesters. Some of them have biological activities which are used in medicine as antiseptics.[30] Basic dyes are cationic in nature and are utilized in dyeing acid-group-containing fibres, typically synthetic fibres. When basic dyes are dissolved in water they form a coloured cationic salt which reacts with the anionic surface of the substrate. They were discovered to be powerful colouring agent when used on acrylic fibre. Crystal violet and brilliant green which form part of the Basic dyes, are known potent clastogens, and are found to be most acutely toxic and may advance tumour growth in certain types of fishes especially dyes with a triphenylmethane structure.[6]

The major non-ionic dyes are disperse dyes, which do not ionise in the aqueous atmosphere. Disperse dyes utilized in dyeing synthetic fibres are generally sparingly water-soluble compounds, yet they can be found in the water section, because of their commercial formulation. Some disperse dyestuffs have been found to cause allergic

reactions such as eczema or contact dermatitis and their presence in the aquatic systems were connected to the observed mutagenic activity of the water and sediments.[6,35,40]

## 2.5 Treatment of water pollution

Dye bearing effluents from industries are problematic to the environment unless adequately treated before being discharged. Dyes are designed with complex aromatic structures that have a strong affinity for the substrate and less affinity for the medium from which they are applied. They are highly stable and do not fade when exposed to water and sunlight. Furthermore, they are able to resist biological activities, ozone and most degradative environmental conditions. There are several processes such as primary, secondary and tertiary processes that have been utilized in the treatment of wastewater effluents. These processes include chemical coagulation, aerobic activated sludge, flocculation, sedimentation and reverse osmosis.[41,42]

These conventional treatment methods take a very long time for the degradation of organic pollutants to complete and also implementing them for the small-scale applications is extremely difficult. In these methods, large amounts of secondary pollutants are produced and released into the environment. These secondary pollutants include poisonous gases and odours. Organic pollutants treated through biological methods produce large amounts of sludge after treatment of wastewater.[43] **Figure 2.2** illustrates the differences between conventional and photocatalysis wastewater treatment methods.

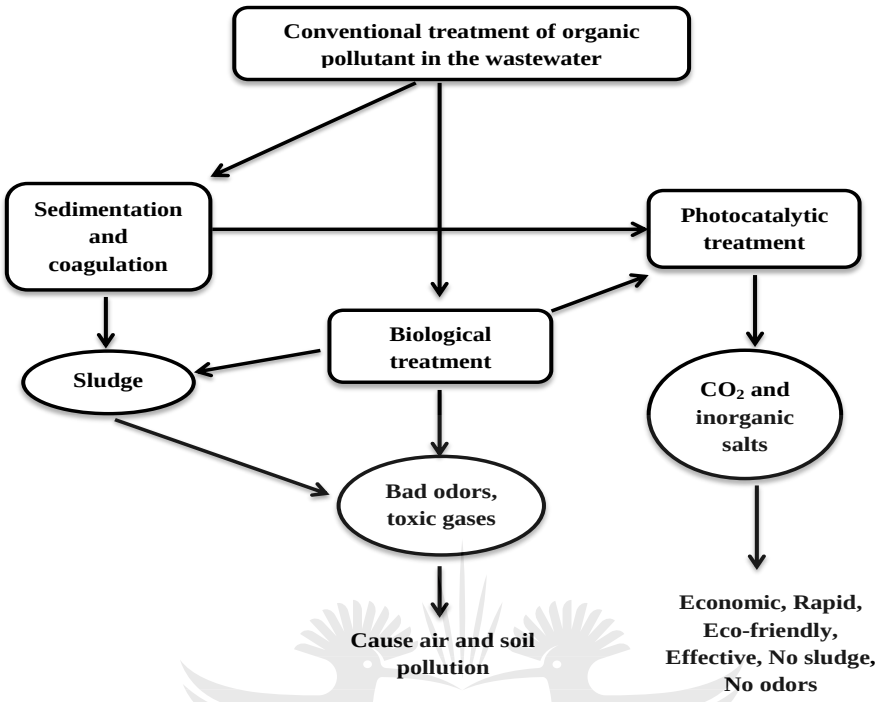


**Figure 2. 2:** Schematic diagram illustrating the differences between conventional and photocatalysis waste water treatment.[43]



However, these treatment methods have been found to be ineffective against the elimination of all types of dyes and other chemicals that are used in the industry.[30] The technologies that are used in wastewater treatment can be classified into three categories. The first one is a non-destructive procedure, which is grounded on physical adsorption, removal, stripping processes. The second is a biological destructive process, which is based on active mud process. Lastly, the oxidative destructive procedure centred around oxidative chemical procedure such as wet oxidation (WO) functioning at high temperature and pressure, then liquid oxidation (LO). Liquid oxidation procedures are advanced oxidation processes (AOPs), which operate at temperature and pressure conditions using oxidative agents $O_3$, $O_2$, $H_2O_2$, catalysts and/ or UV radiations.[44] The wastewater treatment methods can be classified into three categories: physical methods including membrane filtration, adsorption, and

coagulation/flocculation, chemical methods such as photocatalytic oxidation, chemical oxidation, Fenton reagent and electrolysis, then lastly is the biological methods such as biosorption and enzymatic degradation.[6]

### 2.5.1 Conventional methods

Effluents released from the textile industries go through several physical and chemical methods of treatment including chemical coagulation, precipitation, flocculation, photooxidation, reverse osmosis, ozonation, ion exchange, adsorption, and membrane filtration to remove pollutants such as nitrogen, organics, phosphorus and metals.[6,30] These conventional treatment methods have been less effective in completely degrading the pollutants found in the municipal wastewater. Some conventional technologies include adsorption, coagulation, flocculation, precipitation, electrochemical reduction, biosorption and enzyme degradation treatment.[6,45]

It is reported that most of these conventional water treatment methods are not designed to remove small quantities of organic pollutants and as a result, high amounts of these pollutants and their metabolites find their way into the aquatic surroundings.[46,47] The major shortcoming of conventional methods is high operating costs, they have limited versatility, low efficiency, they require specialized equipment, they might incur interference from other wastewater elements, and the process of handling the generated waste. It is reported that these methods may be successful in removing the colour, however, are ineffective in the complete degradation of the dye molecules. In this way, the dyes become concentrated and demanding proper disposal methods.[48] Hence, the use of photocatalytic methods as pre-treatment steps preceding the conventional water treatment is of importance and has attracted the attention of researchers.[48]

#### 2.5.1.1 Biological methods

Biological wastewater treatment may take place by means of biodegradation by the cells or through biosorption on the microbial biomass. In biosorption, the dye is entrapment in the framework of the adsorbent without obliteration of the pollutant.[47] Biological methods involve the use of the by-product of industrial fermentations which have various functional groups on the fungal cell wall such as carboxyl, amino, phosphate and thiol groups. It is reported that these groups can fix dye particles onto the surface of fungal cells. This process is quick and can reach completion in a few hours. Numerous process parameters are reported to affect the dye biosorption process. These parameters include pH, dye concentration, temperature and nature of dye in the solution.[6] Whereas biodegradation is depicted as the complete breakdown of organic molecules into harmless products such as carbon dioxide, water and/or inorganic products. This breakdown is facilitated by the activity of biological enzymes.[6,47] Biological methods are broadly functional for the management of residual wastewater and it has a need for long residence time so that the microorganisms can degrade pollutants and it's not applicable to tread the toxic pollutants due to biomass poisoning.[49]



Biological methods are cost-effective, higher efficiency and less secondary pollution and are frequently the economical alternatives in comparison with other physical and chemical processes. However, in this method, there are toxic heavy metals in the runoff which influence the development of microorganism, also the vast majority of the dyes used are a non-biodegradable in nature, thirdly the method requires a long time for treating the effluent.[30] They require a large-scale commercial application. The adsorption process may be influenced by biosorbents having numerous functional groups and intricate adsorption mechanisms. The biosorbents lack the selectivity hence the recovery of sorbate and the production of biosorbents could be difficult. These methods are unsatisfactory in colour elimination with current biodegradation processes. The discarding of biomaterials polluted with toxic organic ions frequently poses public

and environmental hazards, particularly in emerging countries, where incinerators and engineered landfills are lacking.[47,50]

### 2.5.1.2 Physical methods

Physical methods comprise of adsorption on activated carbon, coagulation/flocculation, peat, fly ash, coal, wood, membrane-filtration procedures and sorption techniques.[51] Adsorption occurs when the substances accumulate at the surface or interface. In water treatment, the procedure takes place at an interface between the solid adsorbent and polluted water. The adsorbed pollutants are called adsorbates whereas the adsorbing phase is called adsorbent.[29]

Adsorption is considered an effective method for removal of colour from dye wastewater since it is dependence on the type and the molecular structure of the dye, as well as the position and the number of substituents in the dye molecule. In this way, there may be interactions between the dyes and the active groups on the surface of the cell via adsorption process in which it is widely acknowledged that the mechanism of ion-exchange is involved in the selectivity and the efficiency of adsorption by microbial biomass.[6] The advantages of the adsorption method of wastewater treatment are its worldwide nature, less expensive and easy to operate. It has the capacity to eliminate soluble and insoluble organic compounds with the removal of up to 99.9%. Physical methods using activated bentonites and powdered activated carbon have been reported to generate large amounts of sludge and their use has thus been limited due to is low treatment efficiency toward specific dyes. Their effectiveness is observed only when the effluent volume treated is small. Furthermore, it is a big challenge to dispose of the solid adsorbent.[33,48,51]

In biocoagulation method, the extracellular polymers comprise of surface functional groups. These functional groups improve the sorption the dye pollutants onto the

polymer surface and settle throughout the process of dye removal. Processes that have been used intensively include coagulation, flocculation, and precipitation for the pre-treatment of raw wastewater before releasing to wastewater treatment plants. These processes have been reported to be satisfactory in reducing COD and partial decolourization. However, it has been found that alone they are ineffective in treating textile/dye waste.[6]

#### 2.5.1.3 Chemical methods

Chemical treatment techniques involve oxidation process using oxidizing agents such as sodium hypochlorite, Fenton's reagent, photochemical, ozone and electrochemical degradation. They also consist of precipitation and flocculation or coagulation in combination with floatation and filtration. Dye removal using ozone is reported to be effective and much quicker. However, it does not provide satisfactory results, particularly for some dispersed dyes.[33] These methods remove the dyes completely however they are expensive. Furthermore, it becomes a challenge to dispose of concentrated sludge that has buildup. Some methods are is not suitable for all type of dyes.[48,51]



### 2.5.2 Advanced oxidation processes

Advanced oxidation processes (AOPs) refers explicitly to processes whereby organic pollutants are primarily oxidized through interactions with hydroxyl radicals ($OH^-$). AOPs were development in the 1990s and comprise a variety of methods for producing $OH^-$ and other reactive oxygen species such as hydrogen peroxide ($H_2O_2$), superoxide anion radical ($O_2^{\bullet -}$) and singlet oxygen ($O_2$).[52–54] the attention that photocatalysis has attracted arises from the unique route it takes to effectively achieve better mineralization of organic contaminants to less harmful products under light irradiation.[53] This process is directed by the desired flow rate, the target effluent contaminant concentration, and the pH of the background water.[52]

AOPs are broadly utilized in removing organic pollutants that are difficult to remove by conventional methods, thereby providing remediation for wastewater because of their ability to completely degrade different types of pollutants. The AOP technology is capable of removing persistent organic pollutants and microorganisms present in water even at low concentration levels. The generated free radicals in AOP process were observed to degrade pollutants that are not easily degraded by conventional oxidation methods. This technology is being researched and applied worldwide especially in developing nations.[30,53,54] Water systems rooted in urban areas are typically predisposed to severe pollution a collection of pollutants including organic and inorganic pollutants.[44]

These processes are based on the production of highly oxidizing agents, such as hydroxyl radicals with high oxidation potential (E°=+2.72 V vs. NHE). They can oxidize organic pollutants present in the environment to produce harmless by-products such as $H_2O$ and $CO_2$). Hence, they are deemed environmentally friendly.[30,43] The processes are based on different classes including photocatalysis, AOPs based on ozone, AOPs based on $H_2O_2$, AOP "hot" technologies based on ultrasound, oxidation with an electron beam, electrochemical oxidation process.[44]



### 2.5.2.1 Advanced oxidation process based on Ozone

Ozonation encompasses an important coadjutant process for treating different effluents that are highly loaded with recalcitrant pollutants. The discolouration process via ozonation is a speedy one that takes place in both alkaline and acid medium. This behaviour can be ascribed to the electrophilic nature of the ozonation process, whereby the reaction with the azo groups in the pollutants is facilitated through the direct attack by $O_3$ molecules and the indirect attack of $HO^{\bullet}$ radicals.[37] But this process of cleaving the conjugated double bonds frequently results of the formation of poisonous products. However, extended ozonation can eradicate toxic products.[51] The electron affinity of $O_3$ which is at 2.1 eV is much higher as compared to that of $O_2$ at 0.44 eV, therefore

addition of $O_3$ in pure $O_2$ or in air could be a means of enhancing the scavenging of the photo-promoted electrons from the VB into the CB, either directly as illustrated in **Equation (2.1) and (2.2)**.

$$e^- + O_3 = O^{\bullet -} + O_2 \quad \textbf{(2.1)}$$

or indirectly

$$O_2^{\bullet -} + O_3 \rightarrow O_2 + O_3^{\bullet -} \quad \textbf{(2.2)}$$

The radical anion $O_3^{\bullet -}$ is more unstable than $O_3$ and can probably split effortlessly at the surface: according to **Equation 2.3**. It may also react with adsorbed water as illustrated in **Equation 2.4**.

$$O_3^{\bullet -} \rightarrow O^{\bullet -} + O_2 \quad \textbf{(2.3)}$$

$$O_3^{\bullet -} + H_2O \rightarrow OH^{\bullet} + OH^- + O_2 \quad \textbf{(2.4)}$$



An increased scavenging rate of photogenerated $e^-$ due to the ozone process should reduce the recombination rate of $e^-$ and $h^+$. However, $O_3$ can also scavenge hydroxyl radicals thereby restraining the favourable effect.[53]

### 2.5.2.2 Advanced oxidation process based on Hydrogen peroxide

Included in AOPs are Fenton, Fenton-like, $H_2O_2$ /UV, and photo-Fenton reactions (UV/$H_2O_2$/$Fe_2$+ or $Fe^{3+}$). In 1894, Fenton discovered that hydroxyl radicals could be generated by mixing $H_2O_2$ and ferrous iron, hence the name Fenton's reagent.[55] These are effective alternatives to remove textile industrial dyes, due to the ability to completely discolour and partially mineralize them, in relatively short reaction times. In

Fenton reaction, the ferrous iron ($Fe^{2+}$) starts and catalyzes the breakdown of $H_2O_2$, which result in the production of hydroxyl radicals. The production of these radicals occurs in a sequential complex reaction in an aqueous solution.[55] In this process, the initial $Fe^{2+}$ ions are consumed as the oxidation of the dye occurs, then the rate of oxidation is dependent on the rate of dissolution of $Fe^0$. The dye oxidation mechanism in the $H_2O_2/Fe^0$ system is illustrated in **Equations (2.5)** and **(2.6)**.[56,57]

$$Fe^0 \rightarrow Fe^{2+} \quad \textbf{(2.5)}$$

$$Fe^{2+} + H_2O_2 \rightarrow OH^{\bullet} + Fe^{3+} + OH^- \quad \textbf{(2.6)}$$

$$OH^- + Dye \rightarrow Oxidized\ dye + H_2O \quad \textbf{(2.7)}$$

In the photo-Fenton process, an extra number of $HO^{\bullet}$ is created each through direct $H_2O_2$ photolysis as well as by UV radiations interaction with the ion species that are present in aqueous solutions. The mechanisms are illustrated in **Equations (2.8)-(2.10)**.

$$H_2O_2 + UV \rightarrow 2HO \quad \textbf{(2.8)}$$

$$Fe^{3+} + H_2O + UV \rightarrow Fe^{2+} + H^+ + H^{\bullet} \quad \textbf{(2.9)}$$

$$[Fe(OH)]^{2+} + UV \rightarrow Fe^{2+} + HO^{\bullet} \quad \textbf{(2.10)}$$

The effectiveness of the oxidation method is determined by the organic compound structures, $H_2O_2$ and the concentrations of the catalyst, the wavelength and UV radiation intensities, the initial pH of the solution and the duration of the reaction.[44] The drawbacks of traditional Fenton reaction include low efficiency in utilizing $H_2O_2$, narrow working pH (pH <3.0) range, excessive loss of iron ions and generation of solid sludge and challenges in recycling catalysts.[58]

#### 2.5.2.3 Advanced oxidation process based on Photolysis

Heterogeneous photocatalysis is defined as the acceleration of a photoreaction within the sight of a catalyst. It is a green innovation technology with the distinctive benefits of operating at room temperature and usage of fresh, sustainable solar light as the propulsion. It is effective for other reactions, for example, organic transformations, reduction of carbon dioxide and photocatalytic water splitting. Furthermore, a variety of alternative photoactive organic species and photocatalytic semiconductors can apply to these photocatalytic reactions.[53,54] The interest in photocatalytic processes is on the utilization of photocatalytic semiconductors for the abatement of both organic and inorganic species present in effluents as a result of cleaning up the environmental, treatment of drinking water. This photocatalysis application in drinking water, as well as wastewater treatment, has been well recognized as a technique that transforms toxic organic pollutants into harmless mineral acids, $CO_2$ and water.[44,54]

The photocatalysis process is illustrated in **Figure 2.3**. At the point when a semiconductor absorbs an ultraviolet photon that has energy that is equivalent to or exceeds its band gap, electrons may be ejected from the VB to the CB ($e_{cb}$), leaving behind an electron vacancy known as ‘‘hole’’ in the VB ($h_{vb}^{+}$). These electrons and holes then relocate to the surface of the catalyst and take part in redox reactions.[8,59].

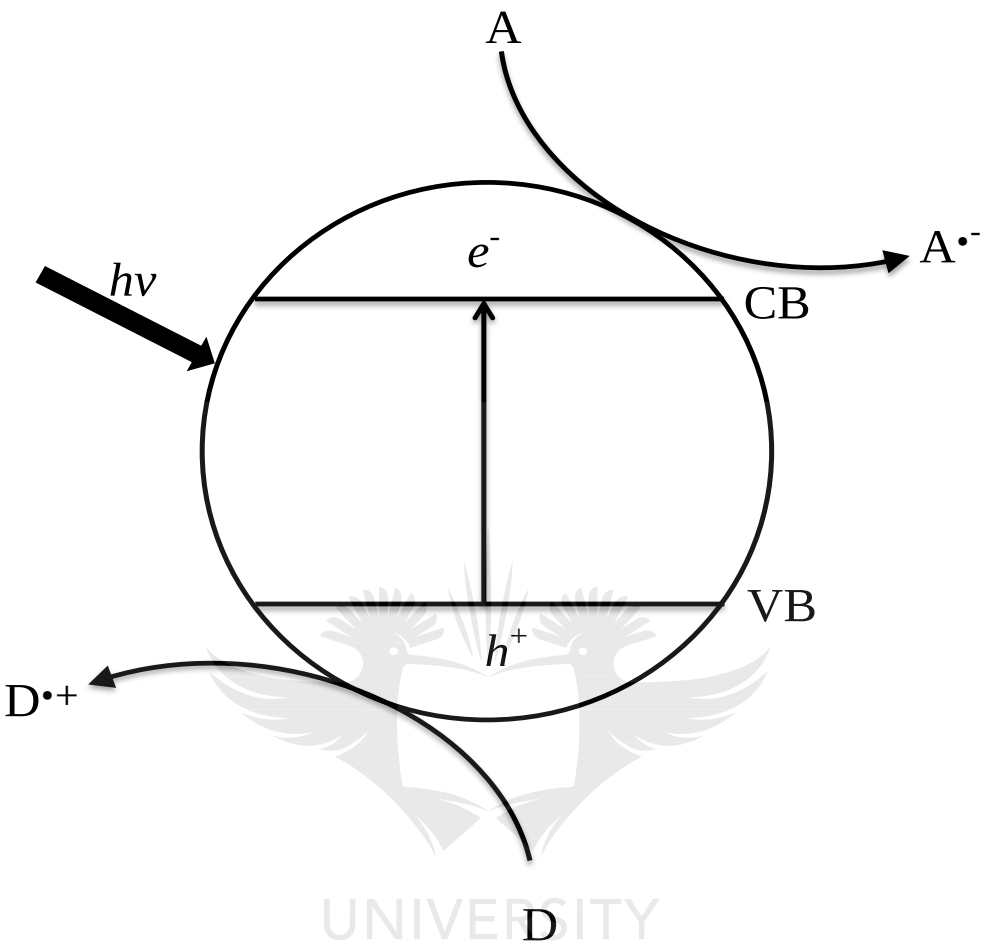




**Figure 2. 3:** Schematic illustrating electron/hole pair generation at semiconductor particle, D- electron donor; A- electron acceptor.[41]

In the VB, the oxidation may take place either as a result of indirect oxidation by means of reaction with the hydroxyl radical (•OH) that are bound on the surface or by direct attachment of $h^+$ on the metal surfaces, before it is trapped inside the particle or at its surface.[58]

$$h^+ + H_2O_{ads} \rightarrow {}^{\bullet}OH_{ads} + h^+ \quad \textbf{(2.11)}$$

$$h^+ + HO^-_{ads} \rightarrow {}^{\bullet} OH_{ads} \quad \textbf{(2.12)}$$

$$h^+ + M_{ads}{}^{n+} \rightarrow \cdot M_{ads}{}^{(n+1)+} \quad \textbf{(2.13)}$$

Furthermore, the photogenerated electrons may also react with adsorbed oxygen as illustrated in **Equation (2.14) to (2.19)**, to form superoxide radical ions ($O2^{\bullet -}$) in order to avoid build-up of excess charges within the particles of the catalyst and thus lead to electron/hole recombination. These species are strongly oxidizing and can mineralize organic pollutants as indicated below.[58]

$$O_2 + e^- \rightarrow O_2^{\bullet -} \quad \textbf{(2.14)}$$

$$O_2^{\bullet -} + h^+ \rightarrow HO_2^{\bullet} \quad \textbf{(2.15)}$$

$$2\,HO_2^{\bullet -} \rightarrow H_2O_2 \quad \textbf{(2.16)}$$

$$H_2O_2 + hv \rightarrow {}^{\bullet}OH \quad \textbf{(2.17)}$$

$$H_2O_2 + O_2^- \rightarrow {}^{\bullet}OH + {}^-OH + O_2 \quad \textbf{(2.18)}$$

$$H_2O_2 + e^- \rightarrow {}^{\bullet}OH + {}^-OH \quad \textbf{(2.19)}$$



## 2.6 Photocatalysis overview

The usage of photocatalytic semiconductors as a method of degrading organic and inorganic pollutants is currently drawing in a great deal of attention. Photocatalysis processes can be utilized to completely degrade and mineralize dyes and chemicals to $CO_2$ and $H_2O$ and are additionally useful in the degradation of stable compounds which are recalcitrant under other processes. They are relatively cheap and also able to function efficiently at ambient temperature and pressure conditions, requiring no special supply of oxygen.[58] Earlier studies have demonstrated that $TiO_2$ and oxygen can completely photomineralized a large scope of organic compounds including alkanes, fungicides, insecticides, pesticides, and aromatics.[60]

Metal oxide semiconductors are reported to be very efficient photocatalysts and have been widely researched. However, a number of metal oxides have a wide band gap, and that has restricted their visible-light absorption capacity. For example, $TiO_2$, as a standout amongst the most regularly considered photocatalysts can only absorb the UV portion at a wavelength lower than 388 nm, which covers just 4-6% of the solar radiation because of its wide band gap that is reported to be 3.2 eV and shows low quantum yield. The other disadvantage is the rapid recombination of photogenerated $e^-/h^+$ pairs, which diminish the efficiency of photocatalytic reactions quite significantly. Moreover, they are not suitable for recycling.[41,61]

The semiconducting particle works simultaneously throughout the lifetime of charge separation. It works as an oxidizing agent by catching electrons found on the substrate and putting them at the positive holes and as a reducing agent by transporting electrons to substrates. This reduction and oxidation in the photocatalytic procedure have to occur simultaneously. If the redox reaction does not occur at the same rate, there will be an accumulation of electrons in the conduction band which will result in electron/ hole pair recombination as illustrated in **Figure 2.4**. The state of charge separation can be affected through different pathways, such as charge recombination of photogenerated $e^-$ or $h^+$ in the similar occasion of photon absorption and by charge recombination after unsystematic migration of $e^-$ or $h^+$ through the material.[53]

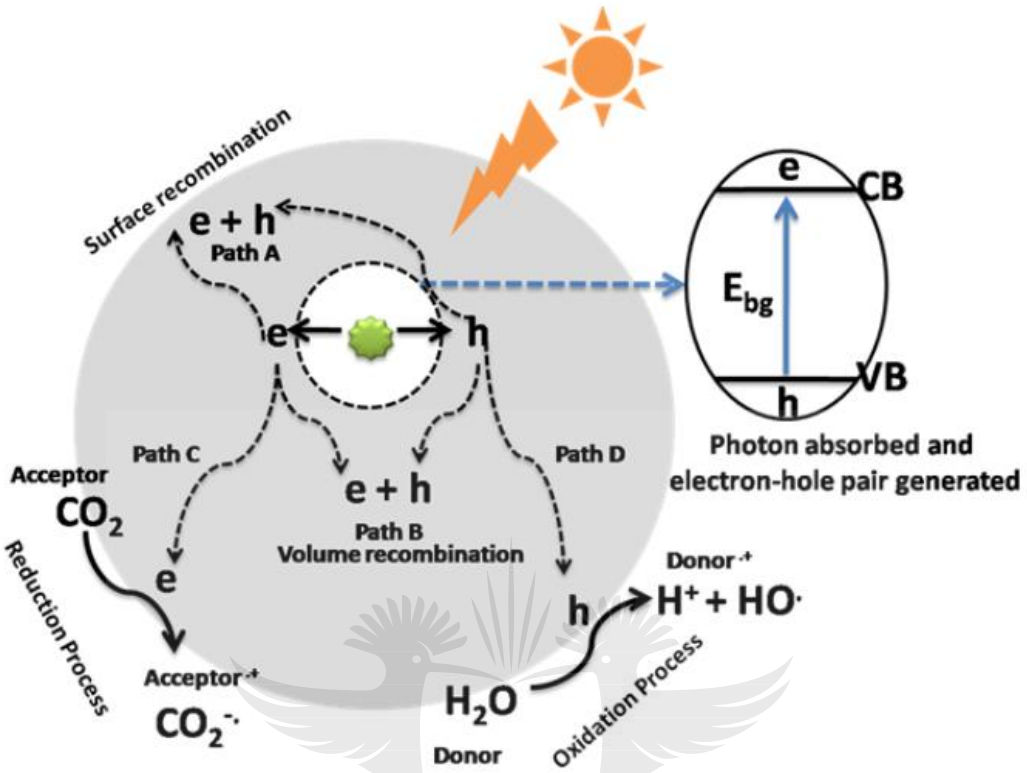


**Figure 2. 4:** Schematic diagram showing the typical photocatalysis process.[62]



To significantly reduce the recombination rate of the photogenerated electrons and holes, the charge-carrier species may be separated through the addition of appropriate scavenger or addition of trap sites on the surface in order to produce defects, surface adsorbents, or different sites. Modification methods used to improve the performance of the catalyst comprised of heterojunction structural development, ion-doping, morphological control and noble metal deposition.[58] The differences in corresponding conduction and valence bands energy levels between the dopants and the catalyst, resulting in the increase in the photocatalytic efficiency as charge separation is increased which allows absorption not only in UV but also visible light range.[61,63,64]

Numerous visible-light absorbing photocatalysts have been effectively pursued in recent years.[65] A diversity of photocatalytic semiconductors including $TiO_2$, ZnO, CdS, $SnO_2$,

$Ag_3PO_4$, $FeTiO_3$, their composites have been fabricated without failure and also their photocatalytic properties have been widely explored.[66] These nanocrystalline composite frameworks show a significantly improved photocatalytic degradation of organic pollutants as the composite could facilitate the transfer of charges and conquer the recombination of photoexcited electron-hole pairs. Amongst other visible-light absorbing photocatalysts, tungsten oxide ($WO_3$) has been viewed as a standout amongst the best candidates because of its physicochemical properties that are stable, including relatively small band-gap energy (2.4-2.8 eV) and valence band (VB) holes having high oxidation power.[61]

## 2.7 Tungsten trioxide ($WO_3$)

Amongst countless visible active photocatalysts, is Tungsten oxide ($WO_3$), also referred to as tungsten trioxide. It is an n-type semiconductor having a narrow band gap reported to range between 2.5-3.2 eV and is thermally stable and water-insoluble. Prior studies have indicated that temperature and pressure have an influence on the different crystalline phases and phase transitions that $WO_3$ possess.[67–69] $WO_3$ is a transition metal oxide composed of perovskite units and is better known for its nonstoichiometric properties. Its lattice can endure a substantial amount of oxygen deficiency.[70]



The metal tungsten (W) can for oxides quite easily when oxidized in air. The oxidation process of tungsten with water and the reduction process of tungsten oxides with hydrogen are similar, especially if the reaction is driven in a specific direction by the high partial pressure of $H_2O$ or hydrogen.[71] The sequential reactions are illustrated below

$$W + 2H_2O \rightarrow WO_2 + 2H_2 \quad \textbf{(2.20)}$$

$$W + 3H_2O \rightarrow WO_3 + 3H_2 \quad \textbf{(2.21)}$$

$$WO_3 + xH_2O \rightarrow WO_3 \cdot xH_2O \quad \textbf{(2.22)}$$

The reaction with water is a slow reaction at 38ºC and it is temperature and pressure dependent. Prior studies have shown that the reaction increases with increasing temperatures and pressures. It is reported that reactions with water vapour at temperatures ranging from 20 and 500ºC resulted in the formation of $WO_3$ only without forming other oxides. Since the rate of the reaction is dependent on temperature and partial pressure of water to that of hydrogen, proper adjustments of the partial pressures may result in the formation of all known oxides.[71]

The structure is constructed with corner sharing of $WO_6$ octahedra, where the oxygen atoms are located at the corner and the tungsten atom are at the centre position of each octahedron as illustrated in **Figure 2.5**. Concerning the perfect $ReO_3$ cubic structure, the symmetry is brought down by two distortions originating from the tilting of the $WO_6$ octahedra and the dislocation of tungsten from the centre position of its octahedron.[72] The structure is held together largely by ionic bonds since there are also significant covalent bonds. $WO_3$ has a stoichiometric that can be visualized as being made out of $W^{6+}$ and $O_2^{2-}$ ions. The VB is largely composed of O 2p orbitals, while the CB originates largely from W 5d orbitals.[73]

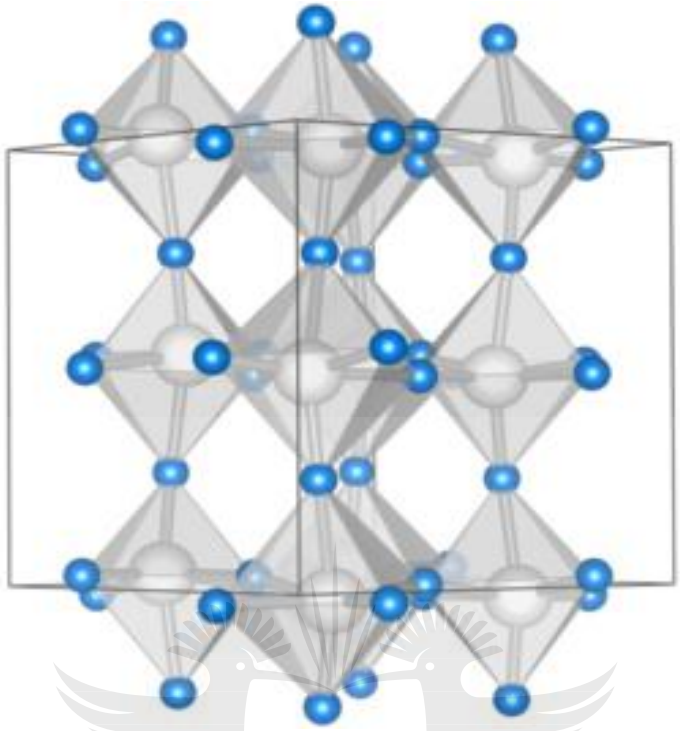

**Figure 2. 5:** Crystal structure of anhydrous monoclinic γ-phase of tungsten oxide.[75]

They can be synthesized in nanostructures with varying morphology as illustrated in **Figure 2.6**, crystallinity and the alteration of each octahedron results in the following phases, monoclinic (ε-phase), monoclinic (γ-phase), triclinic (δ-phase), tetragonal (α-phase) and orthorhombic (β-phase), The mixture of monoclinic and triclinic phases are commonly present at room temperature.[72] All these four phases of $WO_3$ have essentially a similar chessboard-like arrangement of $WO_6$ octahedra. The difference between them is only in the degree to which the W atoms are dislodged from the centre of $WO_6$ octahedra.[75] $WO_3$ has demonstrated great photocatalytic efficiency under visible light for abatement of most organic pollutants. The monoclinic phase has been reported to be a good candidate for applications in the presence of solar irradiation since it displays suitable band-gap energy for visible light absorption.[61]

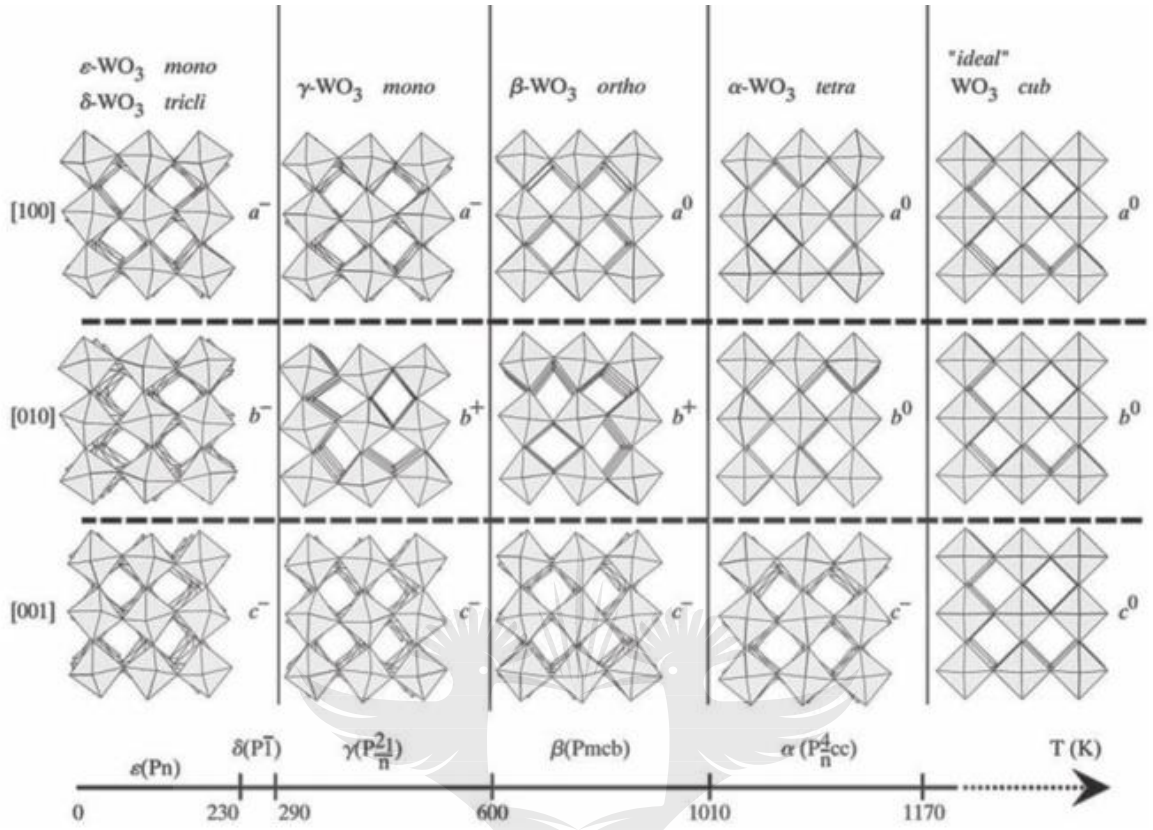


**Figure 2. 6:** Tilt patterns and stability temperature domains of the different polymorphs of $WO_3$.



The focus has been on tungsten because of their distinctive attributes that have prompted various applications and guaranteed further improvement. Methods that have been used to prepare tungsten oxide include sol-gel, chemical precipitation, hydrothermal, and microwave irradiation methods.[68,73] Because of such outstanding characteristics, $WO_3$ has interesting optical and electrical behaviour,[76] making it a suitable candidate in electrolysis,[77] photoelectrochemistry,[78] gas sensing,[73] photocatalysis, [81] electrochromic,[81] and photoelectrolysis.[82]

### 2.7.1 Advantages and disadvantages

$WO_3$ is an interesting photocatalyst because it is inexpensive, non-toxic, holds physical and chemical stability toward harsh conditions including consistent contact with water and solar irradiation. Furthermore, it is comparatively abundant in nature.[63,67] The ability of $WO_3$ photocatalyst to absorb visible light in the region of up to 480 nm qualifies to be an interesting option for photocatalytic applications. It can, as a result, be utilized indoors for pollutant treatment. $WO_3$ can use internal light sources in which ultraviolet light is limited to degrade volatile organic compound (VOC) gases. It also has the potential to be applied in outdoors where it is able to utilize light from the sun as energy for the treatment of harmful pollutants that are released from industrial wastewater. Moreover, it can be used for the production of hydrogen.[59,67,68] On the other hand, $WO_3$ in a pure state still suffers some drawbacks such as lower conduction band level. In $WO_3$ semiconductor, the VB edge is reported to be located at approximately 3 eV, but due to the lower CB edge value (+0.3 to 0.5 V NHE) does not have adequate potential to decrease $O_2$ [$E^0$ ($O_2/O_2^{2-\bullet}$) -0.33 V NHE and $E_0(O_2/HO_2^{\bullet})$ -0.05 V NHE]. The consequence of $O_2$ failing to scavenge CB electrons leads to the build-up of electrons in the CB which subsequently results in less separation of the photogenerated $e^-$ and $h^+$ and thus resulting in inefficient photocatalytic activity of $WO_3$.[23]



### 2.7.2 Modification

Even though $WO_3$ is able to absorb visible light, research has shown that using dopants can modify properties including the optical, electronic and physical properties of the nanomaterial and also further reduce the material's bandgap. The method of supporting and altering the surface of the photocatalyst is an effective one that also improves the adsorption capacities. The improved adsorption capacity enables a reactant-rich environment which then results in strengthened interaction between the pollutant and the catalyst surface.[66] Considering that each photocatalyst has advantages and disadvantages, there are different approaches that have been used to improve the

efficiency of the photocatalyst. These include altering the morphology and particle size, using composite materials, doping with transition/noble metal, non-metals, and surface sensitization.[67] Doping considered to be an effective and basic approach to increase free carries and decrease potential and conduction band levels by presenting impurity elements. The process involves the incorporation of foreign components into the parent photocatalyst without offering to ascend to another thus improving the separation of photogenerated charges. In this way, the wide visible-light component of the solar spectrum can be harnessed efficiently by the photocatalyst as compared to the narrow UV component.[83]

Tungsten oxide as an interesting photocatalyst has limitations which can be compensated by applying modification strategies. Modifying functionalities of the $WO_3$ is critical for its wide applications and can be effectively accomplished predominantly in three different ways. The first is the attachment of mono- or divalent cations into the interstitial positions of the $WO_3$, secondly by producing surface oxygen vacancies and lastly by doping the $WO_3$ semiconductor in either oxygen site or W site.[23,83] Furthermore, nanoscale metal oxides have extremely increased the photocatalytic activity due to the availability of larger specific surface area for reactions.[54] However, large surface areas may facilitate electron and hole recombination. Thus modifying the surface area of the semiconductor delays the fast electron-hole recombination, and increases the photocatalytic efficiency.[54,84]



#### 2.7.2.1 Metal doping

Extensive research has been done on the use of transition metals as dopants. This has been done in order to enhance their physical properties, explicitly to induce electronic structure with a small energy band gap.[23] Noble metals like platinum (Pt), silver (Ag), gold (Au) display excellent visible light absorption and interfacial charge transfer due to their surface plasmon resonance (SPR) effect which adds to improve the visible-light absorbance and the efficiency of solar-energy conversion. It is well known that SPR is

based on the resonant oscillation of charges between the metal-dielectric interface, occurring as the exciting light frequency equals the natural frequency of the surface metal electrons that are oscillating to resist the restoring force of positive nuclei.[61]

Li et al.[83] used the density functional theory to research the crystal structure of Niobium (Nb) and Rhenium (Re) doped $WO_3$. The research revealed that doping with Nb distorted the $WO_3$ lattice, whilst Re-doping transformed $WO_3$ from monoclinic to cubic phase. In the investigation of the effects of Ag on the structural and optical properties $WO_3$ synthesised via a microwave-assisted route, it was discovered that the Ag substituted on the host lattice of $WO_3$ resulting in intensity increase of the observed diffraction bands. This substitution causes lattice defects due to different atomic radii of the transition metals Ag (1.26) and W (0.6Å).[85]

#### 2.7.2.2 Non-metal doping

Non-metal doping has attracted attention and has been thoroughly researched. This technique has been used to decrease the Eg of wide bandgap semiconductors so that they can absorb in the visible light range. In nitrogen-doped semiconductor such as $TiO_2$, the element has been considered a suitable dopant because of its ionic radii and the band structure which is equivalent to oxygen. Nitrogen has lower electronegativity than oxygen, hence its 2p states produce trap sites that influence the narrowing of the band gap energy of nitrogen-doped $TiO_2$ nanoparticles.[23] Successful results were observed upon alteration of nanostructured $WO_3$ films when doped with boron. The non-metal substituted on the interstitial positions in the pristine $WO_3$ lattice, decreased the crystallite size due to $B^{3+}$ having smaller atomic radii than that of $W^{6+}$ (0.23Å vs 0.54Å) thus occupying partial tungsten sites. Furthermore, the morphology of the films having a pronounced increase in roughness factor was observed and resulted in a larger surface area that was visible to the aqueous solution and thus increased surface hydroxylation contributing to improved photoelectrochemical (PEC) performance.[69,78]

#### 2.7.2.3 Binary semiconductors

In binary semiconductor compounds, the character of the valence band is generally linked with the anion and the character of the conduction band is generally linked with the cation. Therefore, the transition of a band to band deteriorates the interatomic bond, so that the when in the solution, the photoexcitation can promote the decomposition and dissolution of the solid.[23] Stojadinovic et al.[86] have reported that the Bi-component $WO_3$ and $TiO_2$ nanoparticles have demonstrated improved photocatalytic activity regarding their plain component analogues since their VB and CB energy levels favour the transfer of electrons from the $TiO_2$ conduction band to $WO_3$ conduction band. The holes are transferred between valence bands in reverse direction. In this way, the electron-hole recombination process is reduced in both semiconductors. The results indicated higher photocatalytic activity achievement for a shorter Plasma electrolytic oxidation process time.[86] It was also discovered that by coupling with $CaFe_2O_4$ (CFO), the photocatalytic efficiency of $WO_3$ was basically improved and the composite photocatalysts could completely break down acetaldehyde.[87]



## 2.8 Characterization tools

### 2.8.1 X-ray diffraction (XRD)

Various X-ray diffractometry techniques have been utilized for the analysis of crystal structure as a means to understand the properties that the material displays. An example of a diffractometer system is depicted in **Figure 2.7**. XRD is based on the productive interference of the X-rays monochromatic beam that is scattered at particular angles from each set of lattice planes in a sample allowing a precise study of the structure of crystalline phases providing information on the degree of crystallinity, phase transitions as well as average grain size.[88] The structure of a material alludes to its arrangement at different complexity levels, which ranges from a simple molecular formula to the precise locations of all atoms in the molecule. The structural features such as electrostatic/polar effects have a great influence on the macroscopic behaviour

and properties of the material. Hence, structural characterization assumes an important role in identifying material structures. X-ray diffractometry technique such as powder method which uses a wide-angle goniometer and an automatic diffractometer with counter has been of interest for years.[89,90]

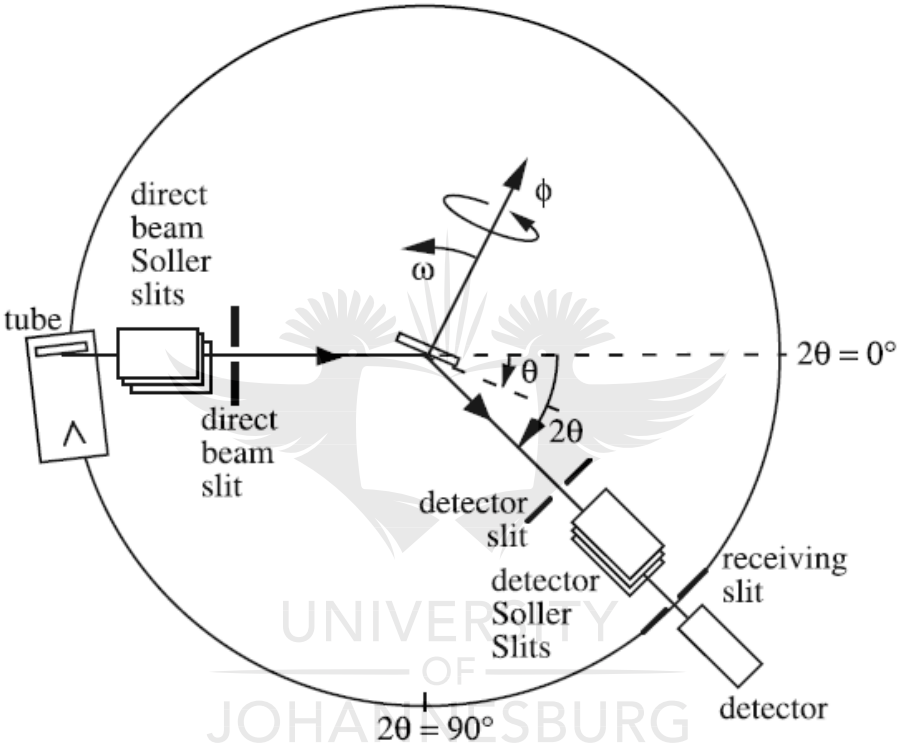


**Figure 2. 7:** Schematic diagram of a diffractometer system.[92]

X-rays are generated in a cathode ray tube. Upon heating the filaments, electrons are produced and accelerated towards the target material by means of applying a voltage. Characteristic X-ray spectra are created at the time when electrons have acquired enough energy to remove electrons from the material's inner shell. These spectra illustrated in **Figure 2.8** and comprise of $K_{\alpha}$ and $K_{\beta}$. Whereby $K_{\alpha}$ consists of $K_{\alpha 1}$ and $K_{\alpha 2}$. The specific wavelengths are subject of the target material (Cu, Fe, Mo, Cr) from which X-ray beams are produced. For filtration, foils or crystal monochrometers are used in

order to create monochromatic X-rays necessary for diffraction. Copper (Cu) is the most widely recognized target material for single-crystal diffraction with $CuK_{\alpha}$ (1.5418 Å).[92]

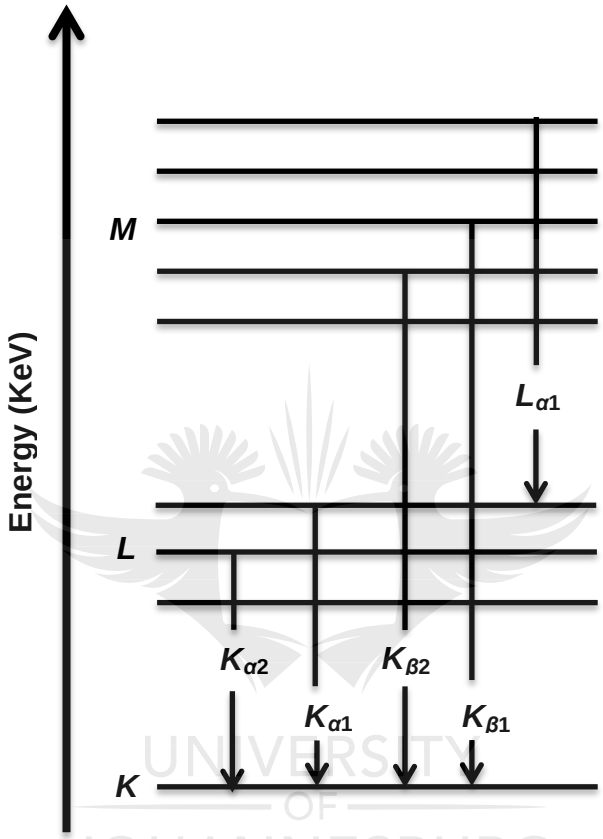


**Figure 2. 8:** Schematic of the atomic energy levels and emission of characteristic X-ray radiation.[89]

When the crystal structure is stricken at an angle $\theta$ by incident X-rays with respect to the crystalline planes, they can enter the crystal up to a reasonable distance and will interrelate with a great number of parallel planes. In general, each plane will be inclined to reflect the minimum amount of the incident X-ray beam and the reflected X-rays will likewise leave at an angle $\theta$ with respect to the planes as illustrated in **Figure 2.9**.[92]

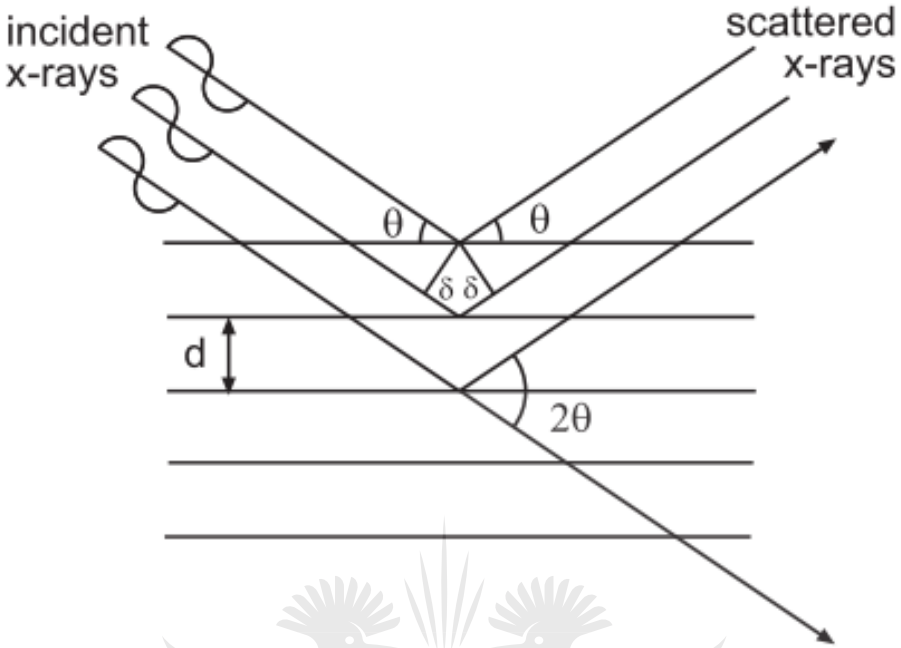


**Figure 2. 9:** Geometrical description of X-rays scattering.[94]

When conditions satisfy Bragg's Law (**Equation 2.23),** constructive interference and a diffracted ray are generated as incident rays interact with the target material. Bragg's law relates the wavelength, diffraction angle and the lattice spacing in a crystalline sample

$$n\lambda = 2dsin\theta \qquad \textbf{(2.23)}$$

Where *n* =an integer, *d* =interplanar spacing producing the diffraction, *λ* = wavelength of the X-rays and *θ* =diffraction angle.[92,93]

### 2.8.2 Raman spectroscopy

Raman spectroscopy is a technique named after its inventors. C.V. Raman together with K.S. Krishnan, experimented on the phenomenon of inelastic scattering of light which was first proposed by Smekal.[94,95] Raman spectroscopy is for the most part

utilized to distinguish vibrations in molecules, giving data on the physical forms and chemical structures in order to recognize materials from the spectral patterns.[95] This technology utilizes a single frequency of radiation in irradiating the sample. Raman detects the radiation that is scattered from the molecule and from one vibrational unit of energy that differs from the incident beam. Consequently, Raman does not need to match the incident radiation with the energy difference that is between the ground and excited states.[95]

The Raman scattering is a two-photon process, which involves light interactions with molecules. At the time when the light interacts with a material, the photons may either be absorbed or scattered. The photons may also be in contact with the material but rather pass straight through it. However, if the incident photon energy matches the energy gap between the ground state and the excited state of the molecules, the photon could be absorbed and the molecule excited to the higher energy state. Upon the interaction of the light with the molecule, the cloud of electrons nearby the nuclei is distorted to form an unstable short-lived state in which the photon can re-radiate. Then Rayleigh scattering is due to the emitted photon energy that remains the same as the energy of the incoming photon. An emitted photon with energy that is weaker than that of the incoming photon implies that the molecule gained energy from the photon while at ground state and then got promoted to the excited state. This process is known as Stokes Raman scattering. Furthermore, when the incoming photon gains energy from the molecule that is already in an excited vibrational state, it will produce a much stronger photon while the molecule in the excited state falls back to the ground state, this process is known anti-Stokes Raman scattering. These three types of scattering processes are summarised in **Figure 2.10**.[94,95]

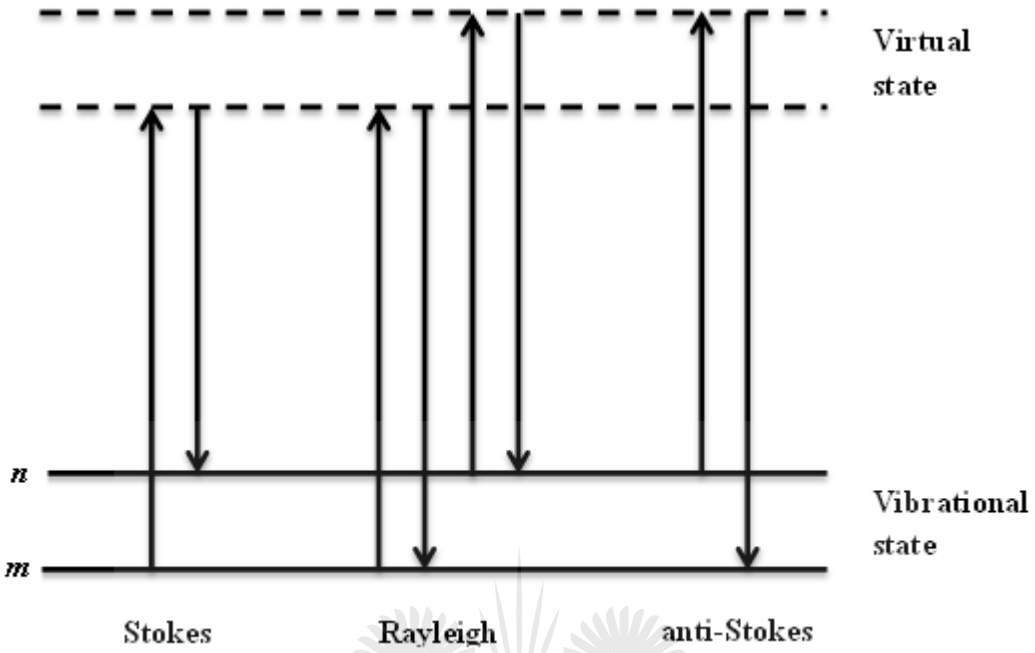


**Figure 2. 10:** Mechanism of the Raman scattering process.[96]

### 2.8.3 FTIR spectroscopy

FTIR spectroscopy was invented by Michelson in the 80s. it was a concept which started as an invention of the interferometer. Then Lord Rayleigh proposed a new way in which the produced interference patterns could be interpreted into a spectrum by Fourier transformation.[96] The instrumentation has been improved and advanced over the years and to date, FTIR spectroscopy is considered to be one of the most powerful techniques to date that can identify functional groups and molecular bonds between chemical compounds.[97] Chemical compounds can easily be identified by observing the position of IR absorption bands in the spectrum. FTIR has the capacity to provide the IR spectrum at a faster rate than other spectrophotometers. The main components of a simple FTIR spectrophotometer are illustrated in **Figure 2.11**.[97]

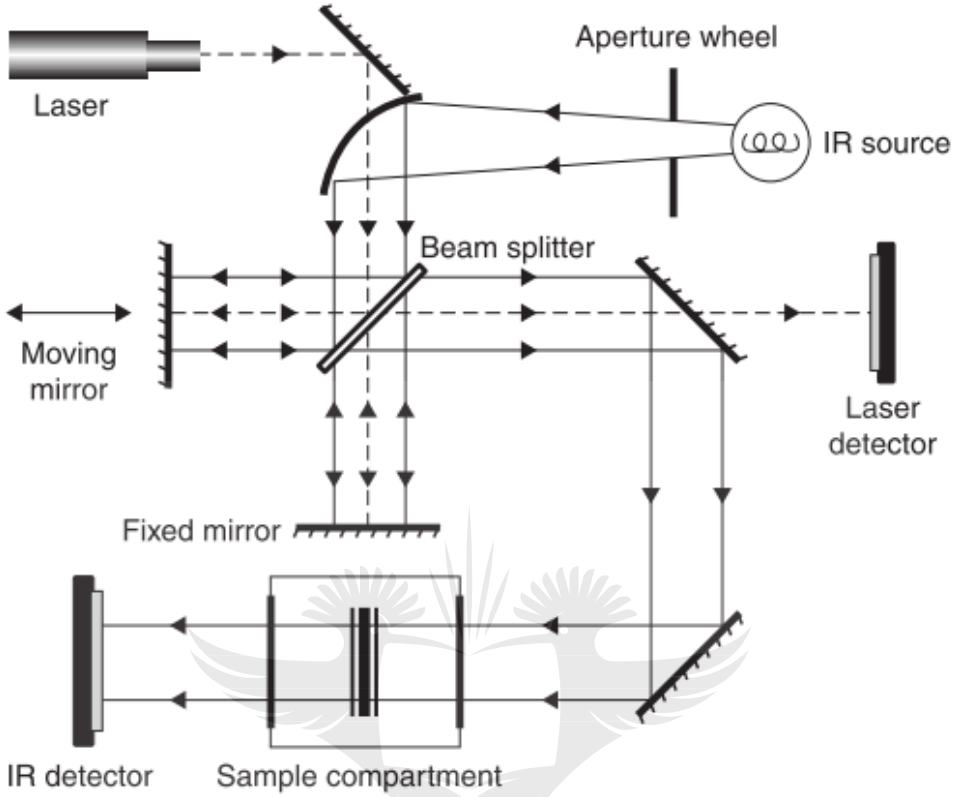


**Figure 2. 11:** Layout of a typical FTIR spectrometer.[97]



In the FTIR process, the intended light passes through the aperture wheel and is focussed on the mirror which then directs and focuses the light onto the beam splitter. Then the interferogram, which is the constructive and destructive interference, is created in the interferometer because of the recombination of the beams having different path lengths. The mirror directs the beam to enter the sample compartment from which a specific frequency of energy is absorbed by the sample. The detector interprets the interferogram signal in energy as a function of time. Then the interferogram subtracts the background noise from the sample by Fourier transformation software before releasing the anticipated.[96,98]

There are two modes used to collect FTIR spectra, namely, the transmission modes and reflection modes. The transmission modes which involve the use of KBr pallets, disposable cards and gas cells, whiles the reflection modes comprise of diffuse reflectance, attenuated total reflection, and specular reflectance. For liquid samples, the solution is placed between pairs of salt plates, for example, potassium bromide or sodium chloride. These plates are then placed into a holder in the spectrometer to produce a neat spectrum since no solvent is used. In solid samples, KBr pellet is obtained by crushing the sample into powder and then mixing it with potassium bromide (KBr) at a ratio of 1:100, followed by pressing it under high pressure of about 12,000 psi for 1-2 minutes. The obtained KBr pellet can then be placed into a holder inside the FTIR spectrometer for analysis. The IR spectrum is in the mid-IR region ranging from 2.5-15 µm between 4000 and 666 $cm^{-1}$. The mid-IR region is used to determine the existence of specific functional groups within the molecule because that is where the transition energies corresponding to vibrational energy state changes occur.[98,99]

### 2.8.4 Morphological analysis

The morphology studies of the nanoparticles were determined using transmission electron microscopy (TEM) coupled with energy dispersive X-ray (EDX), and scanning electron microscopy (SEM). TEM was invented in 1931 by a German electrical engineer Max Knoll and Ernst Ruska who was a German physicist. It was further improved from using a horizontal lens to using the vertically aligned lens in a column in order to sustain good alignment for an extended time. TEM is said to offer incredible choices to examine materials with characteristic dimensions that are under 100 nm or down to atomic scale. It quantifies the nanomaterial particle size, which is essential for the determining factor of the particle diameter. It is also an important instrument in characterizing the size distribution and the morphology of nanoparticles.[100] The basic structure of TEM is comprised of an electron gun and glass lenses with magnetic lenses. The lens system that forms the images comprises three lenses, which are the objective, intermediate and

projection lenses. These lenses ensure high magnification from some tens to up to million times. The schematics the basic structure of TEM is shown in **Figure 2.12**.[101]

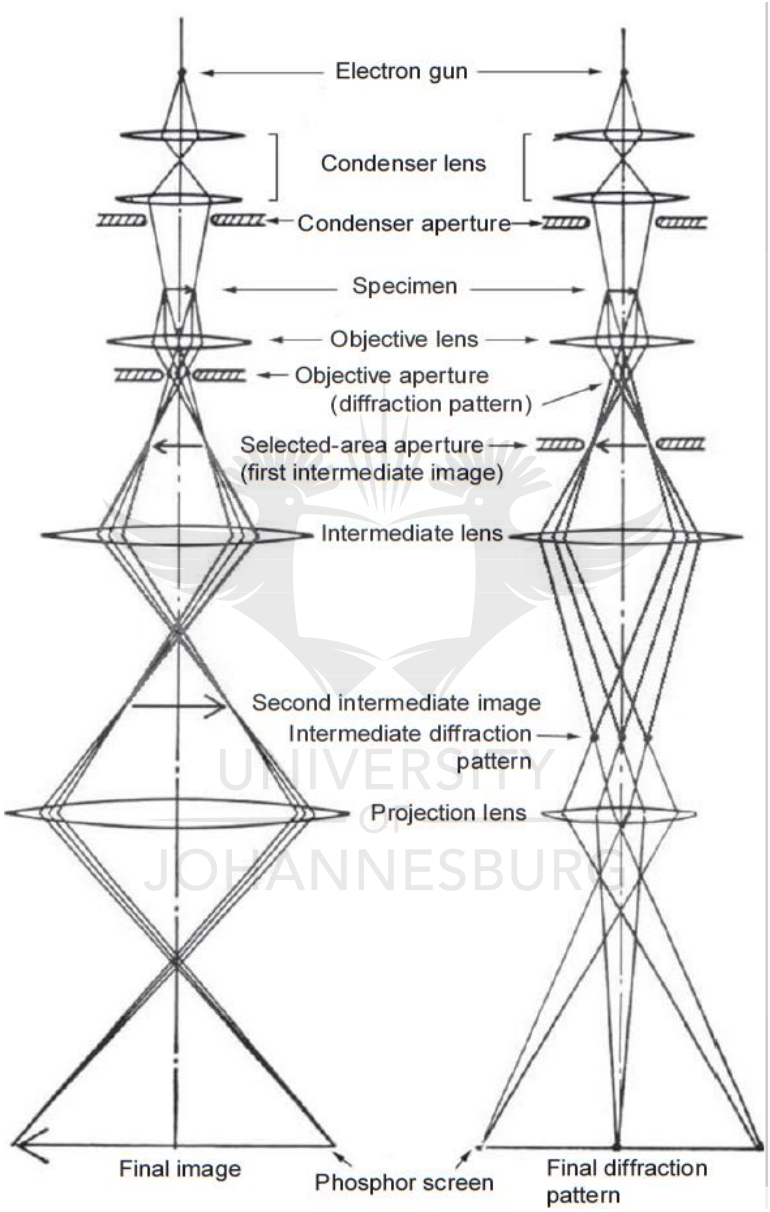


**Figure 2. 12:** Schematic diagram of transmission electron microscope.[102]

In TEM, there are electron beams that are generated from an electron gun, these beams are focused by the metal apertures and electromagnetic lens in the column. The

electrons are focused as the wave-like character of electrons behaving as negatively charged particles are deflected by magnetic or electric fields and only a small range of energy could pass through in this process. This leads to an energy electron beam that is well defined. In the TEM column, the specimen placed onto the sample holder is bombarded with transmitted electrons. This specimen should have a thickness that is within 100 nm for electrons to go through it.[100]

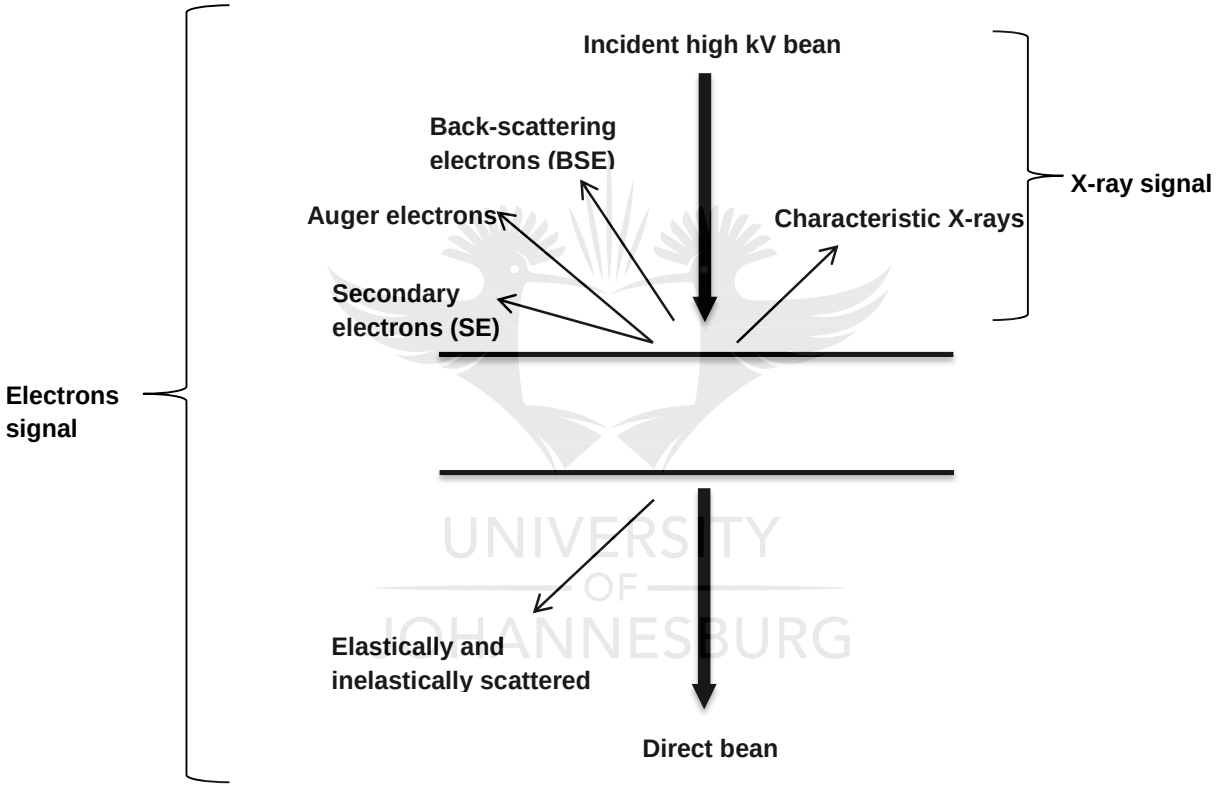


**Figure 2. 13:** Types of signals produced by the hitting of a specimen with a high-energy electron beam.[101]

**Figure 2.13** illustrates X-ray and numerous types of electrons that are generated between an electron beam and specimen. Density and the composition of a specimen are factors that may affect the transmission of electrons. More electrons would go through permeable metal, while fewer electrons would go through much denser

material. The application of a condenser lens could lead to the acquisition of the specimen's crystal structure data by the paralleled electrons beams.[100] TEM instruments can be combined EDX. EDX is an X-ray-based system, which is perceived as a nondestructive testing device to explore the elementary structure of materials. EDX studies deal with the properties, composition and structure of materials.[102]

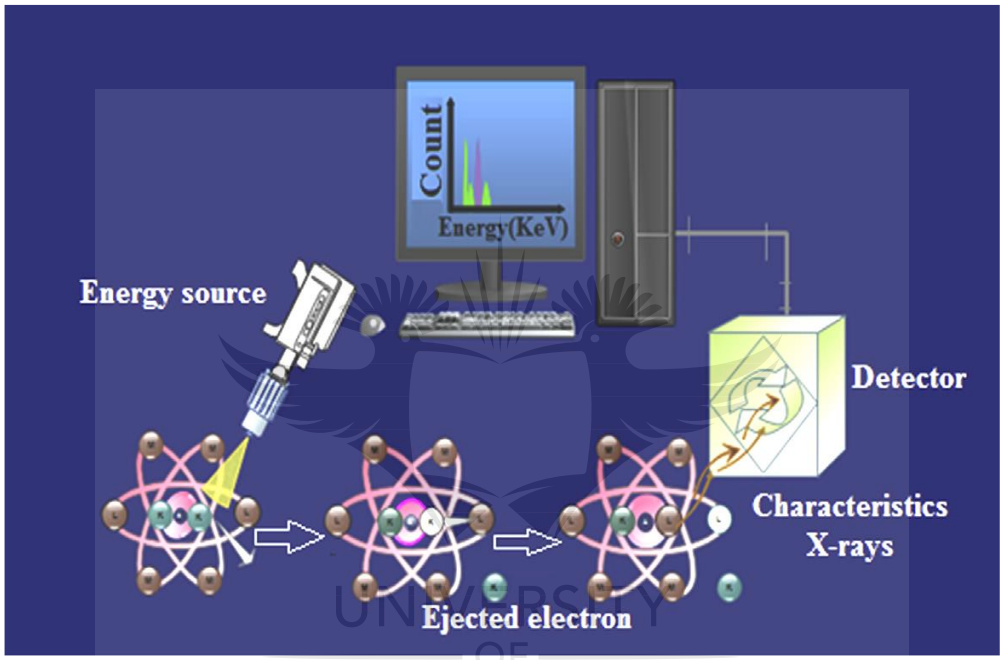


**Figure 2. 14:** Description of energy-dispersive X-ray spectroscopy principle.[103]



In the EDS spectrum, peaks are attained through X-rays. These X-rays are created by characteristic fluorescence radiation. This characterization of EDS is viewed as an instrument for estimating the X-ray mapping and elemental composition, in which every atom is characteristic of its electronic configuration. In EDX, the sample is bombarded with X-ray or g-ray to knock out the electrons from the inner shell. This leaves a hole behind and thereafter the higher energy of the electrons is shifted to lower energy level delivering energy to the EDX where is detected as X-rays.[102] The process is illustrated in **Figure 2.14.**

SEM is a technique that provides the surface image of samples. It was constructed by Manfred von Ardenne in the years 1937-1938 and is one of the best resourceful instruments for the analysis of microstructures and nanostructures. SEM as an electron microscope focuses electron beams to react with the sample in order to produce images and composition of the sample. The focused electron beam creates backscattered electrons, secondary electrons, and characteristic X-ray. These are then detected and displayed on the screen monitor. The schematic drawing of the SEM function is illustrated in **Figure 2.15**.[103,104]

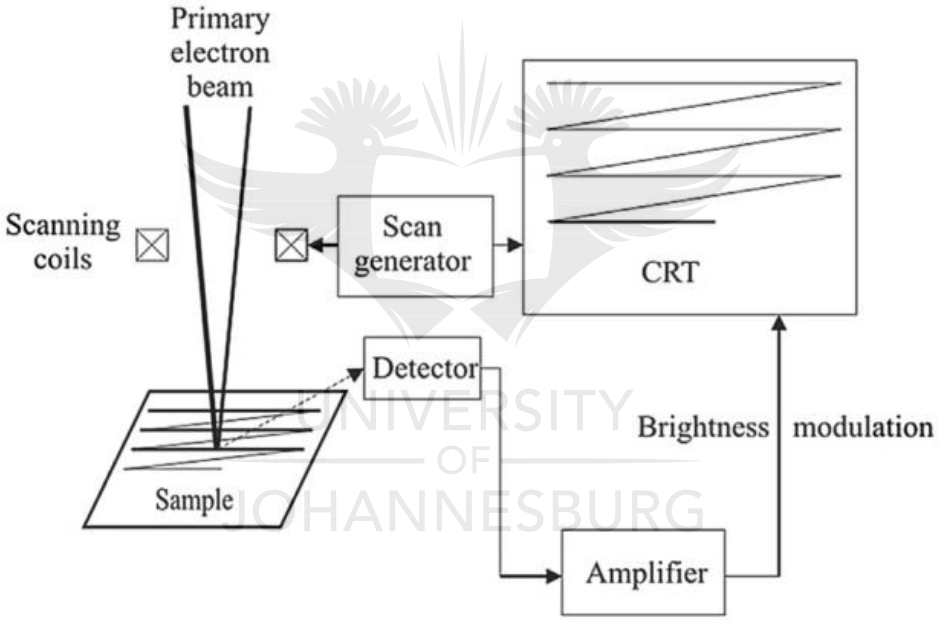


**Figure 2. 15:** Schematic drawing of the SEM function.[104]

### 2.8.5 UV-Vis absorbance spectra analysis

UV-Vis spectroscopy is an exceptional instrument that characterizes nanomaterial properties. In UV-Visible spectroscopy, the photons of light are measured in the UV-Vis range. In this process, the light intensity going through the sample is measured against the light intensity before passing through the sample. This technique can be used for absorption measurements of UV and visible light. The measurement may either occur

as single wavelength or scan a whole range in the spectrum. The UV-Vis spectral region extends over a UV range (190-400 nm) and visible range (400-780 nm). The complete spectrum can be obtained by using dispersive multichannel or dual beam dispersive scanning techniques. The instrument setup is illustrated in **Figure 2.15**. It consists of a light source, a chopper, a monochromator, a sample, a reference beam, a reference section, and a detector.[105,106]

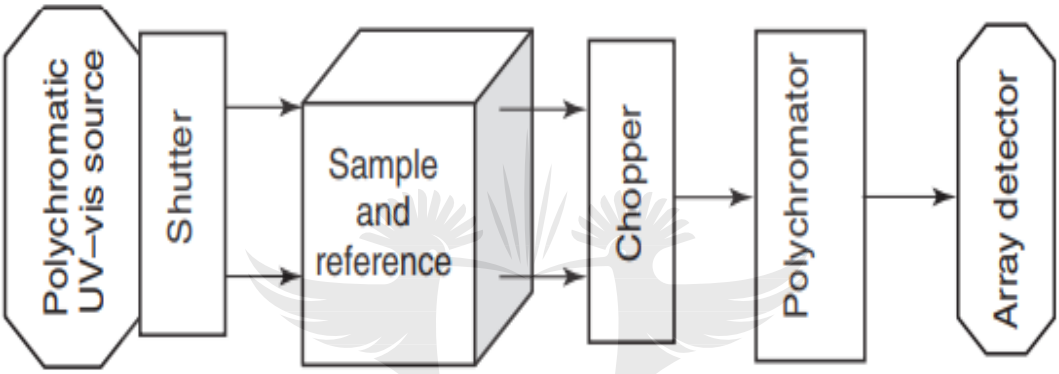


**Figure 2. 16:** Block schematic diagram of UV-Vis multichannel spectrometer.[108]



The extinction of light that is measured by the spectrophotometer is a fraction of light that is isolated from the incident beam. This extinction can be derived from the relation given by the Lambert-Beer law (**Equation 2.24**). Based on the Beer-Lambert Law, the concentration of the substance is direct to the absorbance that is in the solution and consequently UV-visible spectroscopy can be utilized to quantify the concentration of a sample.

$$A = \varepsilon c l \qquad \textbf{(2.24)}$$

Where A =absorbance of a solution, *l* =optical path length of the cell (cm), *c* =solution concentration (mol $dm^{-3}$), and $\varepsilon$ = molar absorptivity of the absorbing molecule. The molar absorptivity is constant for a specific substance at a specific wavelength ($dm^3$ $mol^{-}$

$^{1}$ cm$^{-1}$). The plot of concentration against the absorbance of a series of sample solutions having known concentrations should give a linear graph if the Beer-Lambert Law was obeyed. The graph is identified as a calibration graph.[106]

### 2.8.6 X-ray photoelectron spectroscopy

XPS is a technology that was developed by K. Siegbahn and his research group in the mid-1960s. It is based on the phenomenon of the photoelectric effect delineated by Einstein. In the year 1905, Einstein used the concept of a photon to describe how electrons are ejected from a surface when impinged upon by photons.[108,109] XPS is a very resourceful technique for surface chemistry analysing of materials. It is a quantitative and a nondestructive method, which has the ability to detect most elements and obtain information relating to the atomic compositions, chemical bonds, quantification of elements, oxidation states and determination of contaminants. A schematic diagram of an XPS measurement system is illustrated in **Figure 2.16**.[110,111]

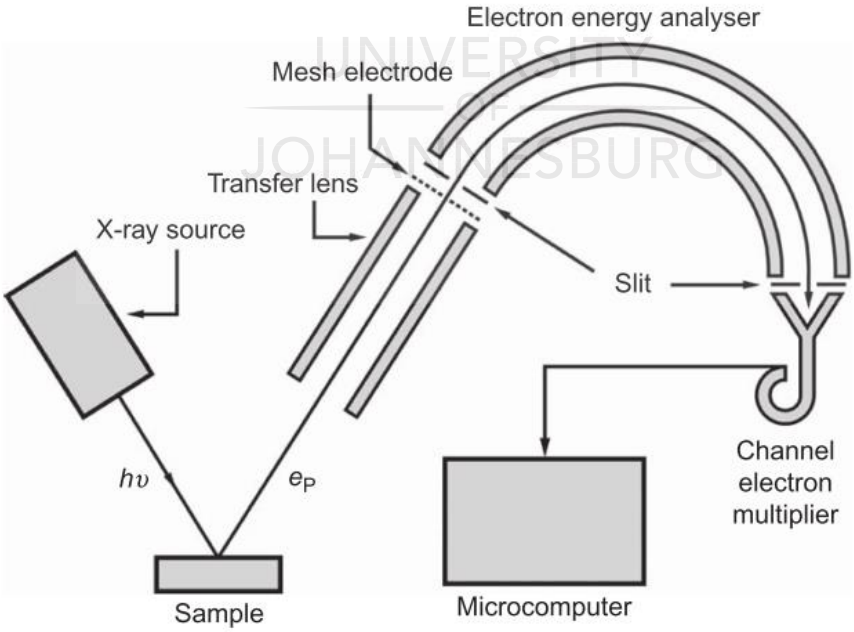


**Figure 2. 17:** Schematic diagram of an XPS measurement system.[111]

Concentric hemispherical analyzer determines the photoelectrons energies ejected from the material and this produces a spectrum of photoelectron peaks. Each peak has binding energy (BE) which is characteristic of each element and this is useful in identifying species. The number of electrons that are related to the energy quantifies the states and in turn, the number of electrons as an element of BE in a given sample.[108,109]

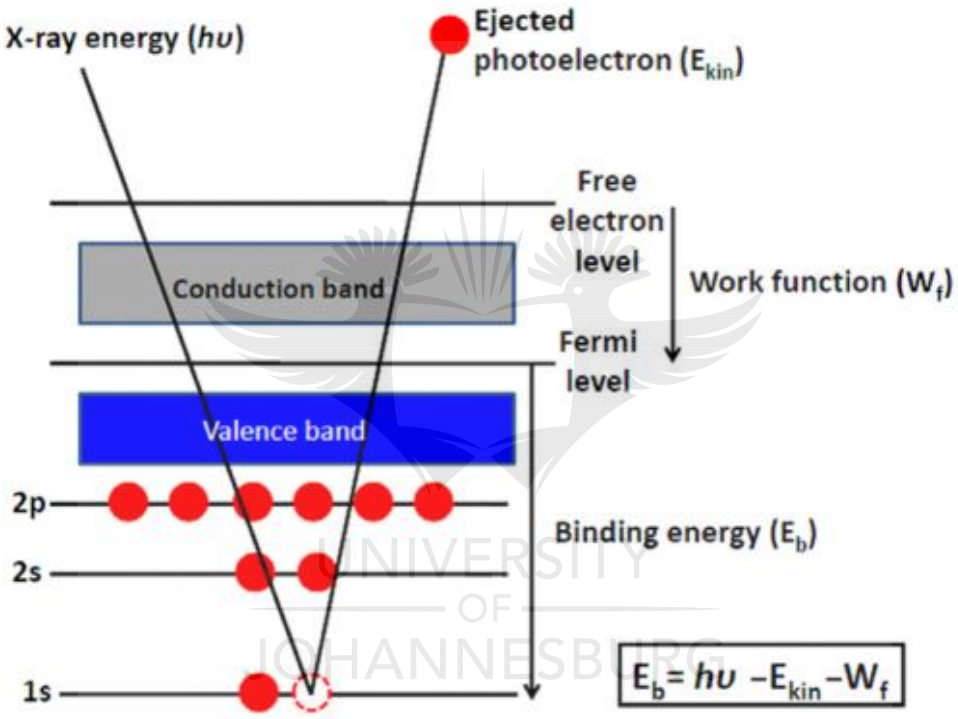


**Figure 2. 18:** Schematic representation of the XPS process.[109]

With respect to the tilting angle of the sample as depicted in **Figure 2.17**, the X-ray penetrates for about 1-10 nm under the surface. When there is an interaction between a photon that has higher energy than the BE of the electron in an atom, electrons will be emitted from an atomic energy level by X-ray photons. The following steps characterize this process: (1) optical excitation; (2) transport to the surface; (3) escape into the vacuum. The kinetic energy (KE) of the ejected electron is related to the incident beam

energy, the BE of the electron and the spectrometer work function.[108,109,111] KE is given by **Equation 2.25**.

$$KE = hv - BE - e\emptyset \quad \textbf{(2.25)}$$

Where KE = kinetic energy, BE = binding energy of the atomic orbital from which the electron originates, *hv* = energy of the incident beam and *eØ* = spectrometer work function. The spectrometer work function is the least amount of energy that each electron requires to dislodge from the surface. Each element generates an exclusive set of electrons with specific energies. Then an XPS spectrum is obtained by quantifying the number of electrons as a function of BE and KE.[111]

## 2.9 Application

### 2.9.1 Gas sensing

Nanotechnology has been used to manufacture gas chemical nanosensors devices. These nanosensors are designed to quantitatively determine chemicals present in a gaseous medium. The nanosensors include two main components, the sensing element and the measuring transducer. The measuring transducer measures the change in optical, electrical and mechanical properties. Gas sensing is a surface effect hence nanostructured materials that are mesoporous have been largely researched in the development of catalytic and gas sensing systems. These mesoporous materials have a large and controllable pore size and high surface area. An increased active surface area of semiconductors enhances the material's properties used as gas sensors.[112]

Tungsten oxide has attracted great attention for its distinctive photocatalytic properties that have the potential for catalysis, solar energy, electrochromic devices and gas sensors. Tungsten oxide has demonstrated tremendous capabilities as a sensor for various gasses such as $H_2$, CO, $C_2H_5OH$, $CH_3OH$, HCHO, and $NH_3$.[113]. Furthermore,

ultrafine $WO_3$ nanoparticles produced via nanocasting synthesis route were investigated on sensing $NO_2$. The results indicated that the nanoparticles are sensitive enough to detect $NO_2$ gas even at low concentrations.[112]

### 2.9.2 Electrochromic properties.

$WO_3$ nanoparticles display sub-stoichiometric phase transitions and structural transformations, which have sought the attention in the nanotechnology research field. The electrochromic effect of $WO_3$ is highly dependent on the crystal stoichiometry, having significantly diverse properties that have been reported for crystalline and amorphous films. Electrochromic materials are materials that are capable of changing their optical properties, reversibly and persistently, by applying an electrical voltage. They exhibit electrochromic properties that make them appropriate for dazzle-free mirrors that are in automobiles, variable reflection mirrors, and smart windows.[114]

Tungsten trioxide (hydrate) and its electrochromic properties were investigated in their applications in the electrochromic device where a complementary electrochromic device which was founded on the nanoparticle $3WO_3{\cdot}H_2O$ film and PB film was synthesized and the resultant demonstrated faster-switching response, larger optical contrast and better colouration efficiency.[115,116] In smart windows, they spare energy by decreasing the heating or cooling loads of the interiors in buildings.[70,73,116] The investigation of the electrochromic and morphological effect of dry-lithiated nanostructured $WO_3$ thin films resulted in improved normal state transmission as well as suppression of interference extrema in nanostructured films that are highly porous. The high normal state transmission, together with the open structure of the films, made the films highly anticipated applicants for electrochromic applications.[117]

### 2.9.3 Photoelectrochemical properties

Photoelectrochemical (PEC) water splitting has the same principles as the natural photosynthesis-solar energy conversion through numerous electron transfers and generation of high energy chemicals like hydrogen.[118] Metal oxide semiconductors are regarded as ideal candidate for photoelectrodes due to their nontoxicity, and low cost and inherent stability in water. $WO_3$ has been considered a promising photoanode material for PEC water oxidation. PEC is extensively used in water splitting devices that involve water electrolysis using solar energy.[118–120]

Kwong et al.[121] demonstrated the effectiveness of the deposition potential on different mechanisms for deposition as well as the morphological, mineralogical, and optical properties of electrodeposited $WO_3$ thin films and how these characteristics influence the photoelectrochemical performance of the $WO_3$ thin films. Yang, et al.[120] modified the surface states as well as the performance of PEC water oxidation of $WO_3$ nanoflakes film photoanode with amorphous $TiO_2$ (α-$TiO_2$). This led the photogenerated-electrons or dissolved-oxygen method for the formation of $H_2O_2$ to be depressed and accelerated the $H_2O_2$ oxidation throughout PEC water oxidation. In the removal of pollutants from wastewater, Fernández-Domene et al.[122] investigated parameters that influenced the PEC performance of $WO_3$ nanomaterials via statistical analysis. He reported that the photoelectrochemical and chemical stability of $WO_3$ in highly acidic atmospheres improved the PEC performance of $WO_3$ photoelectrodes. The result further indicated that the high degree of crystallinity of $WO_3$ nanostructure enhanced the electrochemical as well as the photoelectrochemical interfacial phenomena. These $WO_3$ photoanodes were used in the degradation of chlorfenvinphos under visible-light illumination.

### 2.9.4 Photocatalytic properties

$WO_3$ nanoparticles have been evaluated for their photocatalytic efficiency in Methylene blue under UV-vis irradiation and alkaline reaction pH indicated that the more porous and large surface area samples provided a more active site for faster photocatalytic reaction rate and almost complete discolouration of the organic dye.[59] Moreover, the photocatalytic activity of the $WO_3$ in the degradation reaction of the organic dyes such as indigo carmine (IC), Rhodamine blue (RhB), Congo red (CR) and methyl orange (MO) under UV and UV-vis irradiation has been remarked as one of the peak applications of $WO_3$.[123]

Furthermore, $WO_3$ nanoparticles have been employed for the treatment of wastage form pharmaceutical contaminated effluents. The study on the photocatalytic degradation of Lidocaine drug achieved 95.48% and 97.5% degradation of the drug in 60 minutes under visible and sunlight respectively.[80] Modification of $WO_3$ proves to enhance the photocatalytic activity of the catalyst. Upon deposition of Silver nanoparticles on $WO_3$ nanorods, the resultant was better optical properties and more optical visible-light response-ability. The enhancement of photocatalytic activity was attributed to the intrinsic nature of charge separation and also on the SPR effect which contributes towards the reduction of electron-hole pair recombination.[61]



## 2.10 Synthesis

### 2.10.1 Sol-gel technique

Sol-gel methods grant the means to obtain well-crystallized nanomaterials with high chemical homogeneity at warm temperatures. It is reported to be a powerful technique for synthesizing metal oxides to fit particular applications due to the ability to regulate a number of parameters such as the pH, the type of the precursors, reaction time and temperature, concentration of the reagent, concentration and type of the catalyst and

ageing temperature and time. In this process, the metal-oxo-polymer networks are formed from metal salt or metal alkoxides precursors. However, alkoxides tend to hydrolyse rapidly which may result in the difficulty in controlling the sol-gel synthesis. Hence, products can be obtained as a result of introducing different variations in the preparation routes.[23]

Ageing of the sol, particularly at high temperatures, produces coarse particles. The hydrolysis step is promoted by the electrophilic attack of $H^+$, hence it is typically catalysed by the addition of either an inorganic or carboxylic acid. Preparation at low pH generally produces more crystalline powders. However, high pH levels promote condensation, which results in less ordered solids. It is possible to control the rates of nucleation and growth of the particle by adjusting the water-to-alkoxide ratio. An increase in this ratio favours nucleation, whereas low water content or excess $TiO_2$ alkoxide favours particle growth.[23]

### 2.10.2 Acid precipitation

As one suitable and inexpensive method, chemical co-precipitation is able enough to meet high demands for the direct preparation of nanoparticles that are well dispersed. This method is energy saving by using low-temperature substitutes to conventional powder synthesis methods in the synthesis of nanoparticles. The method also offers the ability to control the sizes of nanoparticles by an apt surfactant. Chemical co-precipitation can generate high-purity, fine, stoichiometric particles of single and multicomponent metal oxides. The synthesis route includes metal ion complexation by polyfunctional carboxyl with one hydroxyl group, its precipitation and lastly, thermal treatment decomposition.[124,125]

### 2.10.3 Microwave irradiation method

Microwave heating is one of the promising technologies, whose applications have been a research interest due to its unique effects including increased reaction rates, rapid volumetric heating and shortened reaction time, enhanced reaction selectivity and energy saving. Microwave irradiation methods have been used effectively to modify the properties which have enormous effects on the photocatalytic performance of semiconductor metal oxides, these properties include particle size, morphology and high surface areas.[86]

Moreover, the simplicity of the microwave irradiation method arises from its operation, less time consuming, purity of the material in comparison with other methods. In a typical experiment, the prepared precursor solution is placed into the microwave oven operating at 360W in an air atmosphere. Thereafter, the resulting substance is dried at a temperature of 100°C for 5 min. Abhudhahir and Harshulkhan[127] synthesized pristine and Manganese doped $WO_3$ nanoparticles without hydrate group using Microwave irradiation method for the photodegradation of Methylene Blue.



## 2.11 References

1. Ndoricimpa, A. Analysis of asymmetries in the nexus among energy use, pollution emissions and real output in South Africa. *Energy* **125,** 543-551 (2017).
2. Amdany, R., Chimuka, L., Cukrowska, E., Kukučka, P., Kohoutek, J., Tolgyessy, P., & Vrana, B. Assessment of bioavailable fraction of POPs in surface water bodies in Johannesburg City, South Africa, using passive samplers: an initial assessment. *Env. Monit Assess* **186,** 5639-5653 (2014).
3. Verhaert, V., Newmark, N., Hollander, W. D., Covaci, A., Vlok, W., Wepener, V., Addo-Bediako, A., Jooste, A., Teuchies, J., Blust, R. & Bervoets, L. Persistent organic pollutants in the Olifants River Basin, South Africa: Bioaccumulation and trophic transfer through a subtropical aquatic food web. *Sci. Total Environ.* **586,**

792-806 (2017).

4. Liu, L., Ma, W., Jia, H., Zhang, Z. & Song, W. Research on persistent organic pollutants in China on a national scale: 10 years after the enforcement of the Stockholm Convention. *Environ. Pollut.**217,*** 1-12 (2016).
5. Gao, H., Zhou, L., Ma, M., Chen, X. & Hu, Z. Composition and Source of Unknown Organic Pollutants in Atmospheric Particulates of the Xigu District, Lanzhou, People's Republic of China. *Bull. Environ. Contam. Toxicol* **72,** 923-930 (2004).
6. Sigh, S. N. *Microbial Degradation of Synthetic Dyes in Wastewaters*. *Springer International Publishing Switzerland* (Springer International Publishing Switzerland, 2015).
7. Lahkimi, A., Oturan, M. A., Oturan, N. & Chaouch, M. Removal of textile dyes from water by the electro-Fenton process. *Env. Chem Lett* **5,** 35-39 (2007).
8. Rizzo, L., Koch, J., Belgiorno, V. & Anderson, M. A. Removal of Methylene Blue in a photocatalytic reactor using polymethylmethacrylate supported $TiO_2$ film. in *International Conference on Environmental Science and Technology* A1256 - A1261 (2005).
9. Mehmetli, E. & Koumanova, B. *The Fate of Persistent Organic Pollutants in the Environment*. (Springer, 2007).
10. Kordouli, E., Bourikas, K., Lycourghiotis, A. & Kordulis, C. The mechanism of azo-dyes adsorption on the titanium dioxide surface and their photocatalytic degradation over samples with various anatase/rutile ratios. *Catal. Today* **252,** 128-135 (2015).
11. Srinivasan, K. in *Chemistry and Water* 329–351 (Elsevier Inc., 2017).
12. Murray, K., Slabbert, L. & Moloi, B. *Needs assessment and development framework for a tested implementation plan for the initialisation and execution of a National Toxicants Monitoring Programme ( NTMP ) Final Report*. *National Toxicants Monitoring Programme* (2003).
13. Mouele, E. S. M., Tijani, J. O., Fatoba, O. O. & Petrik, L. F. Degradation of organic pollutants and microorganisms from wastewater using different dielectric

barrier discharge configurations - a critical review. *Env. Sci Pollut Res* **22,** 18345-18362 (2015).

14. Govender, T., Barnes, J. M. & Pieper, C. H. Contribution of Water Pollution From Inadequate Sanitation and Housing Quality to Diarrheal Disease in Low-Cost Housing Settlements of Cape Town , South Africa. *Res. Pract.* **101,** 4-9 (2011).
15. Racine, D., Muchapondwa, E. & Kirsten, J. Implications of water policy reforms for agricultural productivity in South Africa: Scenario analysis based on the Olifants river basin. *Water Resour. Econ.* **9,** 60-79 (2015).
16. Watts, M. J., Atwood, J. & Beattie, B. R. Water degradation implications when whole-farm irrigation water is binding. *Water Resour. Econ.* 3-22 (2015).
17. Puvaneswari, N., Muthukrishnan, J. & Gunasekaran, P. Toxicity assessment and microbial degradation of azo dyes. *Indian J. Exp. Biol.* **44,** 618-626 (2006).
18. Nasuha, N., Zurainan, H. Z., Maarof, H. I., Zubir, N. A., Amri, N., Pauh, P., & Pinang, P. Effect of cationic and anionic dye adsorption from aqueous solution by using chemically modified papaya seed. *Int. Conf. Environ. Sci. Eng.* **8,** 50-54 (2011).
19. Sharma, V. K. Oxidation of inorganic contaminants by ferrates (VI , V, and IV) - kinetics and mechanisms: A review. *J. Environ. Manage.* **92,** 1051-1073 (2011).
20. Fabietti, G., Biasioli, M., Barberis, R., & Ajmone-Marsan, F. Soil contamination by organic and inorganic pollutants at the regional scale: the case of Piedmont , Italy. *J Soils Sediments* **10,** 1-11 (2009).
21. Masindi, V., Gitari, M. W., Tutu, H. & Beer, M. De. Fate of inorganic contaminants post treatment of acid mine drainage by cryptocrystalline magnesite: Complimenting experimental results with a geochemical model. *Biochem. Pharmacol.* **4,** 1-11 (2016).
22. Al, E. T. Removal of Chromium (III) from the Waste Solution of an Indian Tannery by Amberlite IR 120 Resin. *Int. J. Nonferrous Metall.* **1,** 32-41 (2012).
23. Hernández-Ramírez, A. & Medina-Ramírez, I. *Photocatalytic Semiconductors: Synthesis, Characterization, and Environmental Applications*. *Springer International Publishing Switzerland* (Springer International Publishing

Switzerland, 2015).

24. Teklehaimanot, G. Z., Coetzee, M. A. A. & Momba, M. N. B. Faecal pollution loads in the wastewater effluents and receiving water bodies: a potential threat to the health of Sedibeng and Soshanguve communities, South Africa. *Env. Sci Pollut Res* **21,** 9589-9603 (2014).
25. Baudišová, D. Microbial pollution of water from agriculture. *Plant Soil Env.* **55,** 429-435 (2009).
26. Bertrand, J., Bonin, P., Caumette, P., Gattuso, J. & Gérald Grégori, Rémy Guyoneaud, Xavier Le Roux, Robert Matheron, F. P. in *Environmental Microbiology: Fundamentals and Applications: Microbial Ecology* 511-617 (2015).
27. Cann, P. Le, Roig, B., Thomas, O. & Baurè, E. Microbial Contamination Detection in Water Resources: Interest of Current Optical Methods, Trends and Needs in the Context of Climate Change. *Int. J. Environ. Res. Public Heal.* **11,** 4292-4310 (2014).
28. Zhou, Y., Zhang, L. & Cheng, Z. Removal of organic pollutants from aqueous solution using agricultural wastes : A review. *J. Mol. Liq.* **212,** 739-762 (2015).
29. Ali, I., Asim, M. & Khan, T. A. Low cost adsorbents for the removal of organic pollutants from wastewater. *J. Environ. Manage.* **113,** 170-183 (2012).
30. Ghaly, A. E., Ananthashankar, R., Alhattab, M. & Ramakrishnan, V. V. Production, Characterization and Treatment of Textile Effluents: A Critical Review. *J Chem Eng Process Technol* **5,** 1-19 (2014).
31. Saggioro, E. M., Oliveira, A. S., Pavesi, T., Maia, C. G., Filipe, L., Ferreira, V., & Moreira, J. C. Use of Titanium Dioxide Photocatalysis on the Remediation of Model Textile Wastewaters Containing Azo Dyes. *Molecules* **16,** 10370-10386 (2011).
32. Bari, Q. & Bhardwaj, N. Role of bio-sorbents in the decolorization of some commonly used dyes. *J. Sci.* **4,** 637-642 (2014).
33. Buthelezi, S. P., Olaniran, A. O. & Pillay, B. Textile Dye Removal from Wastewater Effluents Using Bioflocculants Produced by Indigenous Bacterial Isolates. *Molecules* **17,** 14260-14274 (2012).

34. Kehinde, F. & Aziz, H. A. Textile Waste Water and the advanced Oxidative Treatment Process, an Overview. *Int. J. Innov. Res. Sci. Eng. Technol.* **3,** 10-12 (2014).
35. Carmen, Z. & Daniela, S. in *Organic Pollutants Ten Years After the Stockholm Convention - Environmental and Analytical Update* 55-80 (2010).
36. Kyzas, G. Z., Fu, J. & Matis, K. A. The Change from Past to Future for Adsorbent Materials in Treatment of Dyeing Wastewaters. *Materials (Basel).* **6,** 5131-5158 (2013).
37. Santana, M. H. P., Silva, L. M. Da, Freitas, A. C., Boodts, J. F. ., Fernandes, K. C., & Faria, L. A. De. Application of electrochemically generated ozone to the discoloration and degradation of solutions containing the dye Reactive Orange. *J. Hazard. Mater.* **164,** 10-17 (2016).
38. Mirkhani, V., Tangestaninejad, S., Moghadam, M. & Habibi, M. H. Photocatalytic Degradation of Azo Dyes Catalyzed by Ag Doped $TiO_2$ Photocatalyst. *J. Iran. Chem. Soc* **6,** 578-587 (2009).
39. Jo, W.-K. & Tayade, R. J. Recent developments in photocatalytic dye degradation upon irradiation with energy-efficient light emitting diodes. *Elsevier* **35,** 1781-1792 (2014).
40. Ribeiro, A. R. & Umbuzeiro, G. D. A. Effects of a textile azo dye on mortality, regeneration, and reproductive performance of the planarian, Girardia tigrina. *Ribeiro Umbuzeiro Environ. Sci. Eur.* **26,** 1-8 (2014).
41. Mahlambi, M. M., Ngila, C. J. & Mamba, B. B. Recent Developments in Environmental Photocatalytic Degradation of Organic Pollutants: The Case of Titanium Dioxide Nanoparticles - A Review. *J. Nanomater.* **2015,** 1-30 (2015).
42. Dafare, S., Deshpande, P. S. & Bhavsar, R. S. Photocatalytic degradation of congo red dye on combustion synthesised $Fe_2O_3$. *Indian J. Chem. Technol.* **20,** 406-410 (2013).
43. Shivaraju, H. P. Removal of Organic Pollutants in the Municipal Sewage Water by $TiO_2$ based Heterogeneous Photocatalysis. *Int. J. Environ. Sci.* **1,** 911-923 (2011).
44. Segneanu, A. E., Orbeci, C., Lazau, C., Sfirloaga, P., Vlazan, P., Bandas, C., &

Grozescu, I. in *Intech* 53-80 (2013).

45. Hettige, A. I. & Lanka, S. Reduction of Colour in Treated Wastewater from Textile Industry Using Sawdusts as Bio-sorbents. *Trop. Agric. Res.* **26,** 666-676 (2015).
46. Mohamed, F. A., Fali, N., El-mohamedy, R. S. R. & Hebeish, A. A. Biodegredation of Reactive and Reactive Disperse Dyes by Aspergillius nigar. *J Bioremed Biodeg* **5,** 1-5 (2014).
47. Ogugbue, C. J. & Sawidis, T. Bioremediation and Detoxification of Synthetic Wastewater Containing Triarylmethane Dyes by Aeromonas hydrophila Isolated from Industrial Effluent. *Biotechnol. Res. Int.* **2011,** 1-11 (2011).
48. Karthik, V., Saravanan, K. & Nadu, T. An overview of treatments for the removal of textile dyes. *J. Chem. Pharm. Sci.* **7,** 301-307 (2014).
49. Luan, M., Jing, G., Piao, Y., Liu, D. & Jin, L. Treatment of refractory organic pollutants in industrial wastewater by wet air oxidation. *Arab. J. Chem.* **10,** S769-S776 (2017).
50. Chaukura, N., Gwenzi, W., Tavengwa, N. & Manyuchi, M. M. Biosorbents for the removal of synthetic organics and emerging pollutants: Opportunities and challenges for developing countries. *Environ. Dev.* **19,** 84-89 (2016).
51. Ratna & Padhi, B. S. Pollution due to synthetic dyes toxicity & carcinogenicity studies and remediation. *Int. J. Environ. Sci.* **3,** 940-955 (2012).
52. Glaze, W. H., Kang, J. & Chapin, D. H. The Chemistry of Water Treatment Processes Involving Ozone, Hydrogen Peroxide and Ultraviolet Radiation. *Ozone Sci. Eng.* **9,** 335-352 (1987).
53. Colmenares, J. C. & Xu, Y.-J. *Heterogeneous Photocatalysis*. (2016).
54. Ibhadon, A. O. & Fitzpatrick, P. Heterogeneous Photocatalysis: Recent Advances and Applications. *Catalysts* **3,** 189-218 (2013).
55. Ebrahiem, E. E., Al-Maghrabi, M. N. & Mobarki, A. R. Removal of organic pollutants from industrial wastewater by applying photo-Fenton oxidation technology. *Arab. J. Chem.* **10,** S1674-S1679 (2017).
56. Silva, L. C. da, Neto, B. de B. & Silva, V. L. da. Homogeneous degradation of the Remazol Black B dye by Fenton and photo-Fenton processes in aqueous

medium. *Afinidad LXVI* **541,** 232-237 (2009).

57. Barbusiński, K. & Majewski, J. Discoloration of Azo Dye Acid Red 18 by Fenton Reagent in the Presence of Iron Powder. *Polish J. Environ. Stud.* **12,** 151-155 (2003).
58. Zhang, J., Tian, B., Wang, L., Xing, M. & Lei, J. *Photocatalysis*. (2018).
59. Vamvasakis, I., Georgaki, I., Vernardou, D., Kenanakis, G. & Katsarakis, N. Synthesis of $WO_3$ catalytic powders: evaluation of photocatalytic activity under NUV/visible light irradiation and alkaline reaction pH. *J. Sol-Gel Sci. Technol.* **76,** 120-128 (2015).
60. Muneer, M., Philip, R. & Das, S. Photocatalytic degradation of waste pollutants. Titanium dioxide mediated oxidation of textile dye, Acid blue 40. *Res. Chem. Intermed* **23,** 233-246 (1997).
61. Ding, J., Chai, Y., Liu, Q., Liu, X., Ren, J., & Dai, W. Selective Deposition of Silver Nanoparticles onto $WO_3$ Nanorods with Different Facets: The Correlation of Facet-Induced Electron Transport Preference and Photocatalytic Activity. *J. Phys. Chem.* **120,** 4345-4353 (2016).
62. Sahoo, P. C., Martha, S. & Parida, K. Solar Fuels from $CO_2$ Photoreduction over Nano-Structured Catalysts Solar fuels from $CO_2$ photoreduction over nano-structured catalysts Prakash Chandra Sahoo, Satyabadi Martha, Kulamani Parida. *Mater. Sci. forum* **855,** 1-9 (2016).
63. Nešić, J., Manojlović, D. D., Anđelković, I., Dojčinović, B. P., Vulić, P. J., Krstić, J., & Roglić, G. M. Preparation, characterization and photocatalytic activity of lanthanum and vanadium co-doped mesoporous $TiO_2$ for azo-dye degradation. *J. Mol. Catal.* **378,** 67-75 (2013).
64. Sun, J., Wang, Y., Sun, R. & Dong, S. Photodegradation of azo dye Congo Red from aqueous solution by the $WO_3$-$TiO_2$/activated carbon (AC) photocatalyst under the UV irradiation. *Mater. Chem. Phys. J.* **115,** 303-308 (2009).
65. Song, H., Li, Y., Lou, Z., Xiao, M., Hu, L., Ye, Z., & Zhu, L. Synthesis of Fe-doped $WO_3$ nanostructures with high visible-light-driven photocatalytic activities. *Appl. Catal. B Environ.* **166-167,** 112-120 (2015).

66. Chakraborty, A. K., Rhaman, M. M., Hossain, M. E. & Sobahan, K. M. A. Preparation of $WO_3/TiO_2/In_2O_3$ composite structures and their enhanced photocatalytic activity under visible light irradiation. *React. Kinet. Mech. Catal.* **111,** 371-382 (2014).
67. Asim, N., Syuhami, M. F., Badiei, M. & Yarmo, M. A. $WO_3$ Modification by Synthesis of Nanocomposites. *Procedia - Soc. Behav. Sci.* **9,** 175-180 (2014).
68. Harshulkhan, S. M. & Krishnaraj, S. Structural and optical properties of Ag doped tungsten oxide ($WO_3$) by microwave-assisted chemical route. *J. Mater. Sci. Mater. Electron.* **27,** 3158-3163 (2016).
69. Marschall, R. & Wang, L. Non-metal doping of transition metal oxides for visible-light photocatalysis. *Catal. Today* **225,** 111-135 (2014).
70. Zheng, H., Ou, J. Z., Strano, M. S., Kaner, R. B., Mitchell, A., & Kalantar-zadeh, K. Nanostructured Tungsten Oxide - Properties, Synthesis, and Applications. *Adv. Funct. Mater* **21,** 2175-2196 (2011).
71. Han, S., Raja, R. & Somorjai, G. A. *Nanotechnology in Catalysis*. **3,** (Springer, 2007).
72. Baserga, A., Russo, V., Fonzo, F. Di, Bailini, A., Cattaneo, D., Casari, C. S., Bassi, A. L., Bottani, C. E. Nanostructured tungsten oxide with controlled properties: Synthesis and Raman characterization. *Thin Solid Films* **515,** 6465-6469 (2007).
73. Niklasson, G. A. & Granqvist, C. G. Electrochromics for smart windows: thin films of tungsten oxide and nickel oxide, and devices based on these. *J. Mater. Chem.* **17,** 127-156 (2007).
74. Lin, H., Zhou, F., Liu, C.-P., & Vidvuds, O. Non-Grotthuss Proton Diffusion Mechanism in Tungsten Oxide Dihydrate from First-Principles Calculations. *J. Mater. Chem. A* **2,** 12280-12288 (2014).
75. Szilágyi, I. M., Fórizs, B., Rosseler, O., Szegedi, Á., Németh, P., Király, P., Tárkányi, G., Vajna, B., Varga-Josepovits, K., László, K., Tóth, A. L., Baranyai, P. & Leskelä, M. $WO_3$ photocatalysts: Influence of structure and composition. *J. Catal.* **292,** 119-127 (2012).

76. Gajera, H. P., Bambharolia, R. P., Hirpara, D. G., Patel, S. V., & Golakiya, B. A. Molecular identification and characterization of novel Hypocrea koningii associated with azo dyes decolorization and biodegradation of textile dye effluents. *Process Saf. Environ. Prot.* **98,** 406-416 (2015).
77. Tan, L., He, M., Song, L., Fu, X. & Shi, S. Aerobic decolorization , degradation and detoxification of azo dyes by a newly isolated salt-tolerant yeast Scheffersomyces spartinae TLHS-SF1. *Bioresour. Technol.* **203,** 287-294 (2016).
78. Barczuk, P. J., Krolikowska, A., Lewera, A., Miecznikowski, K., Solarska, R., & Augustynski, J. Structural and photoelectrochemical investigation of boron-modified nanostructured tungsten trioxide films. *Electrochim. Acta* **104,** 282-288 (2013).
79. Jaimy, K. B., Ghosh, S., Sankar, S. & Warrier, K. G. K. An aqueous sol-gel synthesis of chromium (III) doped mesoporous titanium dioxide for visible light photocatalysis. *Mater. Res. Bull.* **46,** 914-921 (2011).
80. Fakhri, A. & Behrouz, S. Photocatalytic properties of tungsten trioxide ($WO_3$) nanoparticles for degradation of Lidocaine under visible and sunlight irradiation. *Sol. Energy* **112,** 163-168 (2015).
81. Bi, Z., Zhang, S., Xu, X., Hu, X., Li, X., & Gao, X. A novel nanocomposite of $WO_3$ modi fi ed Al-doped ZnO nanowires with enhanced electrochromic performance. *Mater. Lett.* **160,** 186-189 (2015).
82. Zhao, W., Wang, Z., Shen, X., Li, J., Xu, C., & Gan, Z. Hydrogen generation via photoelectrocatalytic water splitting using a tungsten trioxide catalyst under visible light irradiation. *Int. J. Hydrogen Energy* **37,** 908-915 (2011).
83. Li, Z., Wu, S., Wang, Z. & Fu, Y. Q. Doping Induced Structural Transformation in Tungsten Trioxide. *J. Alloys Compd.* **672,** 155-160 (2016).
84. Fallis, A. . Study on Water Purification Using Tungsten Trioxide Photocatalyst under Visible Light. *Journal of Chemical Information and Modeling* (2013).
85. Harshulkhan, S. M., Ganapthy, S. R., Janaki, K., Velraj, G. & Nagarajan, M. Effect of Ag doping on structural, optical and photocatalytic activity of tungsten oxide ($WO_3$) nanoparticles. *J. Mater. Sci. Mater. Electron.* **27,** 3-10 (2016).

86. Stojadinovic, S., Radic, N., Vasilic, R., Petkovic, M., Stefanov, P., Zekovic, L. & Grbic, B. Photocatalytic properties of $TiO_2$ /$WO_3$ coatings formed by plasma electrolytic oxidation of titanium in 12-tungstosilicic acid. *Appl. Catal. B Environ.* **126,** 334-341 (2012).
87. Liu, Z., Zhao, Z.-G. & Miyauchi, M. Efficient Visible Light Active $CaFe_2O_4$/$WO_3$ Based Composite Photocatalysts: Effect of Interfacial Modification. *J. Phys. Chem. C* **113,** 17132-17137 (2009).
88. Epp, J. in *Materials Characterization Using Nondestructive Evaluation (NDE) Methods* 81-124 (Elsevier Ltd, 2016).
89. Iwashita, N. *X-ray Powder Diffraction*. *Materials Science and Engineering of Carbon* (Tsinghua University Press Limited., 2016).
90. Giannini, C., Ladisa, M., Altamura, D., Siliqi, D., Sibillano, T., & Caro, L. De. X-ray Diffraction: A Powerful Technique for the Multiple-Length-Scale Structural Analysis of Nanomaterials. *Crystals* **6,** 1-22 (2016).
91. Fultz, B. & Howe, J. *Transmission Electron Microscopy and Diffractometry of Materials*. (Springer, 2013).
92. Bunaciu, A. A., Udristioiu, E. G. & Aboul-enein, H. Y. X-Ray Diffraction: Instrumentation and Applications. *Crit. Rev. Anal. Chem.* **45,** 289-299 (2015).
93. Idziak, S. H. J. *Powder X-ray Diffraction of Triglycerides in the Study of Polymorphism*. *Structure-Function Analysis of Edible Fats* (Elsevier Inc., 2018)
94. Wen, Z. Raman Spectroscopy of Protein Pharmaceuticals. *J. Pharm. Sci.* **96,** 2861-2878 (2007).
95. Smith, E. & Dent, G. *Modern Raman Spectroscopy - A Practical Approach*. (John Wiley & Sons, Ltd, 2005).
96. Subramanian, A. & Rodriguez-saona, L. in *Infrared Spectroscopy for Food Quality Analysis and Control* 145-178 (Elsevier Inc., 2009).
97. Dufour, É. in *Infrared Spectroscopy for Food Quality Analysis and Control* 1-27 (Elsevier Inc., 2009).
98. Mohamed, M. A., Jaafar, J., Ismail, A. F., Othman, M. H. D. & Rahman, M. A. in *Membrane Characterization* 3-29 (Elsevier B.V., 2017).

99. Tao, J. in *Methods in Enzymology* **532,** 533-556 (Elsevier Inc., 2013).
100. Tang, C. Y. & Yang, Z. in *Membrane Characterization* 145-159 (Elsevier B.V., 2017).
101. Kogure, T. in *Developments in Clay Science* **5,** 275-317 (Elsevier Ltd., 2013).
102. Mishra, R. K., Zachariah, A. K. & Thomas, S. in *Microscopy Methods in Nanomaterials Characterization* 383-405 (Elsevier Inc., 2017).
103. Henning, S. & Adhikari, R. in *Microscopy Methods in Nanomaterials Characterization* 1-30 (Elsevier Inc., 2017)
104. Mutalib, M. A., Rahman, M. A., Othman, M. H. D., Ismail, A. F. & Jaafar, J. in *Membrane Characterization* 161-179 (Elsevier B.V., 2017).
105. Kumar, C. S. S. R. *UV-VIS and Photoluminescence Spectroscopy for Nanomaterials Characterization*. (Springer, 2013).
106. Anderson, R. J., Bendell, D. J. & Groundwater, P. W. in *Organic Spectroscopic Analysis* 7-23 (Royal Society of Chemistry, 2004).
107. Gauglitz, G. & Moore, D. S. *Handbook of Spectroscopy*. (Wiley-VCH, 2014).
108. Mane, A. T. & Patil, V. B. in *Spectroscopy of Polymer Nanocomposites* 452-467 (Elsevier Inc., 2016).
109. Aziz, M. & Ismail, A. F. in *Membrane Characterization* 81-93 (Elsevier B.V., 2017).
110. Seyama, H., Soma, M. & Theng, B. K. G. in *Developments in Clay Science* **5,** 161-176 (Elsevier Inc., 2013).
111. Yahia, L. H. & Mireles, L. K. in *Characterization of Polymeric Biomaterials* 83-97 (Elsevier Ltd., 2017).
112. Heidari, E. K., Marzbanrad, E., Zamani, C. & Raissi, B. Nanocasting Synthesis of Ultrafine $WO_3$ Nanoparticles for Gas Sensing Applications. *Nanoscale Res Lett.* **5,** 370-373 (2010).
113. Xiang, Q., Meng, G. F., Zhao, H. B., Zhang, Y., Li, H., Ma, W. J., & Xu, J. Q. Au Nanoparticle Modified $WO_3$ Nanorods with Their Enhanced Properties for Photocatalysis and Gas Sensing. *J. Phys. Chem* **114,** 2049-2055 (2010).
114. Prabhu, N., Agilan, S., Muthukumarasamy, N., Senthilkumaran, C. K. Effect of temperature on the structural and optical properties of $WO_3$ nanoparticles

prepared by solvo thermal method. *Dig. J. Nanomater. Biostructures* **8,** 1483-1490 (2013).

115. Rao, M. C. Structure and properties of $WO_3$ thin films for electrochromic device application. *J. Non-Oxide Glas.* **5,** 1-8 (2013).
116. Jiao, Z., Wang, J., Ke, L., Liu, X., Demir, H. V., Yang, M. F., & Sun, X. W. Electrochromic properties of nanostructured tungsten trioxide (hydrate) films and their applications in a complementary electrochromic device. *Electrochim. Acta* **63,** 153-160 (2012).
117. Beydaghyan, G., Bader, G. & Ashrit, P. V. Electrochromic and morphological investigation of dry-lithiated nanostructured tungsten trioxide thin films. *Thin Solid Films* **516,** 1646-1650 (2008).
118. Kim, J. H., Lee, B. J., Wang, P., Son, M. H. & Lee, J. S. General Facile surfactant driven fabrication of transparent $WO_3$ photoanodes for improved photoelectrochemical properties. *Appl. Catal. A, Gen.* **521,** 233-239 (2016).
119. Prabhu, S., Cindrella, L., Kwon, O. J. & Mohanraju, K. Photoelectrochemical and photocatalytic activity of $TiO_2$-$WO_3$ heterostructures boosted by mutual interaction. *Mater. Sci. Semicond. Process.* **88,** 10-19 (2018).
120. Yang, M., He, H., Zhang, H., Zhong, X., Dong, F., Ke, G., Chen, Y., Du, J. & Zhou, Y. Enhanced photoelectrochemical water oxidation on $WO_3$ nano flake films by coupling with amorphous $TiO_2$. *Electrochim. Acta* **283,** 871-881 (2018).
121. Kwong, W. L., Qiu, H., Nakaruk, A., Koshy, P. & Sorrell, C. C. Photoelectrochemical Properties of $WO_3$ Thin Films Prepared by Electrodeposition. *Energy Procedia* **34,** 617-626 (2013).
122. Fernández-Domene, R. M., Roselló-Márquez, G., Sánchez-Tovar, R., Lucas-Granados, B. & García-Antón, J. Photoelectrochemical removal of chlorfenvinphos by using $WO_3$ nanorods: Influence of annealing temperature and operation pH. *Sep. Puri fi cation Technol.* **212,** 458-464 (2019).
123. Sánchez-Martínez, D., Martínez-de la Cruz, A. & López-Cuéllar, E. Synthesis of $WO_3$ nanoparticles by citric acid- assisted precipitation and evaluation of their photocatalytic properties. *Mater. Res. Bull.* **48,** 691-697 (2013).

124. Mahdavi, M., Ahmad, M. Bin, Haron, M. J., Namvar, F., Nadi, B., Rahman, M. Z. A., & Amin, J. Synthesis, Surface Modification and Characterisation of Biocompatible Magnetic Iron Oxide Nanoparticles for Biomedical Applications. *Molecules* **18,** 7533-7548 (2013).
125. Sanchez-Martı´nez, D., Cruz, A. M. la & Llar, E. L.-C. Synthesis of $WO_3$ nanoparticles by citric acid-assisted precipitation and evaluation of their photocatalytic properties. *Mater. Res. Bull.* **48,** 691-697 (2013).
126. Abhudhahir, H. M. S. & Kandasamy, J. Photocatalytic effect of manganese doped $WO_3$ and the effect of dopants on degradation of methylene blue. *J. Mater. Sci. Mater. Electron.* **26,** 8307-8314 (2015)

# CHAPTER 3
# METHODOLOGY AND CHARACTERIZATION

## 3.1 Introduction

This chapter gives detailed procedures employed in the synthesis, characterization and photodegradation of the synthesized nanoparticles. Pristine monoclinic tungsten trioxide (*m*-$WO_3$) and lanthanum doped $WO_3$ nanoparticles were synthesized using the impregnation method. Various characterization techniques such as X-ray diffraction (XRD), Raman spectroscopy, scanning electron spectroscopy, transmission electron microscopy (TEM), FTIR spectroscopy, and X-ray photoelectron spectroscopy (XPS) were used to characterize the samples. The UV-Vis spectroscopy and ion chromatography (IC) were used in photocatalytic measurements of the nanoparticles.

## 3.2 Materials and reagents

Tungstic acid (99%, Sigma-Aldrich Co.), Nitric acid (30%, Sigma-Aldrich Co.), Lanthanum nitrate hydrate (99%, Merck), 1000 ppm dye stock solutions were prepared by dissolving Methylene Blue and Congo Red powders (Sigma-Aldrich Co.) in de-ionized water.

## 3.3 Methodology

### 3.3.1 Synthesis of pristine *m*-$WO_3$ and La- $WO_3$ nanoparticles

Pristine *m*-$WO_3$ was synthesized using a thermal treatment of a yellow tungstic acid $H_2WO_4$ (5.0 g) powder in the oven at 450 ºC for 3 hrs. Lanthanum doped samples were prepared via impregnation method. To obtain the desired percentage of dopant (1, and 5 m/m %), lanthanum nitrate and tungstic were dissolved in nitric acid (30%, 10 ml) under continuous stirring for two hrs at 90°C. The materials were then precipitated,

washed with ethanol and dried overnight at room temperature to obtain a yellow powder product. The sample was then calcined in the oven at 450 °C for 3 hours. The samples were labelled *m*-$WO_3$, 1-La-$WO_3$, and 5-La-$WO_3$ for pristine $WO_3$, 1% and 5% (m/m) La-doped $WO_3$ respectively.[1,2]

### 3.3.2 Characterization tools

#### 3.3.2.1 X ray diffraction (XRD)

Structural properties of pristine *m*-$WO_3$ and the La-$WO_3$ nanoparticles were analyzed with X-ray diffraction (XRD, X'Pert Philips). XRD was operated at 40 mA, 40 kV with $CuK_\alpha$ radiation (1.54060 nm) polychromator beam 2θ scan within the scan range of 10–80°, and a step size and step time of 0.0170 and 175.26 s. By using the Debye–Scherrer's equation **(3.1)**, the average grain size was calculated based on the peaks found in the XRD patterns.

$$D = \frac{k\lambda}{\beta cos\theta} \quad \textbf{(3.1)}$$



Where, *D* =mean crystallite size, *λ* =X-ray wavelength (0.1541 nm) for $CuK_\alpha$, *k* =0.89, *β* =full width at half maximum and *θ* =Bragg angle.[3,4]

#### 3.3.2.2 Raman spectroscopy

Raman experiments were conducted using Raman Micro 200, Perkin Elmer spectrophotometer with a 514.5 nm wavelength $Ar^+$ laser. Spectra were obtained by an 1800 lines/mm grating, with a holographic notch filter and cooled TCD tolerating a spectral resolution of about 3 $cm^{-1}$. The power on the samples was maintained below 0.5 mW to avoid local heating and the photoluminescence spectra were recorded by LS 45 Fluorescence spectrometer.

### 3.3.2.3 Fourier transform infrared (FTIR) spectroscopy

The FTIR spectra analysis was done using a Perkin Elmer Precisely spectrum 100 FTIR spectrometer in the range 400-4000 $cm^{-1}$ with KBr as a reference. The specimen discs of nanopowders were prepared by preparing a pellet of a mixture of nanoparticle with KBr. In this experiment, the sample was crushed into powder. Then the sample powder was combined with powdered potassium bromide (KBr) at a ratio of 1:100. The powder mixture was then pressed under high pressure at around 12,000 psi for 1 minute. The produced KBr pellet was then inserted into a sample holder in the FTIR spectrometer and scanned between 4000 – 400 wavenumbers ($cm^{-1}$) to obtain spectra.[5]

### 3.3.2.4 Morphological analysis

The morphology studies of the nanoparticles were resolved using transmission electron microscopy (JOELTEM 2010) at an acceleration voltage of 200 kV. The instrument was coupled with an energy dispersive X-ray (EDX) detector operated at 5 kV. The nanoparticles were dispersed in alcohol followed by ultrasonication for 2 minutes and then with the use of a pipette, a drop of the sample was dispersed on a carbon-coated copper grid, which was left to dry before analysis. The scanning electron microscope (SEM, TESCAN Vega TC instrument with VEGA 3 TESCAN software) was used and operated under nitrogen gas.



### 3.3.2.5 UV-Vis absorbance spectra analysis

UV-Vis spectrometer (Shimadzu UV-2450) operated in diffuse reflectance mode (DRS) was utilized in obtaining the absorbance spectra, followed by the application of Kubelka–Munk transformation and Barium sulphate ($BaSO_4$) was used as reference material in all measurements. The nanoparticles were mixed with $BaSO_4$ and placed in a spherical sample holder and pressed into a smooth surface pallet. The sample was then placed in UV-Vis spectrometer for analysis. The energy gap values ($E_g$) were determined with the following relationship as expressed in **Equation (3.2).**

$$\alpha = A(hv - E_g)^n / hv \quad \textbf{(3.2)}$$

where $\alpha$ =the absorption coefficient that is calculated from the Kubelka–Munk function, $hv$ =the photon energy, $E_g$ = band gap energy, $A$ =constant, and $n$ =constant with a value of n = 1/2 for materials with a direct transition.

The formula was simplified as expressed in equation **3.3**

$$hv = h\frac{c}{\lambda} = \frac{1240}{\lambda} \quad \textbf{(3.3)}$$

The optical band gap of the nanomaterials was calculated by extrapolation from the Tauc linear portion of $(\alpha hv)^2$ against $hv$, to the x-axis, where $\alpha$ = 0, and, consequently, $E_g = hv$.[2,6]



#### 3.3.2.6 X-ray photoelectron spectroscopy

The AXIS SUPRA X-Ray photoelectron spectroscopy (XPS) equipment was used to provide information on the position of the valence band edge of the nanoparticles with respect to the Fermi level. The valence band maximum was determined under the following conditions: working pressure 1.8 × $10^{-8}$ Torr, 15mA emission current, resolution 80, with dwell time 100 and sweeps 2. Furthermore, the application of charge neutralizer mode was carried out due to the non-conductive nature of samples.

### 3.3.3 Photocatalytic degradation

#### 3.3.3.1 Photocatalytic activity

The photocatalytic activity of the as-synthesized nanoparticles was demonstrated by the degradation of Congo Red and Methylene Blue in aqueous solutions. The experiments

were carried using Lelesil Make TQR super degradation reactor. In this experiment, 0.5 g of the catalyst was added into 500 mL of dye (10 ppm). The high-pressure visible lamp attached to a UV controller unit and operating at 250 W was mounted in a glass tube with cooling water system around it which was then placed inside the 1000 mL flask with the dye solution in it. The flask was then placed on a magnetic stirrer and stirred for half an hour in the dark to ensure that the equilibrium between the adsorption-desorption of the dye on the surface of the catalyst is reached; then the solution was kept in the dark for 30 minutes. Thereafter the light source was switched on. During the reaction, 5 mL samples were withdrawn at different time intervals from the reactor to be analyzed with UV-Vis spectrophotometer.

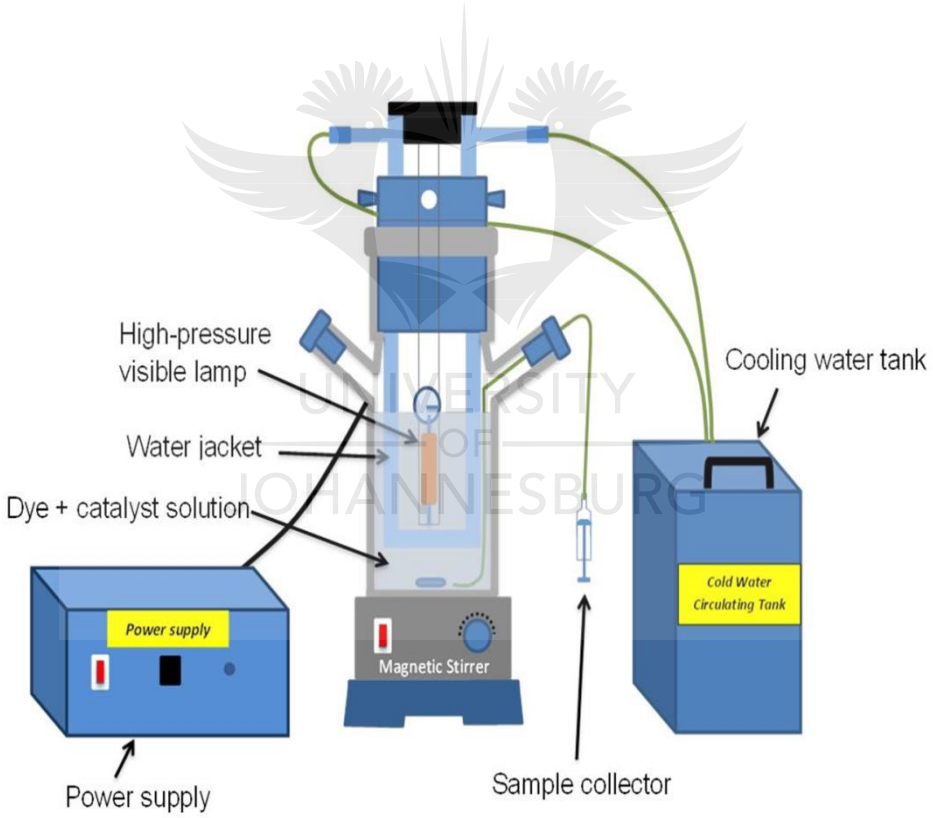


**Figure 3. 1**: Schematic representation of a photocatalytic reactor.

### 3.3.3.2 Surface Charge Analyses

Zeta potential measurements were done using a Zetasizer Nano ZS (Malvern). The zeta potential was determined by suspending nanoparticle (30 mg) in deionized (DI) water. The pH of the suspensions ranging from 2–10 was adjusted using 6 M NaOH and 6 M HCl.[7]

### 3.3.3.3 Ion Chromatography

The resulting $[SO_4]^{2-}$ and $Cl^-$ ions were measured using Ion chromatograph (IC, Dionex-ICS 2000) that was equipped with a Dionex Ion Pac AS18 (2 × 250 mm) column and a conductivity. A cocktail of the two dyes, Methylene Blue and Congo Red were prepared at different concentrations (1ppm, 5ppm, 20ppm, 50ppm, 70ppm, 100ppm) and 10ppm of each dye for the calibration curve. Thereafter, the degradation samples were then injected into the IC for analysis.

## 3.4 References

1. Smith, S. J., Huang, B., Bartholomew, C. H., Campbell, B. J., Boerio-Goates, J., & Woodfield, B. F. La-Dopant Location in La-Doped γ-$Al_2O_3$ Nanoparticles Synthesized Using a Novel One-Pot Process. *J. Phys. Chem. C* **119,** 25053-25062 (2015).

2. Vamvasakis, I., Georgaki, I., Vernardou, D., Kenanakis, G. & Katsarakis, N. Synthesis of $WO_3$ catalytic powders : evaluation of photocatalytic activity under NUV/visible light irradiation and alkaline reaction pH. *J. Sol-Gel Sci. Technol.* **76,** 120-128 (2015).

3. Harshulkhan, S. M., Ganapthy, S. R., Janaki, K., Velraj, G. & Nagarajan, M. Effect of Ag doping on structural, optical and photocatalytic activity of tungsten oxide ($WO_3$) nanoparticles. *J. Mater. Sci. Mater. Electron*. **27,** 3–10 (2016).

4. Harshulkhan, S. M. & Krishnaraj, S. Structural and optical properties of Ag doped

tungsten oxide ($WO_3$) by microwave-assisted chemical route. *J. Mater. Sci. Mater. Electron.* **27,** 3158–3163 (2016).

5. Mohamed, M. A., Jaafar, J., Ismail, A. F., Othman, M. H. D. & Rahman, M. A. in *Membrane Characterization* 3-29 (Elsevier B.V., 2017).

6. Kumar, A., Keshri, S. & Kabiraj, D. Influence of annealing temperature on nanostructured thin films of tungsten trioxide. *Mater. Sci. Semicond. Process.* **17,** 43-52 (2014).

7. Simelane, S., Ngila, J. C. & Dlamini, L. N. The effect of humic acid on the stability and aggregation kinetics of $WO_3$ nanoparticles. *Part. Sci. Technol.* **35,** 632–642 (2017).

# CHAPTER 4
# RESULTS AND DISCUSSIONS

## 4.1 Introduction

Organic dyes including the cationic Methylene Blue and an anionic Congo Red are considered as hazardous chemical due to the high stability of these species. They are able to resist light and oxidation agents. Hence, they are able to by-pass the conventional method of anaerobic digestion. Both CR and MB commonly used in textile industries in for dyeing cotton, wool and silk. These dyes are detrimental to human and animal health and thus their introduction to water stream poses health risks, ecological and environmental concerns. Therefore, it is important that effluents containing MB and CR pollutants must be properly treated before they are released into water bodies.[1–3]

The process of degrading unmanageable organic pollutants is challenging since they cannot be adequately treated by conventional methods.[2] These methods include carbon adsorption, coagulation, ultrafiltration and reverse osmosis.[4] The conventional biological wastewater treatment method is not effective enough to treat dye wastewater since these dyes are less biodegradable. Furthermore, chemical and physical processes create a substantial amount of sludge and also cause secondary pollution owing to hazardous products that are being formed.[5]

Heterogeneous photocatalysis using semiconductor has demonstrated to be a useful means for the degradation of water pollutants.[6,7] Several efforts have been done to understand how it is able to degrade a wide variety of indistinct recalcitrant organics into compounds that are readily biodegradable and ultimately mineralizing them to innocuous $CO_2$ and water.[8,9] In light of the economical use of visible light radiation the development of semiconductor photocatalysts with high photocatalytic activity under visible light radiation is desirable.[10] Among numerous visibly active photocatalysts, is tungsten trioxide ($WO_3$). It is reported to be a nontoxic metal oxide, possessing physical

and chemical resilience toward photo corrosions and it is relatively abundant in nature. It is an *n*-type semiconductor with a wide band gap of between 2.4 and 2.8 eV, which makes it an interesting visible-light-driven photocatalysts.[11,12]

$WO_3$ has a broad display of band-gap values that guarantees considerable photoelectrocatalytic and photocatalytic applications under visible-light radiation.[13] However, pure $WO_3$ has some drawbacks as it has low conduction band level which does not provide potential that is adequate to react with strong oxidizing agents and thus result in fast recombination of photogenerated $e^-$ and $h^+$ and eventually lowering the photocatalytic activity of the catalyst.[12] Different strategies have been employed to modify their catalytic activity including non-metal and transition/noble metal doping.[14,15] Depending on the structure distortions, $WO_3$ exists in several phase transitions such as monoclinic, triclinic, orthorhombic and tetragonal.[16] $WO_3$ has positive valence band (VB) holes (+3.1 - 3.2 $V_{NHE}$), which is generally more positive than the oxidation potential. This makes it capable of efficiently photo oxidising a broad range of organic pollutants.[17] Furthermore, $WO_3$ has incredible stability in acidic conditions, making it a good candidate for the treatment of contaminated water.[18]



In this manuscript, we report the synthesis of pristine and lanthanum doped $WO_3$ nanoparticles, via a modified impregnation method. Furthermore, the influence of lanthanum on the structure and optical properties was investigated. Lanthanum is one of the widely investigated rare-earth metal elements due to its 4f electron configuration that often serve as a catalyst or promote catalysis. They are ideal dopants for modifying the electronic structure, crystal structure, surface adsorption and optical properties. Lanthanide ions can also form complexes with different Lewis bases, this leads to increased adsorption of organic compounds onto the surface of the catalyst and thus results in improved photocatalytic activity.[19–22] The photocatalytic properties of pristine and La-doped $WO_3$ nanoparticles were investigated on the photodegradation of a cationic Methylene blue (MB) and an anionic Congo Red (CR) in an aqueous phase as model pollutants. To the best of our knowledge, the investigation of photocatalytic

properties of La-doped $WO_3$ on these two different classes of dyes has not been carried before. Moreover, the optical bandgap shift depending on carrier concentration, the amount of doped lanthanum, and the pH of the reaction solution were also investigated.

## 4.2 Results and discussions

### 4.2.1. XRD

X-ray diffraction was utilized n determining the phase purity, crystallinity and structural analysis of the pristine *m*-$WO_3$ and La-doped $WO_3$ nanoparticles as shown in **Figure 4.1**. The X-ray patterns of the *m*-$WO_3$ at 2θ = 23.14º, 23.58º and 24.37º corresponding to (002), (020) and (-202) can be ascribed to those of monoclinic phase of $WO_3$. La-doped $WO_3$ exhibited the diffraction peak at 2θ = 23.14º, 23.64º and 24.43º correspond to (001), (020) and (200) planes of $WO_3$ with monoclinic structure. The observed XRD results indicate clear crystallinity of the synthesized nanoparticles. It was observed that there were no obvious diffraction peaks associated with the dopant. This may be due to the differences in the ionic radius. The ionic radius of $W^{6+}$ (0.64 Å), is much lower than that of $La^{3+}$ (1.15 Å) therefore it was difficult for $La^{3+}$ to enter the lattice of $WO_3$. $La^{3+}$ ions were most likely to be found on the surface of $WO_3$. Villa et al[23] also reported a monoclinic $WO_3$ with no crystal phases related to $La_2O_3$ on their investigated into the role of lanthanum in mesoporous $WO_3$ which was used to photocatalytically convert methane into methanol with water. The average crystallite size of the *m*-$WO_3$ and La-doped samples was calculated from the average of the diffraction peak (020) using the following Debye-Scherrer equation:

$$D = \frac{k\lambda}{\beta cos\theta} \quad \textbf{(4.1)}$$

Where *D* is the mean crystallite size, *λ* is the X-ray wavelength (0.1541 nm) for CuKa, *k* =0.89, *β* is the full width at half maximum and *θ* is the Bragg angle. The average crystallite size of *m*-$WO_3$ was found to be 12 nm and it was further decreased to 10 nm for 1-La-$WO_3$ and increased to 15 nm for 5-La-$WO_3$ sample.

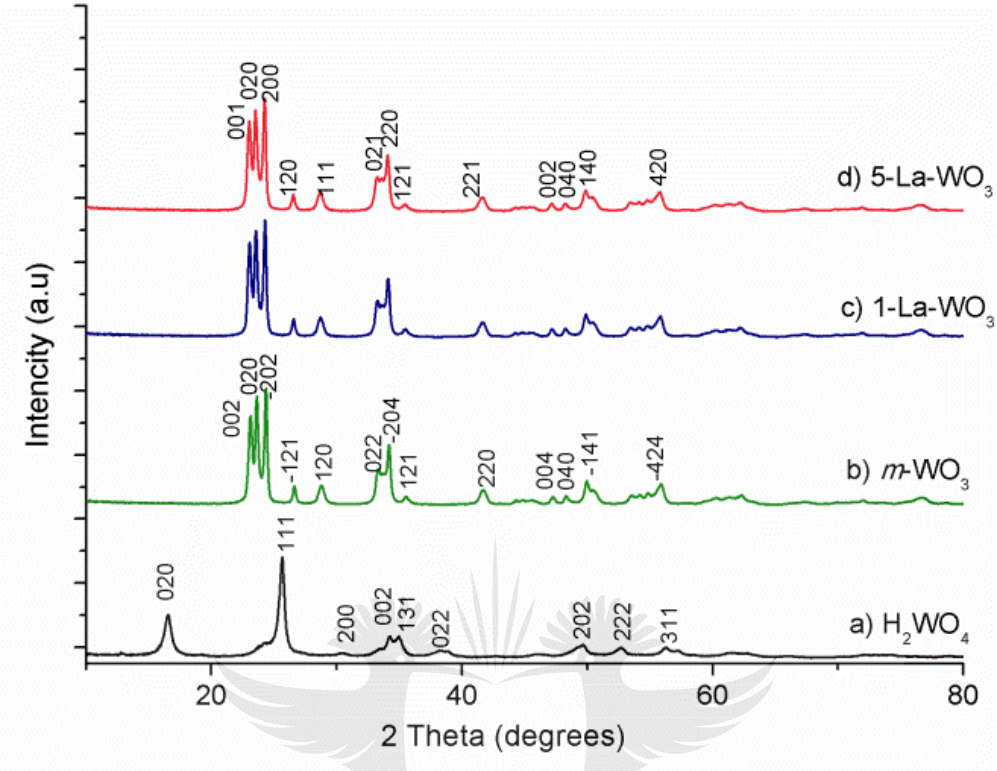


**Figure 4. 1**: XRD patterns for a) Tungstic acid, b) m-WO3, c) 1% La, d) 5% La.



### 4.2.2. Raman spectroscopy

Raman Spectroscopy was used to ascertain the polymorphic nature and bonding environment information about the *m*-$WO_3$ and La-doped $WO_3$ materials. **Figure 4.2** shows the modes at 806 $cm^{-1}$ and 713 $cm^{-1}$ corresponding to the stretching vibrations of O-W-O, whereas the modes at 325 $cm^{-1}$ and 266 $cm^{-1}$ correspond to bending vibrations of W-O-W. All samples contained the characteristic peaks of the monoclinic phase of $WO_3$ nanoparticles, which was consistent with the XRD results. Subsequent to La doping, the peaks intensities were lowered and the most intense peaks at 713 and 806 $cm^{-1}$, become wider. The crystallite size, crystal structure defects had a great influence on the shape, peaks position and relative intensities of the Raman spectra of $WO_3$.[23–25] Furthermore, the Raman bands which typically appear at 104, 191 and 411 $cm^{-1}$ and are assigned to $La_2O_3$ were not observed in the La-doped samples, confirming that lanthanum may be dispersed on the surface of the catalyst.[16,27] Similarly, Villa et al[23]

and Khalid et al[27] reported that the $La^{3+}$ may be found dispersed on the surface of the catalyst due to the difference in their ionic radii.

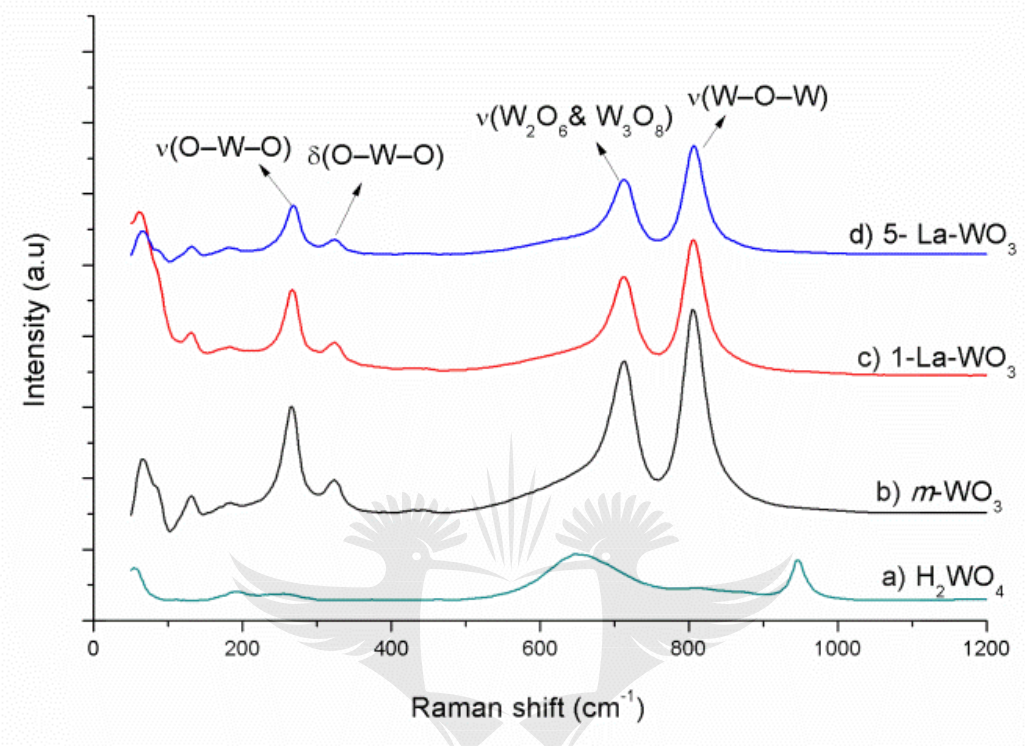


**Figure 4. 2:** Raman spectra of a) Tungstic acid, b) *m*-$WO_3$, c) 1-La-$WO_3$, d) 5-La-$WO_3$.



### 4.2.3. FTIR spectroscopy

$WO_3$ nanoparticles consist of packed corner sharing $WO_6$ octahedral, with W atoms located in the centre and O atoms at the vertices and thus forming W-O-W connections. This arrangement provides IR with fundamental normal modes of vibration of W=O, W-O and W-O-W. The IR spectra in **Figure 4.3** shows the broad absorption peaks in the region 499-972 $cm^{-1}$ which are characteristic of W=O, W-O and O-W-O stretching vibrations in the $WO_3$ crystal lattice. The peaks at 1012- 1197 $cm^{-1}$ are attributed to weak hydrogen bonded W-OH groups and these peaks disappear on the La-doped samples. This decrease is an indication of the presence of lanthanum in the prepared samples. The observed bands at 1380-1651 $cm^{-1}$ are characteristic of OH bands, which are attributed with the surface hydroxyl groups, and solvent those are weakly bound.

Strong broadband at 3021-3685 $cm^{-1}$, characterizes intercalated water molecules (W-OH…..H2O). The decrease in these bands may be due to physisorption.[28–30] The presence of these peaks is an indication of the formation of $WO_3$ nanoparticles. These results are in agreement with FTIR results that are reported by Prabhu et al[28] on their study of the effects that temperature had on the optical and structural properties of $WO_3$ nanoparticles that were prepared by the solvo thermal method.

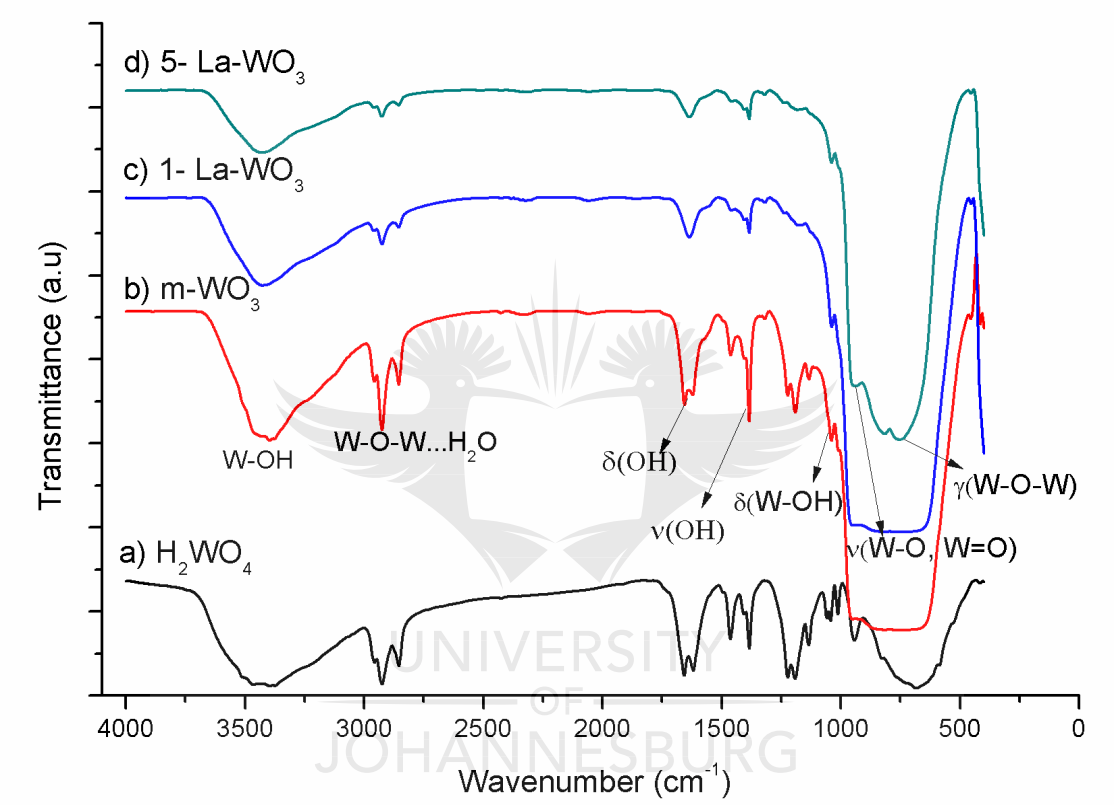


**Figure 4. 3:** FTIR spectrum of a) Tungstic acid, *m*-$WO_3$ and 1% to 5% La doped $WO_3$ nanoparticles.

### 4.2.4. Morphological analysis

Investigation of morphology and particle size was carried through TEM, SAED and EDX. The images of *m*-$WO_3$ and 5-La-$WO_3$ nanoparticles are represented in **Figure 4.4**. **Figure 4.4** (a) and (b) shows the TEM images of both the *m*-$WO_3$ and 5-La-$WO_3$. The nanoparticles have a distinct mixture of spherical and rod-shaped morphology. The spherical shapes sizes of the *m*-$WO_3$ and 5-La-$WO_3$ were found to be 45 nm and 55 nm

respectively. The estimated average particle size from XRD data was much smaller compared to the one extrapolated from TEM images. This may be due to the agglomeration of smaller particles. Similar particle size differences were observed by Harshulkhan et al.[29] During their research on the effects that silver doping has on the optical, structural and photocatalytic activity of $WO_3$ nanoparticles.

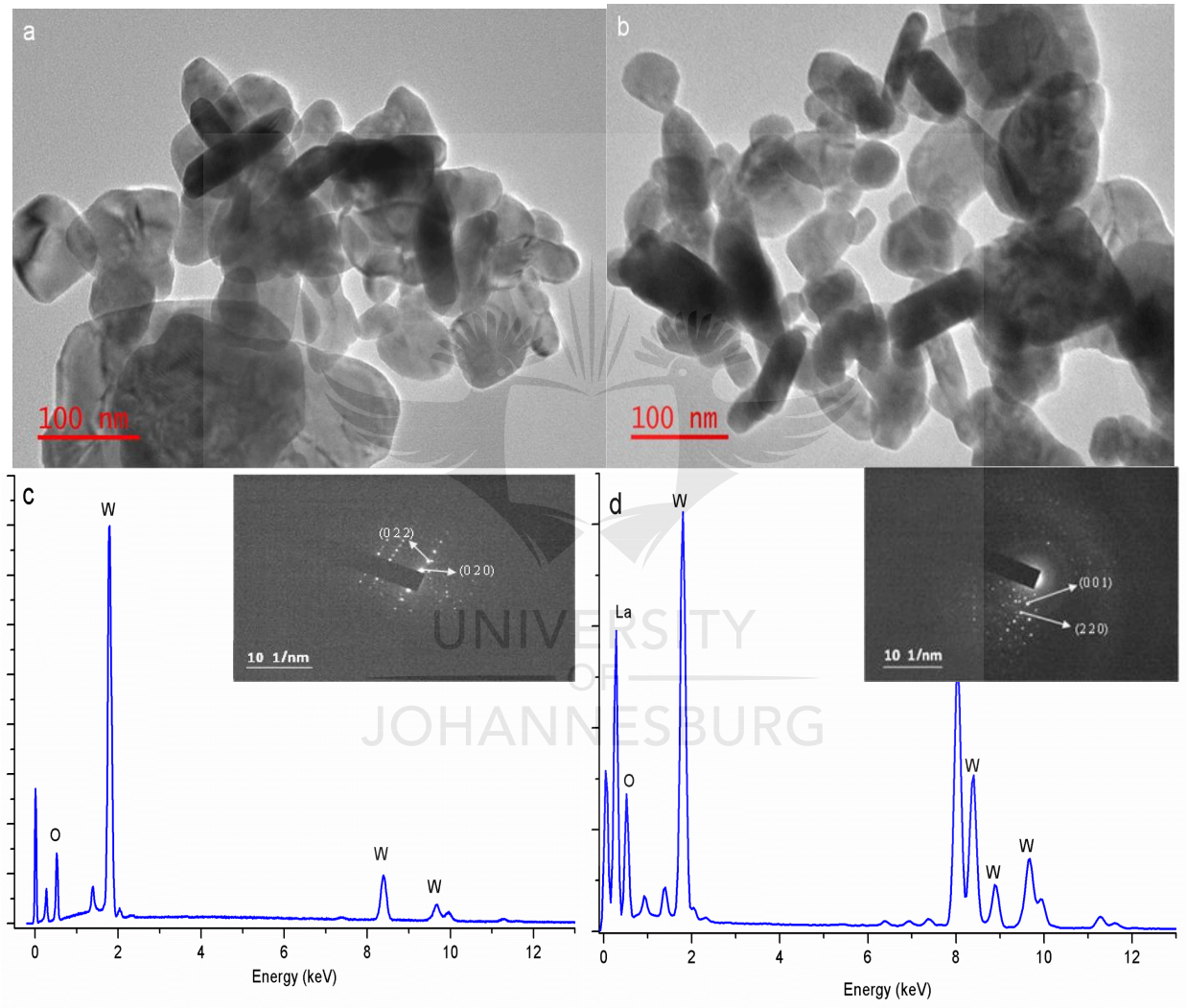


**Figure 4. 4** TEM images for (a) *m*-$WO_3$ and (b) 5-La-$WO_3$; and EDX (c) m-$WO_3$ and (d) 5-La-$WO_3$ with SAED images inserts.

The SEM images in **Appendix A** of *m*-$WO_3$ and 5-La$WO_3$ clearly indicated that the morphology of both the samples is spherical. The EDX spectra represented in **Figure**

**4.4** (c) and (d), showed the presence of oxygen, tungsten and lanthanum. The peaks corresponding to copper and carbon arise from the grid used for EDX analysis. The SAED patterns inserted in **Figure 4.4** (c) and (d), were found to be (022), (020) for the *m*-$WO_3$ and (001), (220) for 5-La-$WO_3$ respectively which compares well with X-ray data.

### 4.2.5. Optical properties

The optical properties of the synthesized samples were explored by solid-state UV-Vis diffuse reflectance. The results are reflected in **Figure 4.5**. The doped samples showed higher intensity than the *m*-$WO_3$, furthermore, it was observed that the absorbance spectrum of La-doped sample slightly shifted toward the shorter wavelength (blue shift). This blue shift is an indication of the increased band gap. The relationship $h\nu = \frac{1240}{\lambda}$ where h*v* and λ are the band gap energy and wavelength respectively was used to estimate the band gap energy of the synthesized samples. The insert is a graph plot of $(\alpha h\nu)^2$ vs $h\nu$, where α is the absorption coefficient, h is the Planck's constant, *v* is the frequency of incident light. The band gap energy of the *m*-$WO_3$, 1-La-$WO_3$ 5-La-$WO_3$ nanoparticles were found to be 2.45, 2.42 and 2.57 eV respectively. A similar band gap of 2.66 eV for monoclinic $WO_3$ was reported by Hunge et al.[31] on their photocatalytic degradation efficiency studies of $WO_3$ thin films on MB. The decrease in the band gap of the La-doped sample is attributed to the doping of lanthanum which could create impurity levels below the conduction band of $WO_3$ nanoparticles.[32] The observed increase in the band gap may be attributed to the high doping of lanthanum.[33–35]

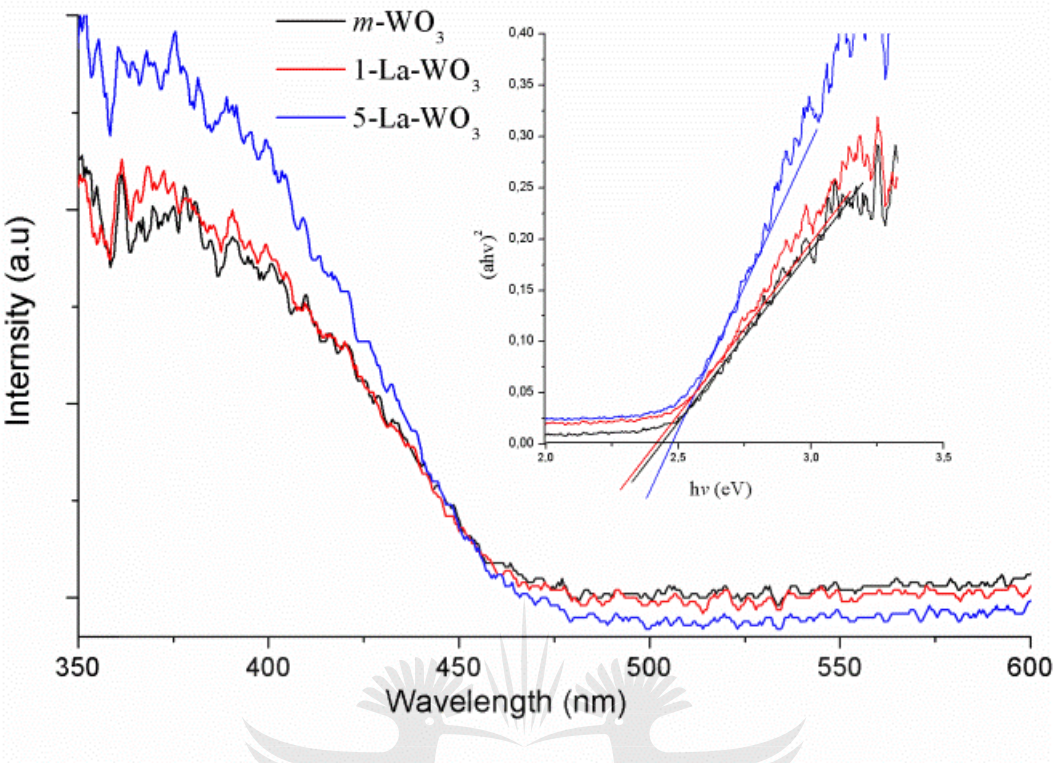


**Figure 4. 5:** UV-Vis diffuse reflectance spectra for pristine m-$WO_3$ and La-doped $WO_3$ nanoparticles. The insert is a plot of $(\alpha h\nu)^2$ versus photon energy.



The band edge positions shown in **Figure 4.6** were calculated to indicate the effect of lanthanum on the band gap of the semiconductor. The valence band (VB) and conduction band (CB) position were calculated using the empirical formulas **(4.2)** and **(4.3)**.

$$E_{CB} = X - E_e - \frac{1}{2}E_g \qquad \textbf{(4.2)}$$

$$E_{VB} = E_{CB} + E_g \qquad \textbf{(4.3)}$$

where *X* =absolute electronegativity of an atom in a semiconductor, and it is described as the arithmetic means of the atomic electron affinity and the first ionization energy; $E_e$

=energy of free electrons of the hydrogen scale (4.5 eV); $E_{CB}$ =CB potential and $E_{VB}$ =the VB potential. **Table 1** Shows the calculated band edge results.[36]

**Table 1**. Band edge for pristine *m*-$WO_3$ and La doped $WO_3$.

| Material | $E_{CB}$ (eV) | $E_{VB}$ (eV) |
|---|---|---|
| *m*-$WO_3$ | 0.855 | 3.305 |
| 1-La-$WO_3$ | 1.140 | 3.560 |
| 5-La-$WO_3$ | 0.795 | 3.365 |

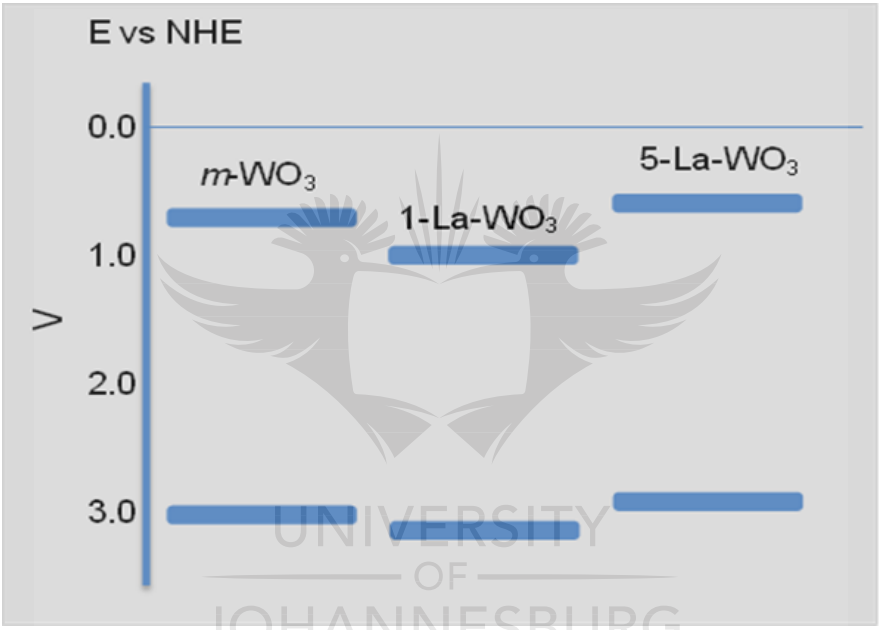


**Figure 4. 6:** The band edge positions of *m*-$WO_3$ and La-doped $WO_3$

The calculated band edge positions infer the change in the position of both VB and CB of the doped samples with respect to the pristine $WO_3$. Further analysis to confirm the band positions was done with XPS. The XPS data provide useful information on the valence band edge position with respect to the Fermi level ($E_F$). In **Figure 4.7** the analysis of valence band edge was performed in order to establish the location of the valence band maximum (VBM) with respect to the Fermi level position (which corresponds to 0 eV binding energy). The VBM was determined by extrapolating two

solid lines from the background and the straight cut off in the spectra. The determined VBM values for *m*-$WO_3$ and 5-La-$WO_3$ were 2.85 eV and 2.82 eV respectively, implying that the VBM was below the Fermi level. The direct band-gap of *m*-$WO_3$ and 5-La-$WO_3$ were estimated to be 2.45 and 2.57 eV from the intercept, as shown in **Figure 4.5** insert.

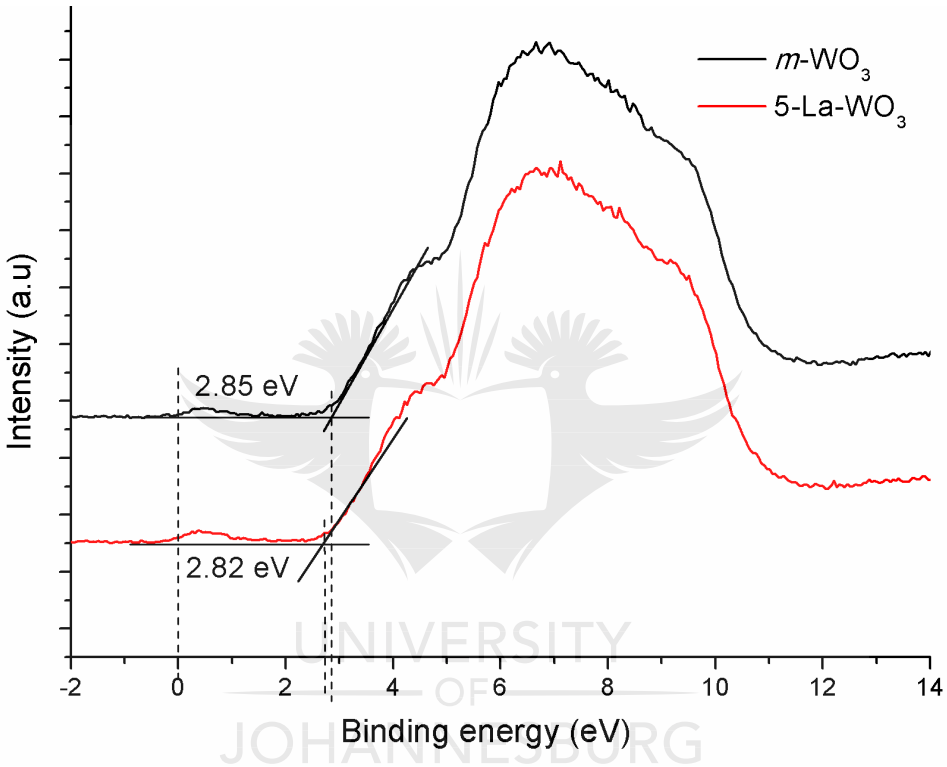


**Figure 4. 7:** XPS spectra for *m*-$WO_3$ and 5-La-$WO_3$ showing the valence band maximum.

Therefore, for *m*-$WO_3$, by combining the measurement from the XPS (VBM is at 2.85 eV) and the optical band-gap value using **Equation 4.3**, the conduction band energy was 0.4 eV below the Fermi level. In 5-La-$WO_3$, the combination of the VBM and optical band gap resulted in conduction band energy of 0.26 eV below the Fermi level.[37,38] Thus when depicting this information in a graphical form in **Figure 4.8**, the results are in agreement with the calculated band edge positions from DRS data depicted in **Figure 4.6**.

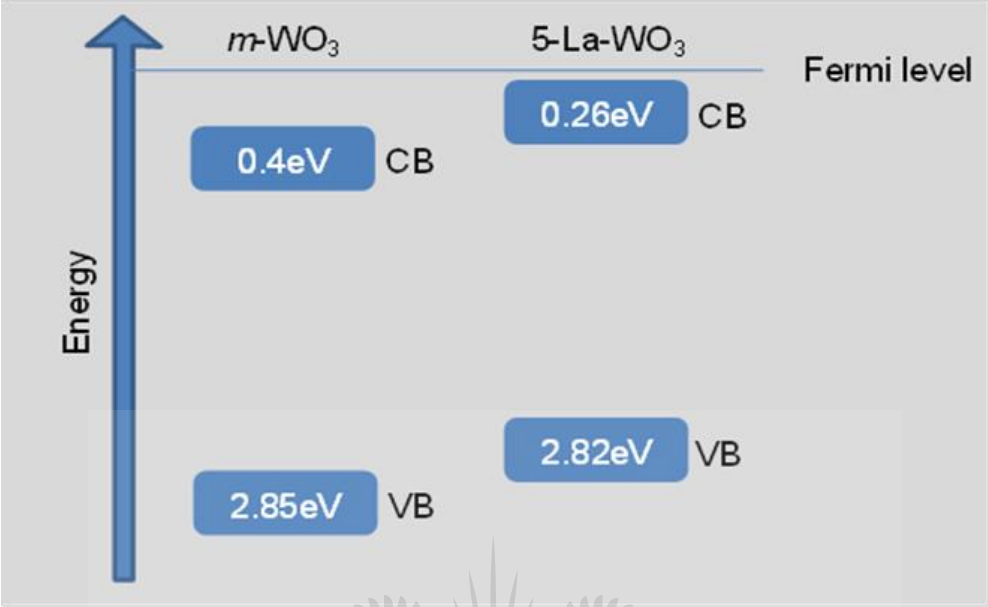


**Figure 4. 8:** Band edge position from the XPS data.

The experimental results demonstrated that 1 and 5% doped $WO_3$ nanoparticles having high VBM are able to generate higher oxidation holes, thus show showing photocatalytic oxidation capabilities. Moreover, the up-shifting of conduction band minimum generates more electrons that react with adsorbed oxygen molecules on the surface.



## 4.3 Photocatalytic activity studies

### 4.3.1 Zeta potential

Zeta potential measurements were used to explains the solid/liquid interfacial charge processes and interactions between the surface of the catalysts and the dyes. The solution pH plays a significant part in characterizing dyes as well as in reaction mechanisms that may influence dye degradation. By making adjustments to the solution pH, the photocatalytic removal efficiency of the catalyst can be significantly enhanced. The Zeta Potential data for the synthesized nanoparticles is presented in **Figure 4.9**. The point at which the Zeta potential shifted to zero (point of zero charge, $P_{zc}$) was

found to be at about pH 3.5-3.8. These results revealed that $WO_3$ surface becomes positively charged at pH < 3.8, and it is negatively charged at pH above 3.8. Similar findings were reported by Simelane et al.[39] on their studies of the effects that humic acid had on the aggregation kinetics and stability of $WO_3$ nanoparticles.

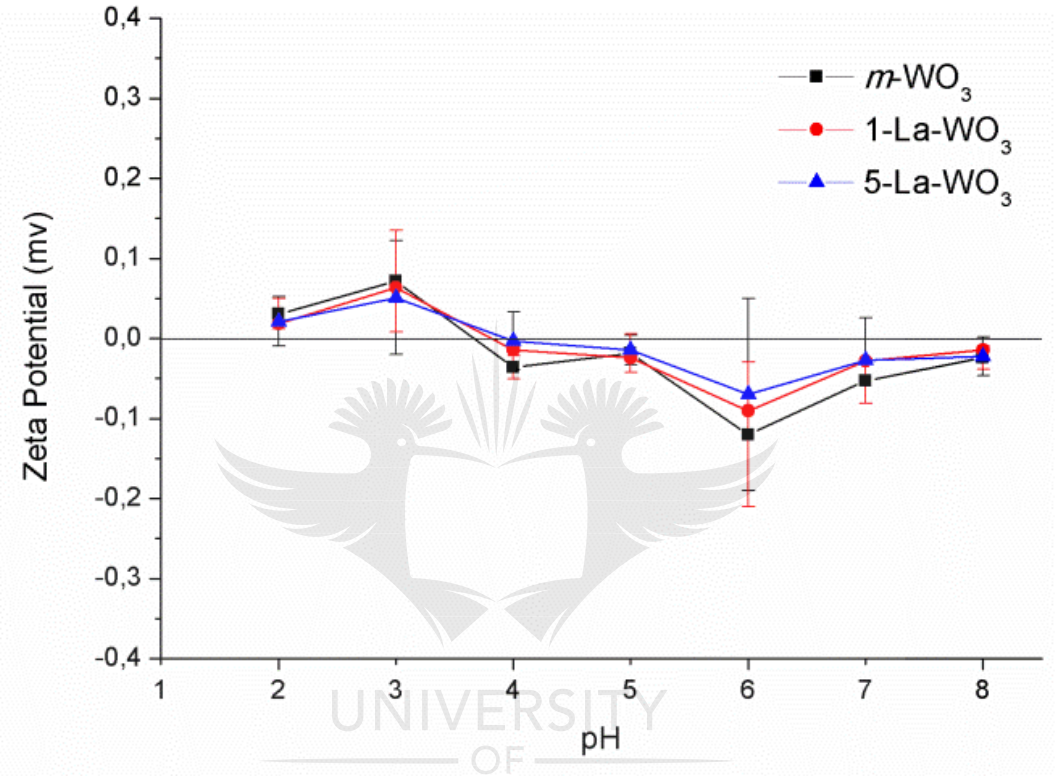


**Figure 4. 9:** Zeta Potential of 1-La-WO3 and 5-La-WO3.

### 4.3.2 The effect of solution pH

The zeta potential data established that the photocatalytic nanoparticles exhibited a transition in potential with respect to pH. At low pH, the nanoparticles had positive potential and at high pH, they had a negative potential. Alkaim et al.[40] studied the effects that pH had on the adsorption process and photocatalytic degradation efficiency of different catalysts when used to remove MB, and reported pH to be an important parameter in the photocatalytic reactions that occurs on surfaces of the catalyst. Methylene Blue is a cationic dye when dissolved in water. It was observed that at higher

pH (pH = 6), MB adsorbed on the surface of the catalyst. As the pH of the dye solution changed to more neutral, the surface to the photocatalyst acquired negative charges. Therefore the increasing electrostatic attraction between the photocatalyst that is negatively charged and positively charged dye resulted in increased adsorption of the MB dye.[41] In contrast, CR is an anionic dye. Hence the adsorption capacity increased when the pH was low (pH = 2), due to CR containing positively charged sulfonic groups. In acidic conditions, the CR molecules with sulfonic groups ionize easily and become a soluble CR anion and thus the interaction between the catalyst surface that is positively charged and the negatively charged CR dye favoured adsorption.[41,42]

### 4.3.3 Photocatalytic and kinetic measurements

The photocatalytic properties of pristine and La-doped $WO_3$ samples were evaluated by the degradation of Methylene blue and Congo red under visible light irradiation. The concentration of the dyes was calculated using the absorbance at maximum wavelengths of both MB and CR dyes vs the initial concentration before and during visible light irradiation. The degradation of MB and CR aqueous solutions was monitored at 664nm and 567nm wavelength respectively as illustrated in **Figure 4.10**. In MB, the decrease that is observed in the absorption band appearing at 664 nm is used to monitor the rate of decolourization of the dye, whereas the reductions in absorbance at 290 nm peak is an indication of the degradation of the aromatic portion of the dye.[3,43]



The photocatalytic experimental results indicated a gradual decrease of the bands at 664 and 290 nm with an increase in exposure time and finally disappearing after 60 minutes of irradiation time, indicating a complete degradation of MB, whereas CR absorption spectra showed almost complete degradation without visible light. Furthermore, it was observed that the absorbance peak shifted from 664 to about 640nm. suggesting that both chromophore and aromatic parts of methylene blue were breaking down and forming byproducts.[44,45] Similar absorbance peaks were reported by Amini et al[46] on their investigation of the photocatalytic degradation activity of MnOx/WO3 nanoparticles on methylene blue.

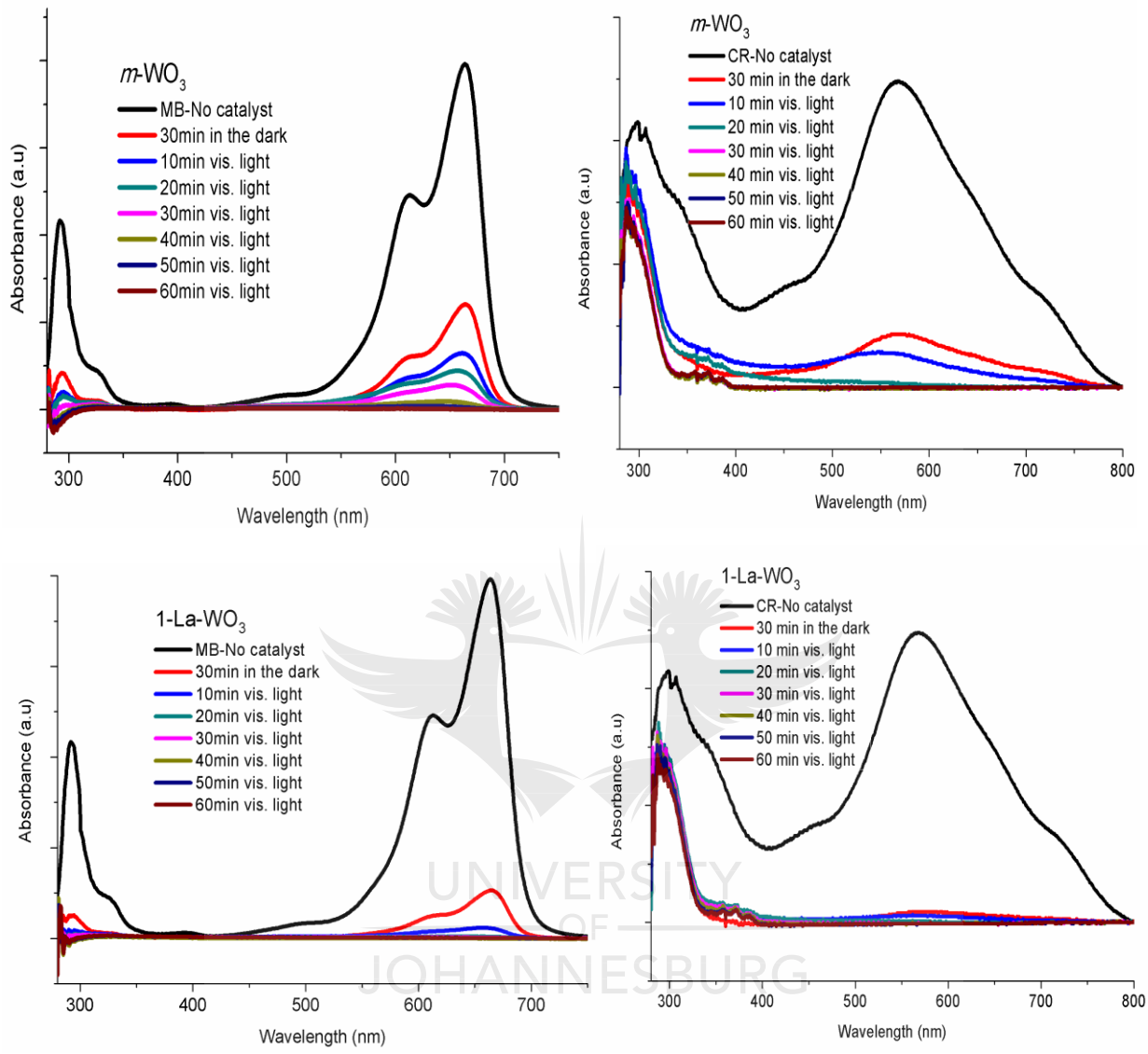


**Figure 4. 10:** Photocatalytic degradation of MB and CR by (a) & (b) *m*-$WO_3$, (c) & (d) 1-La-$WO_3$ and (e) & (f) 5-La-$WO_3$.

During the course of the degradation process, the observed continuous decrease in absorbance peaks indicates a decrease in the concentration of MB and CR. This decrease was confirmed by the reaction solution decolouration and the degradation percentage (%) was obtained by using the formulation illustrated in **Equation 4** and the results representing the degradation percentage of the dye concentration before and

after visible light irradiation in the presence of pristine and La-doped $WO_3$ samples are depicted in **Figure 4.11**.

$$Degradation\ (\%) = \left(1 - \frac{C}{C_0}\right) \times 100 \qquad \textbf{(4.4)}$$

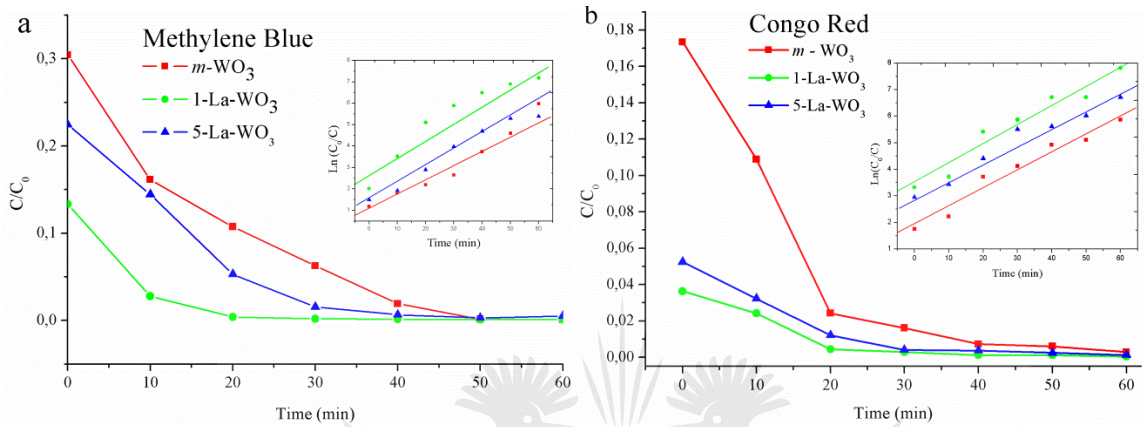


**Figure 4. 11:** Photocatalytic degradation of (a) MB and (b) CR by as synthesized photocatalysts.

It was found that the 89.0, 99.6 and 94.7 of MB and 97.0, 99.6 and 98.5% of CR were degraded in just 20 minutes under visible light by pristine $WO_3$ and La (1 and 5wt%) doped $WO_3$ photocatalysts. The photocatalytic activity increased at 1% La doped $WO_3$ and reduced with 5% $WO_3$. The activity evaluation indicated that low amounts of lanthanum ions could improve the activity by acting as a trap for photogenerated holes and elections and thus inhibit recombination. However further increase in La doping slightly reduced the efficiency of the catalyst, this indicates that there is the presence of an optimal loading. The decreased photocatalytic activity with high La doping may be related to the increased absorption and scattering of a photon by the remaining lanthanum in the photoreaction system.[27] The kinetics of the degradation process of methylene blue was studied and the linear behaviour was verified using the pseudo-first-order kinetic model depicted in **Equation 4.5**. The slope of which upon linear regression equals the apparent first-order rate constant *k*.

$$\ln\left(\frac{C_0}{C_t}\right) = kt \qquad \textbf{(4.5)}$$

Where $C_o$ =the concentration of the first solution (ppm), $C_t$ =the actual concentration (ppm) of each solution at a time 't', t =the irradiation time (min), and $k$ =the degradation rate constant of methyl orange dye solution. The plots ln($C_0$/$C_t$) vs. irradiation time for dyes are inserted in **Figure 4.11**. The highest rate constant, 1.19 × $10^{-1}$ $min^{-1}$ (MB) and 2.60 × $10^{-1}$ $min^{-1}$ (CR) was observed when the photocatalyst with 1% lanthanum loading was used in the degradation of both dyes, which was higher than the pristine (MB, 9.90 × $10^{-2}$ $min^{-1}$ and CR, 1.95× $10^{-1}$ $min^{-1}$) and 5% lanthanum doped $WO_3$ (MB, 8.9 × $10^{-1}$ $min^{-2}$ and CR, 2.2 × $10^{-1}$ $min^{-1}$) nanoparticles. These results indicate that the photocatalytic performances of the 1% La-doped $WO_3$ are more efficient as compared to the pure $WO_3$ and 5% La-doped $WO_3$ under visible-light illumination.

### 4.3.4 Ion Chromatography measurements

To confirm the degradation of MB CR, the evolution of $Cl^-$ and $[SO_4]^{2-}$ ions were measured using IC. As illustrated, in **Figure 13 (a)**, $Cl^-$ ions from MB were liberated at much higher amounts with 1% loading of lanthanum than in both pristine and 5% La doped catalysts. However, in CR, the liberated $[SO_4]^{2-}$ ions were at higher amounts in both 1% La-$WO_3$ and 5% La-$WO_3$. Confirming that all chloride and sulphate atoms were removed from both MB and CR.

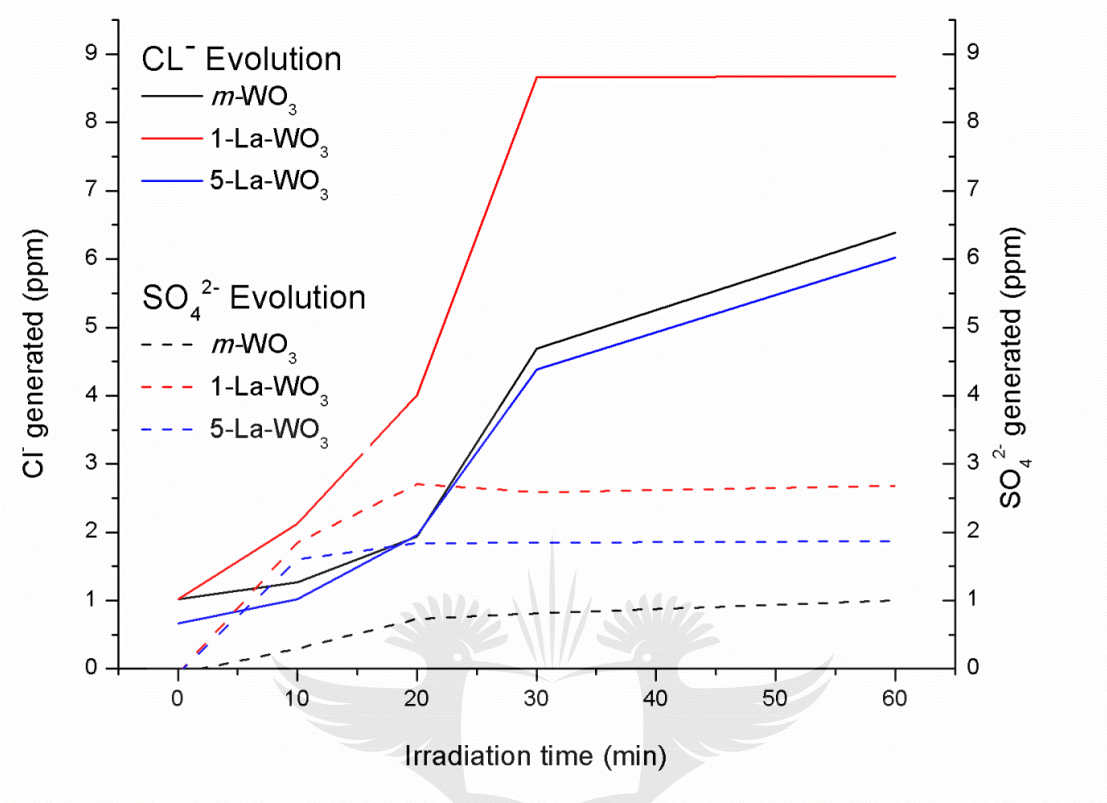


**Figure 4. 12:** Evolution of (a) $IC^-$ and (b) $SO_4^{2-}$



From these outcomes, it is evident that the presence of lanthanum improved the photocatalytic activity of $WO_3$. It has been generally acknowledged that metal oxide particles could act as electron sink in the metal photocatalytic system.[14] In particular, lanthanides are able to form complexes with different Lewis bases including amines, organic acids, aldehydes, thiols and alcohols. They form these complexes via interactions between the functional groups and their f-orbital.[4,27] Thus, doping lanthanide ions provided intends to concentrate organic pollutants on the surface of the semiconductor and therefore improved the separation efficiency of photogenerated electron-hole pairs of $WO_3$ to improve the photocatalytic activity.[47]

When $WO_3$ absorbs the light which has energy that equal to or more than its band gap, electron-hole pairs are created in $WO_3$. While some electron-hole pairs are recombined,

the remaining photogenerated hole/electron pairs are relocated to the surface of the $WO_3$, permitting reaction with chemical compounds that are adsorbed on the surface. The adsorbed oxygen scavenges produced electron which then leads to $H_2O_2$, followed by the production of hydroxyl radicals ($^{\bullet}OH$). The active hydroxyl radicals are the ones that are responsible for the degradation of the dyes.[14,40,48] It can be envisaged that lanthanum played a role in increasing the adsorbed water on the $WO_3$ surface which increased the generation of OH to take part in the photocatalytic reactions.[23]

## 4.4 References


1. Wahi, R. K., Yu, W. W., Liu, Y., Mejia, M. L., Falkner, J. C., Nolte, W., & Colvin, V. L. Photodegradation of Congo Red catalyzed by nanosized $TiO_2$. *Elsevier* **76,** 64-69 (2008).
2. Mahlambi, M. M., Ngila, C. J. & Mamba, B. B. Recent Developments in Environmental Photocatalytic Degradation of Organic Pollutants: The Case of Titanium Dioxide Nanoparticles-A Review. *J. Nanomater.* **2015,** 1-30 (2015)..
3. Abou-Gamra, Z. & Ahmed, M. A. Synthesis of mesoporous $TiO_2$-curcumin nanoparticles for photocatalytic degradation of methylene blue dye. *J. Photochem. Photobiol. B Biol.* **160,** 134-141 (2018).
4. Nešić, J., Manojlović, D. D., Anđelković, I., Dojčinović, B. P., Vulić, P. J., Krstić, J., & Roglić, G. M. Preparation, characterization and photocatalytic activity of lanthanum and vanadium co-doped mesoporous $TiO_2$ for azo-dye degradation. *J. Mol. Catal.* **378,** 67-75 (2013).
5. Bari, Q. & Bhardwaj, N. Role of bio-sorbents in the decolorization of some commonly used dyes. *J. Sci.* **4,** 637-642 (2014).
6. Ibhadon, A. O. & Fitzpatrick, P. Heterogeneous Photocatalysis: Recent Advances and Applications. *Catayst* **3,** 189-218 (2013).
7. Kumar, S. G. & Rao, K. S. R. K. Tungsten-based nanomaterials ($WO_3$ & $Bi_2WO_6$): Modifications related to charge carrier transfer mechanisms and photocatalytic applications. *Appl. Surf. Sci.* **355,** 939-958 (2015).

8. Hernandez-Ramirez, A. & Medina-Ramrez, I. *Photocatalytic Semiconductors: Synthesis, Characterization, and Environmental Applications*. *Springer International Publishing Switzerland* (Springer International Publishing Switzerland, 2015).
9. Ghaly, A. E., Ananthashankar, R., Alhattab, M. & Ramakrishnan, V. V. Production, Characterization and Treatment of Textile Effluents: A Critical Review. *J Chem Eng Process Technol* **5,** 1-19 (2014).
10. Sánchez-Martínez, D., Martínez-de la Cruz, A., López-Cuéllar, E. Synthesis of $WO_3$ nanoparticles by citric acid- assisted precipitation and evaluation of their photocatalytic properties. *Mater. Res. Bull.* **48,** 691-697 (2013).
11. Heidari, E. K., Marzbanrad, E., Zamani, C. & Raissi, B. Nanocasting Synthesis of Ultrafine $WO_3$ Nanoparticles for Gas Sensing Applications. *Nanoscale Res Lett* **5,** 370-373 (2010).
12. Ding, J., Chai, Y., Liu, Q., Liu, X., Ren, J., & Dai, W. Selective Deposition of Silver Nanoparticles onto $WO_3$ Nanorods with Different Facets : The Correlation of Facet-Induced Electron Transport Preference and Photocatalytic Activity. *J. Phys. Chem.* **120,** 4345-4353 (2016).
13. Wicaksana, Y., Liu, S., Scott, J. & Amal, R. Tungsten Trioxide as a Visible Light Photocatalyst for Volatile Organic Carbon Removal. *Molecules* **19,** 17747-17762 (2014).
14. Lee, H., Kim, M., Sohn, D., Kim, S. H., Oh, S.-G., Im, S. S., & Kim, I. S. Electrospun tungsten trioxide nanofibers decorated with palladium oxide nanoparticles exhibiting enhanced photocatalytic activity. *R. Soc. Chem. Adv.* **7,** 6108-6113 (2017).
15. Marschall, R. & Wang, L. Non-metal doping of transition metal oxides for visible-light photocatalysis. *Catal. Today* **225,** 111-135 (2014).
16. Baserga, A., Russo, V., Fonzo, F. Di, Bailini, A., Cattaneo, D., Casari, C. S., Bassi, A. L., Bottani, C. E. Nanostructured tungsten oxide with controlled properties : Synthesis and Raman characterization. *Thin Solid Films* **515,** 6465-6469 (2007).

17. Asim, N., Syuhami, M. F., Badiei, M. & Yarmo, M. A. $WO_3$ Modification by Synthesis of Nanocomposites. *Procedia-Soc. Behav. Sci.* **9,** 175-180 (2014).
18. Sánchez-Martínez, D., Martínez-de la Cruz, A. & López-Cuéllar, E. Synthesis of $WO_3$ nanoparticles by citric acid-assisted precipitation and evaluation of their photocatalytic properties. *Mater. Res. Bull.* **48,** 691-697 (2013).
19. Milanovic, M. & Nikolic, L. M. Modification of TiO2 nanoparticles through lanthanum doping and PEG templating. *Process. Appl. Ceram.* **8,** 195-202 (2014).
20. Smith, S. J., Huang, B., Bartholomew, C. H., Campbell, B. J., Boerio-Goates, J., & Woodfield, B. F. La-Dopant Location in La-Doped γ-$Al_2O_3$ Nanoparticles Synthesized Using a Novel One-Pot Process. *J. Phys. Chem. C* **119,** 25053-25062 (2015).
21. Yao, S., Jia, X., Jiao, L., Zhu, C. & Shi, Z. La-doped $TiO_2$ hollow fibers and their photocatalytic activity under UV and visible light. *indian J. Chem.* **51,** 1049-1056 (2012).
22. Wang, C., Zhu, Q., Gu, C., Luo, X., Yu, C., & Wu, M. Photocatalytic degradation of two different types of dyes by synthesized La/$Bi_2WO_6$. *RSC Adv.* **6,** 85852-85859 (2016).
23. Villa, K., Murcia-lópez, S., Ramón, J. & Andreu, T. An insight on the role of La in mesoporous $WO_3$ for the photocatalytic conversion of methane into methanol. *Appl. Catal. B, Environ.* **187,** 30-36 (2016).
24. Mehmood, F., Iqbal, J., Jan, T., Ahmed, W., Ahmed, W., Arshad, A., Mansoor, Q., Ilyas, S. Z., Ismail., & Ahmad, I. Effect of Sn doping on the structural , optical , electrical and anticancer properties of $WO_3$ nanoplates. *Ceram. Int.* **42,** 14334-14341 (2016).
25. Pal, M., Pal, U., Miguel, J., Jiménez, G. Y. & Pérez-rodríguez, F. Effects of crystallization and dopant concentration on the emission behavior of $TiO_2$: Eu nanophosphors. *Nanoscale Res. Lett.* **7,** 1-12 (2012).
26. Díaz-reyes, J., Castillo-ojeda, R., Galván-arellano, M. & Zaca-moran, O. Characterization of $WO_3$ Thin Films Grown on Silicon by HFMOD. *Hindawi* **2013,** 1-9 (2013).

27. Khalid, N. R., Ahmed, E., Hong, Z. & Ahmad, M. Applied Surface Science Synthesis and photocatalytic properties of visible light responsive La/$TiO_2$-graphene composites. *Appl. Surf. Sci.* **263,** 254-259 (2012).
28. Prabhu, N., Agilan, S., Muthukumarasamy, N., Senthilkumaran, C. K. Effect of temperature on the structural and optical properties of $WO_3$ nanoparticles prepared by solvo thermal method. *Dig. J. Nanomater. Biostructures* **8,** 1483-1490 (2013).
29. Harshulkhan, S. M., Ganapthy, S. R., Janaki, K., Velraj, G. & Nagarajan, M. Effect of Ag doping on structural , optical and photocatalytic activity of tungsten oxide ($WO_3$) nanoparticles. *J. Mater. Sci. Mater. Electron.* 3-10 (2016).
30. Ghosh, S., Acharyya, S. S., Bal, R. & Kumar, M. One-pot preparation of nanocrystalline Ag-$WO_3$ catalyst for the selective oxidation of styrene. *R. Soc. Chem.* **5,** 37610-37616 (2015).
31. Hunge, Y. M., Mahadik, M. A., Mohite, V. S., Kumbhar, S. S., Deshpande, N. G., Rajpure, K. Y., Moholkar, A. V., Patil, P. S. & Bhosale, C. H. Photoelectrocatalytic degradation of methyl blue using sprayed $WO_3$ thin films. *J. Mater. Sci. Mater. Electron.* **27,** 1629-1635 (2016).
32. Ramkumar, S. Rajarajan, G. Effect of Fe doping on structural , optical and photocatalytic activity of $WO_3$ nanostructured thin films. *J. Mater. Sci. Mater. Electron.* **27,** 1847-1853 (2016).
33. Nagy, D., Nagy, D., Szilagyic, I. M. & Fan, X. Effect of the morphology and phases of $WO_3$ nanocrystals on their photocatalytic efficiency. *R. Soc. Chem.* **6,** 33743-33754 (2016).
34. Liu, J., Xu, L., Wei, B., Lv, W. & Zhang, X. One-step hydrothermal synthesis and optical properties of aluminium doped ZnO hexagonal nanoplates on a zinc substrate. *J. Phys. Chem. C* **13,** 1283-1286 (2011).
35. Javaid, S., Akhyar, M., Muneer, I., Shahid, M., Khaleeq-ur-rahman, M., & Ali, A. Super lattices and Microstructures Influence of optical band gap and particle size on the catalytic properties of Sm/$SnO_2$-$TiO_2$ nanoparticles. *Elsevier* **82,** 234-247 (2015).

36. Li, X., Yu, J., Low, J., Fang, Y., Xiao, J., & Chen, X. Engineering heterogeneous semiconductors for solar water splitting. *J. Mater. Chem. A* **3,** 2485-2534 (2015).
37. Taz, H., Sakthivel, T., Yamoah, N. K., Carr, C., Kumar, D., Seal, S., & Kalyanaraman, R. Transparent ferromagnetic and semiconducting behavior in Fe-Dy-Tb based amorphous oxide films. *Nat. Publ. Gr.* **6,** 1-8 (2016).
38. TC, S. K. & Gupta, G. Band alignment and Schottky behaviour of InN/GaN heterostructure grown by low-temperature. *RSC Adv.* **4,** 27308-27314 (2014).
39. Simelane, S., Ngila, J. C. & Dlamini, L. N. The effect of humic acid on the stability and aggregation kinetics of $WO_3$ nanoparticles. *Part. Sci. Technol.* **36,** 1-11 (2017).
40. Alkaim, A. F., Aljeboree, A., Jaafer, S. & Hussein, F. H. Effect of pH on Adsorption and Photocatalytic Degradation Efficiency of Different Catalysts on Removal of Methylene Blue. *Asian J. Chem.* **26,** 8445-8448 (2014).
41. Thu, T. N. T., Thi, N. N., Quang, V. T., Hong, K. N., Minh, T. N., & Hoai, N. L. T. Synthesis, characterisation, and effect of pH on degradation of dyes of copper-doped $TiO_2$. *J. Exp. Nanosci.* **11,** 226-238 (2016).
42. Erdemoğlu, S., Aksu, S. K., Sayılkan, F., Izgi, B., Asiltürk, M., Sayılkan, H., Frimmel , F., & Güçer, Ş. Photocatalytic degradation of Congo Red by hydrothermally synthesized nanocrystalline $TiO_2$ and identification of degradation products by LC-MS. *J. Hazard. Mater.* **155,** 469-476 (2008).
43. Zulkifili, A. N., Fujiki, A. & Kimijima, S. Flower-like $BiVO_4$ Microspheres and Their Visible Light-driven Photocatalytic Activity. *Appl. Sci.* **8,** 1-10 (2018).
44. Rizzo, L., Koch, J., Belgiorno, V. & Anderson, M. A. Removal of Methylene Blue in a photocatalytic reactor using polymethylmethacrylate supported $TiO_2$ film. *Int. Conf. Environ. Sci. Technol.* 1-3 (2005).
45. DePuccio, D. P., Botella, P., O'Rourke, B. & Landry, C. C. Degradation of Methylene Blue Using Porous $WO_3$, $SiO_2$-$WO_3$, and Their Au-Loaded Analogs: Adsorption and Photocatalytic Studies. *ACS Appl. Mater. Interfaces* **7,** 1987-1996 (2015).
46. Amini, M., Pourbadiei, B., Ruberu, T. P. A. & Woo, L. K. Catalytic activity of

$MnOx/WO_3$ nanoparticles: Synthesis, structure characterization and oxidative degradation of methylene blue. *New J. Chem.* **38,** 1250-1255 (2014).

47. Dimitrov, D. T., Milanova, M. M. & Kralshevska, R. P. Lanthanide oxide doped titania photocatalysts for degradation of organic pollutants under UV and visible light illumination. *Bulg. Chem. Commun.* **43,** 489-501 (2011).
48. Zheng, H., Ou, J. Z., Strano, M. S., Kaner, R. B. & Mitchell, A. Nanostructured Tungsten Oxide-Properties, Synthesis, and Applications. *Adv. Funct. Mater* **21,** 2175-2196 (2011).

# CHAPTER 5
# CONCLUSIONS AND RECOMMENDATIONS

## 5.1 Conclusion

In this study, the pristine *m*-$WO_3$ and La-doped $WO_3$ nanoparticles were synthesized using hydrothermal and impregnation method and characterised using Powder X-ray diffraction (PXRD), UV-Vis spectrometer (DRS), Raman spectrophotometer, Fourier transformed infrared (FTIR), transmission electron microscopy (TEM) in combination with an energy dispersive X-ray (EDX) detector, X-Ray Photoelectron Spectroscopy (XPS), Zetasizer Nano ZS, and Ion chromatograph (IC).

The XRD results confirm that the synthesized pristine and lanthanum doped nanoparticles had a monoclinic structure. The observed XRD results further indicated clear crystallinity of the synthesized nanoparticles as there was no presence of diffraction peaks that could be credited to the dopant. The functional groups such as W=O, W-O and W-O-W present in the monoclinic $WO_3$ nanoparticles were affirmed by FTIR and Raman spectroscopy. Furthermore, the typical bands that appear at 104, 191 and 411 $cm^{-1}$ attributed to $La_2O_3$ were not present in the La-doped samples, this may be due to lanthanum being dispersed on the surface of the catalyst.



The morphology studies indicated that as-synthesized nanoparticles are a mixture of spherical and rod-shaped. The spherical shapes sizes of the *m*-$WO_3$ and 5-La-$WO_3$ were found to be 45 nm and 55 nm respectively. The particle size measurement form TEM is higher than the average particle size estimated from XRD and this may be due to the agglomeration of smaller particles.

The effects of lanthanum on optical properties of the nanoparticle analysed using DRS revealed that all synthesized nanoparticles absorb in the visible region (350–800 nm). The calculated band edge positions indicated shifts in valence and conduction bands due to lanthanum doping. Moreover, the valence band maximum (VBM) spectra were

used to calculate the valence and conduction band edge positions and the obtained results were in support of the DRS data.

The photocatalytic activity of the pristine and La-doped nanoparticles was assessed on the degradation of MB and CR. The result showed that low concentration of lanthanum loading can enhance the activity by acting as the lanthanum acted as trap sites for photogenerated holes and elections and thus inhibit recombination. However further increase in La doping slightly reduced the efficiency of the catalyst, and this is an indication of optimal loading of the dopant and that La may be acting as recombination site.

It has been found that the surface charge of the nanoparticles played a significant role in the photodegradation of the dyes. Lanthanum played a role in concentrating the organic pollutants on the surface of the catalyst and therefore improved the separation efficiency of photogenerated electron-hole pairs of $WO_3$ to enhance the photocatalytic activity. The pH of the dye solution was as important as the results showed that the degradation of the cationic dye Methylene blue (MB) was favoured in neutral pH where the photocatalyst was more negatively charged whilst the anionic dye Congo red (CR) had the affinity for positively charged photocatalyst in acidic media. The degradation rate of both MB and CR was about 99.6% in visible-light irradiation for 20 min. The degradation efficiency of the nanoparticles was confirmed by Ion Chromatograph (IC) measurements, which indicated the highest generation of both chloride, and sulphate ions with 1% lanthanum doped $WO_3$ nanoparticles.

## 5.2 Recommendations for future work

The objectives of this research were achieved, however, due to several gaps that were identified; the following recommendations are outlined for future work.

- A study may be conducted to investigate the comparison of the photocatalytic activity between the lab synthesized pristine and commercial tungsten trioxide nanoparticles.

- Wastewater from textile industries is composed of other complex dyestuffs which may also be used in the investigation of the efficiency of lanthanum doped nanoparticles.

- The heterogeneous photocatalysis is reported to be a cheaper and faster method for degrading recalcitrant pollutants. Thus, the degradation efficiency of lanthanum-doped nanoparticle in comparison to the conventional wastewater treatment may also be investigated.

# APPENDIX A: SEM images of pristine 5% La doped $WO_3$ nanoparticles.

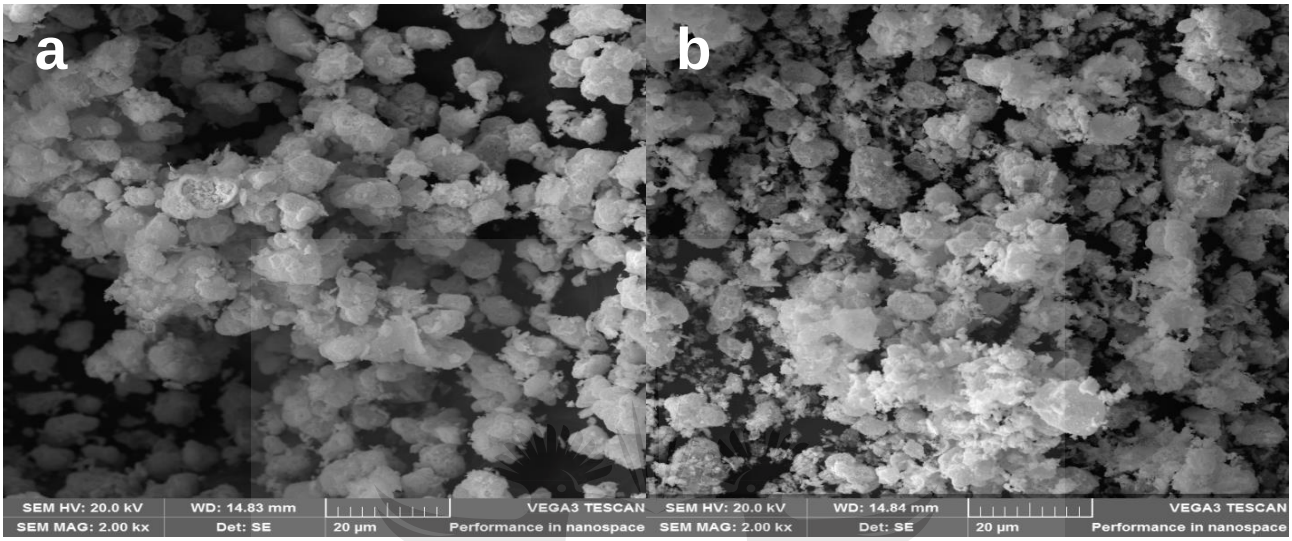


SEM images of pristine $WO_3$ and 5-La-$WO_3$.

# APPENDIX B: Absorbance spectra for the photodegradation of MB and CR by pristine 5% La doped $WO_3$ nanoparticles.

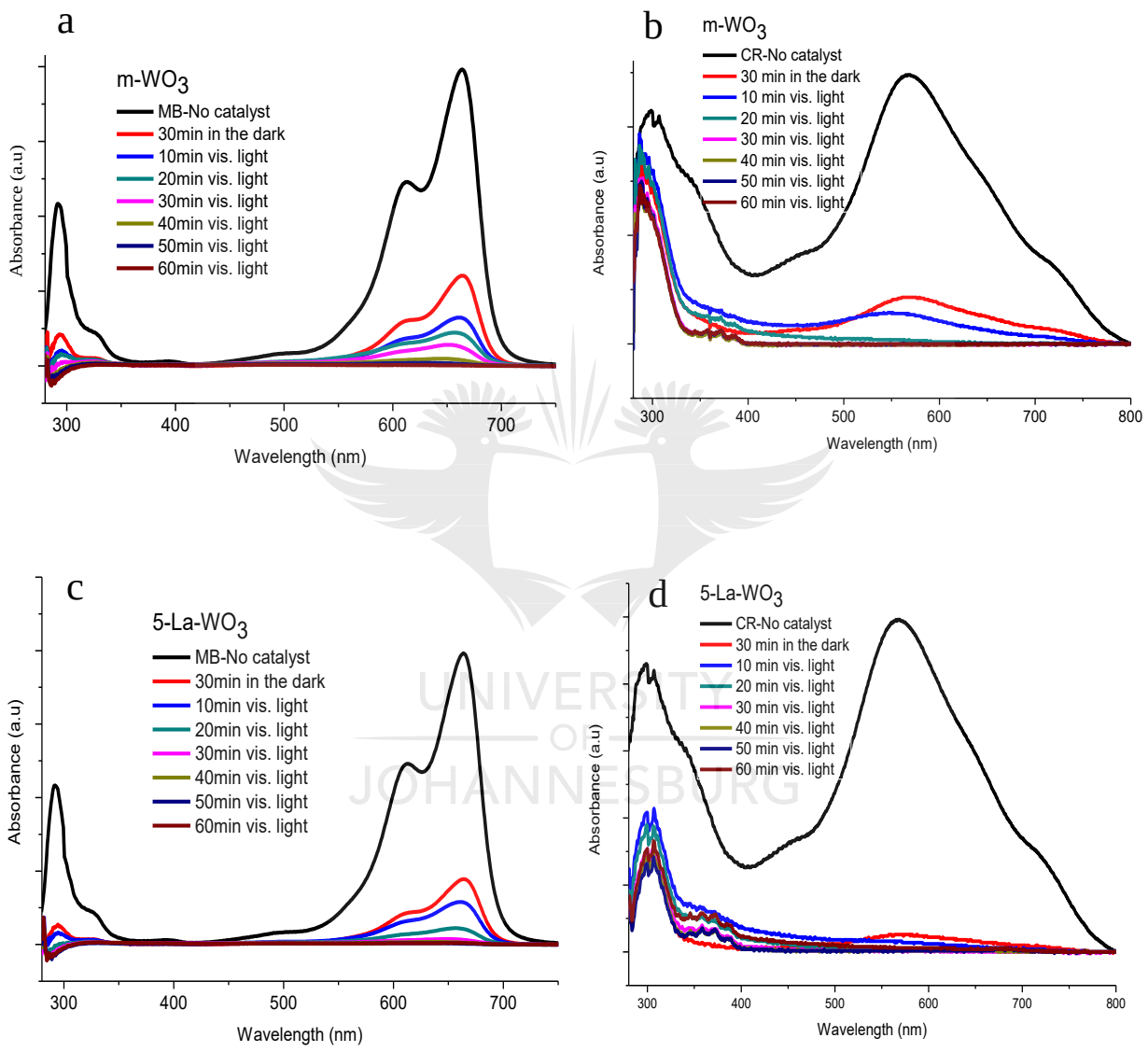


Absorption spectra of the photocatalytic degradation of MB and CR by (a) & (b) m-$WO_3$, and (c) & (d) 5-La-$WO_3$.